Università degli studi di Pavia
Joint Ph.D. program in Mathematics Milano Bicocca - Pavia - INdAM

Doctoral Thesis

Efficient solvers for Isogeometric Analysis

Author:
Gabriele Loli

Supervisor:
Prof. Giancarlo Sangalli
Co-supervisor:
Prof. Annalisa Buffa

Acknowledgements

First of all, I am grateful to my PhD supervisor Prof. Giancarlo Sangalli for his constant support, inspiring ideas and enthusiasm in researching and teaching.

I would like to thank Prof. Annalisa Buffa for having accepted me as a visitor at EPFL and for having co-supervised my thesis. It has been such a great pleasure and honour for me to visit and work with her and her group in Losanna.

I must also express my gratitude to Pouria Behnoudfar, Luca Coradello, Monica Montardini and Mattia Tani for the fruitful collaborations.

A special thanks goes to my collegues and friends, in particular Alessandro, Andrea, Andrea, Gennaro, Mattia and Stefano, for the wonderful time spent together and their precious support.

Finally, I am deeply grateful to my brother for having always encouraged me to do my best and my parents for their unconditional love.

Contents

List of Figures

List of Tables

Chapter 1

Introduction

Isogeometric Analysis (IGA) was introduced by Hughes et al. in [41] to unify computer aided geometric design (CAGD) and numerical simulations. Indeed, IGA uses CAGD mathematical primitives, that are splines, NURBS and their extensions, to represent both the geometry and the unknowns of Partial Differential Equations (PDEs) that model physical phenomena of interest. In this way, thanks to an exact representation of the computational domain, the error due to the approximation of the geometry is eliminated. Moreover, the use of splines and NURBS as building blocks for the construction of discrete spaces turns out to be a key ingredient of numerical schemes enjoying features that would be hard to achieve by standard finite element methods. This is in particular due to the spline smoothness that brings several advantages: it improves the accuracy per degree of freedom (comparing to standard C^0 finite elements), it improves significantly the approximation of the spectrum of the differential operators, it allows direct approximation of PDEs of order higher than two and it facilitates construction of spaces that can be used in schemes that preserve specific fundamental properties of the PDE of interest.
The use of highly refined meshes or high degree splines introduces challenging problems at the computational level. Indeed, the conditioning of the matrices associated to the discrete systems produced by isogeometric methods can degenerate rapidly for decreasing mesh size h and increasing spline degree p. Therefore the design and analysis of efficient and robust iterative solvers and preconditioners for IGA is a very active research topic. In this context, we say that a preconditioner $\mathcal{P}$ for the linear system $\mathcal{A}u = b$ is robust if the condition number $\kappa(\mathcal{P}^{-1}\mathcal{A})$ is bounded from above by a reasonably low number, independent of the mesh size and the spline degree. Further, we say that a preconditioner is computationally efficient if its setup and application has a computational cost comparable to the one of the matrix-vector product for the system matrix $\mathcal{A}$.

This thesis is devoted to the study of efficient method for solving PDEs discretized through IGA. We begin with an efficient and robust preconditioner for the isogeometric mass matrix for single patch domain. Then, we extend it to conforming multipatch geometries where continuity across the patches is imposed strongly. As an application, we combine this preconditioners with the high-order generalized-α method, introduced in [21], as the time integrator to solve a model hyperbolic boundary-value problem. After that, we focus on the analysis of a solver for a fourth-order PDE in the framework of non conforming multipatch domains. In this case the C^1-continuity is imposed weakly through a super-penalty method. The main idea of our method is to eliminate the Lagrange multipliers originated in the mortar formulation of the bilaplace problem by introducing a singular perturbation. Then we propose a preconditioner for the resulting system based on a combination of the Schur Complement Reduction (SCR), introduced in [48, 49], with the Fast Diagonalization technique, developed in [62, 57, 51].

The structure of the work is as follows. Chapter 2 consists of a brief presentation of the main tools we use in this thesis. In particular we start by introducing the basic concepts of Isogeometric Analysis like univariate and multivariate B-spline functions, single patch and conforming multipatch isogeometric spaces. Then we presents the notion of Kronecker product and its main properties.

Chapter 3 deals with the fast solution of linear systems associated with the mass matrix, in the context of isogeometric analysis. We propose a preconditioner that is both efficient and easy to implement, based on a diagonal-scaled Kronecker product of univariate parametric mass matrices. Its application is faster than a matrix-vector product involving the mass matrix itself. We prove that the condition number of the preconditioned matrix converges to 1 as the mesh size is reduced, that is, the preconditioner is asymptotically equivalent to the exact inverse. Moreover, we give numerical evidence of its good behaviour with respect to the spline degree and the (possibly singular) geometry parametrization. We also extend the preconditioner to the multipatch case through an Additive Schwarz method.

Chapter 4 focuses on a novel family of high-order explicit generalized-α methods applied in combination with isogeometric analysis. Our method can deliver $2k$ order of accuracy in time consisting of solving k matrix systems explicitly and updating the other $2k$ variables at each time-step.
Next, to deal with the computational cost, we exploit the preconditioners for the matrix systems presented in Chapter 3. Our high-order schemes require simple modifications of the available implementations of the generalized-α method. Finally, we present numerical examples to prove the performance of the overall methodology regarding single and multipatch IGA discretizations.

Chapter 5 focuses on the development of a super-penalty strategy based on the L^2-projection of suitable coupling terms to achieve C^1-continuity between non-conforming multi-patch for the isogeometric discretization of the bilaplace equation. In particular, the choice of penalty parameters is driven by the underlying perturbed saddle point problem from which the Lagrange multipliers are eliminated and is performed to guarantee the optimal accuracy of the method. Moreover, by construction, the method does not suffer from locking also on very coarse meshes. We demonstrate the applicability of the proposed coupling algorithm to Kirchhoff plates by studying several benchmark examples discretized by non-conforming meshes. In all cases, we recover the optimal rates of convergence achievable by B-splines where we achieve a substantial gain in accuracy per degree-of-freedom compared to other choices of the penalty parameters.

Parts of the results presented in this thesis are contained in papers that have been submitted by the author and coauthors in peer reviewed journals, they are available online or they are in preparation:

- Chapter 3:
  [52] G. Loli, G. Sangalli, and M. Tani. *Easy and Efficient preconditioning of the Isogeometric Mass Matrix.* Submitted to Computers & Mathematics with Applications. 2020. arXiv: `2006.02313`.

- Chapter 4:
  [6] P. Behnoudfar, V. M. Calo, G. Loli, A. Reali, and G. Sangalli. "Explicit high-order generalized-α methods for isogeometric analysis of structural dynamics". In: *In preparation* (2020).

- Chapter 5:
  [13] A. Buffa, L. Coradello, and G. Loli. *A projected super-penalty method for the*

C^1-coupling of multi-patch isogeometric Kirchhoff plates. 2020. arXiv: 2007.14343.
[14] A. Buffa, L. Coradello, and G. Loli. "Isogeometric penalty method for the Bilaplace equation". In: *In preparation* (2020).
[7] A. Benvenuti, G. Loli, G. Sangalli, and T. Takacs. "Isogeometric Analysis for weak C^1-continuous Mortar Method". In: *In preparation* (2020).

Finally, we would like to mention two papers co-authored by the author but not included in this thesis:

- [15] F. Calabrò, G. Loli, G. Sangalli, and M. Tani. "Quadrature Rules in the Isogeometric Galerkin Method: State of the Art and an Introduction to Weighted Quadrature". In: *Advanced Methods for Geometric Modeling and Numerical Simulation*. Ed. by Carlotta Giannelli and Hendrik Speleers. Cham: Springer International Publishing, 2019, pp. 43–55.

- [51] G. Loli, M. Montardini, G. Sangalli, and M. Tani. "An efficient solver for space–time isogeometric Galerkin methods for parabolic problems". In: *Computers & Mathematics with Applications* 80.11 (2020). High-Order Finite Element and Isogeometric Methods 2019, pp. 2586 –2603. ISSN: 0898-1221.

The first one is focused on an efficient method for assembling matrices related to isogeometric analysis, while the second one deals with efficient solution of parabolic problems, approximated with smooth splines in both space and time.

Chapter 2

Preliminaries

This first chapter is devoted to fix the notation and present some preliminary results which will be useful in what follows. In particular, we recall the definitions of B-splines and isogeometric spaces for both single patch and multipatch domain. Finally, we also report the main properties of the Kronecker product.

2.1 B-splines

Given two positive integers p and m, consider an open knot vector

$$\Xi := \{\xi_1, \dots, \xi_{m+p+1}\}$$

such that

$$\xi_1 = \dots = \xi_{p+1} < \xi_{p+2} \leq \dots \leq \xi_m < \xi_{m+1} = \dots = \xi_{m+p+1},$$

where interior repeated knots are allowed with maximum multiplicity $p+1$. Without loss of generality, we assume $\xi_1 = 0$ and $\xi_{m+p+1} = 1$. From the knot vector Ξ, B-spline functions of degree p are defined following the well-known Cox-De Boor recursive formula: we start with piecewise constants ($p = 0$):

$$\widehat{b}_{i,0}(\zeta) = \begin{cases} 1 & \text{if } \xi_i \leq \zeta < \xi_{i+1}, \\ 0 & \text{otherwise,} \end{cases}$$

and for $p \geq 1$ the B-spline functions are defined by the recursion

$$\widehat{b}_{i,p}(\zeta) = \frac{\zeta - \xi_i}{\xi_{i+p} - \xi_i} \widehat{b}_{i,p-1}(\zeta) + \frac{\xi_{i+p+1} - \zeta}{\xi_{i+p+1} - \xi_{i+1}} \widehat{b}_{i+1,p-1}(\zeta),$$

with the convention $0/0 = 0$. Each B-spline $\widehat{b}_{i,p}$ depends only on $p+2$ knots, which are collected in the local knot vector

$$\Xi_{i,p} := \{\xi_i, \dots, \xi_{i+p+1}\},$$

is non-negative and supported in the interval $[\xi_i, \xi_{i+p+1}]$. Moreover, these B-spline functions constitute a partition of unity, that is

$$\sum_{i=1}^{m} \widehat{b}_{i,p}(x) = 1, \qquad \forall x \in (0,1). \tag{2.1}$$

The univariate spline space is defined as

$$\widehat{\mathcal{S}}_h = \widehat{\mathcal{S}}_h([0,1]) := \operatorname{span}\{\widehat{b}_{i,p}\}_{i=1}^{m},$$

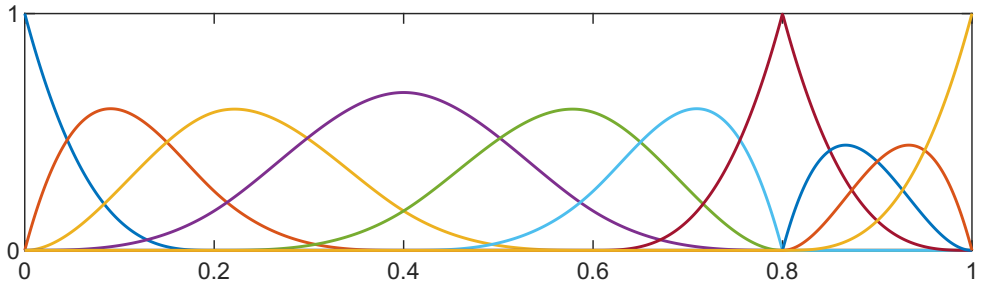

FIGURE 2.1: Example of cubic B-spline basis defined on the open knot vector $\Xi = \{0, 0, 0, 0, 0.2, 0.4, 0.6, 0.8, 0.8, 0.8, 1, 1, 1, 1\}$.

where h denotes the maximal mesh-size, and corresponds to piecewise polynomials of degree p with $p - m_i$ continuous derivatives at the point ξ_i, where m_i is the multiplicity of the knot ξ_i in the knot vector Ξ. We assume that the maximum multiplicity of the internal knots is less than or equal to the degree p, i.e., the B-spline functions are at least continuous. Finally, we remark that B-splines are not in general interpolatory: they are interpolatory at knots ξ_i with multiplicity at least p, that is where B-splines are at most C^0. An example of B-splines is given in Figure 2.1. For brevity, the degree p is not always reported in the notation. For more details on B-splines properties see [18, 19].

Multivariate B-splines are defined from univariate B-splines by tensorization. Let d be the space dimension and consider open knot vectors $\Xi_k = \{\xi_{k,1}, \dots, \xi_{k,m+p+1}\}$ and a set of multi-indices $\mathbf{I} := \{\mathbf{i} = (i_1, \dots, i_d) : 1 \le i_l \le m\}$. For each multi-index $\mathbf{i} = (i_1, \dots, i_d)$, we introduce the d-variate B-spline,

$$\widehat{B}_{\mathbf{i}}(\zeta) := \widehat{b}[\Xi_{i_1,p}](\zeta_1) \dots \widehat{b}[\Xi_{i_d,p}](\zeta_d).$$

Observe that, for the sake of simplicity, the knot vectors are assumed to have the same length and the degree is the same in all directions. The support of each multivariate basis function is

$$Q'_{\mathbf{i}} := \operatorname{supp}(\widehat{B}_{\mathbf{i}}) = \prod_{k=1}^{d} [\xi_{k,i_k}, \xi_{k,i_k+p+1}].$$

For notational convenience, we define the index set for mesh elements

$$\mathbf{I}_e := \{(j_1, \dots, j_d) : 1 \le j_l \le m + p + 1\},$$

$$Q_{\mathbf{j}} := \prod_{k=1}^{d} [\xi_{k,j_k}, \xi_{k,j_k+1}], \qquad \mathbf{j} \in \mathbf{I}_e \tag{2.2}$$

and

$$\mathcal{I}_{\mathbf{j}} := \{\mathbf{i} \in \mathbf{I} : \operatorname{int}(Q_{\mathbf{j}} \cap Q'_{\mathbf{i}}) \neq \emptyset\}. \tag{2.3}$$

The corresponding spline space is defined as

$$\widehat{\mathcal{S}}_h = \widehat{\mathcal{S}}_h([0,1]^d) := \operatorname{span}\{B_{\mathbf{i}} : \mathbf{i} \in \mathbf{I}\},$$

where h is the maximal mesh-size in all knot vectors, that is

$$h := \max_{\substack{1\le k\le d\\ 1\le i\le m+p+1}} \{|\xi_{k,i+1} - \xi_{k,i}|\}.$$

Assumption 1. *We assume that the knot vectors are quasi-uniform, that is, there exists $\alpha > 0$, independent of h, such that each non-empty knot span $(\xi_{k,i}, \xi_{k,i+1})$ fulfils $\alpha h \le \xi_{k,i+1} - \xi_{k,i}$, for $1 \le k \le d$.*

A family of linear functionals $\{\widehat{\varphi}_{\mathbf{i}}\}_{\mathbf{i}\in\mathbf{I}}$ is called a *dual basis* for the set of tensor-product B-splines $\widehat{\mathcal{S}}_h$ if it verifies

$$\widehat{\varphi}_{\mathbf{i}}(\widehat{B}_{\mathbf{j}}) = \delta_{\mathbf{ij}},$$

where $\delta_{\mathbf{ij}}$ is the Kronecker delta.

Theorem 1. *[65, Theorem 12.5] There exists a dual basis and a positive constant C, independent of h, satisfying*

$$|\widehat{\varphi}_{\mathbf{i}}(\widehat{u})| \le Ch^{-\frac{d}{2}} \|\widehat{u}\|_{L^2(Q'_{\mathbf{i}})}, \qquad \forall\, \widehat{u} \in L^2((0,1)^d) \text{ and } \forall\, \mathbf{i} \in \mathbf{I}.$$

2.2 Isogeometric space on a single patch domain

Now, we consider a single patch domain $\Omega \subset \mathbb{R}^d$, given by a d-dimensional spline parametrization $\boldsymbol{F}$, that is

$$\Omega = \boldsymbol{F}(\widehat{\Omega}), \qquad \text{with } \boldsymbol{F}(\boldsymbol{\xi}) = \sum_{\mathbf{i}} \boldsymbol{C}_{\mathbf{i}} \widehat{B}_{\mathbf{i}}(\boldsymbol{\xi}),$$

where $\boldsymbol{C}_{\mathbf{i}}$ are the control points and $\widehat{B}_{\mathbf{i}}$ are tensor-product B-spline basis functions defined on the parametric patch $\widehat{\Omega} := (0,1)^d$. We require that $\boldsymbol{F}$ is an invertible map. Further assumptions will be specified in Assumption 2. Following the isoparametric paradigm, the isogeometric basis functions $B_{\mathbf{i}}$ are defined as $B_{\mathbf{i}} = \widehat{B}_{\mathbf{i}} \circ \boldsymbol{F}^{-1}$. Thus, the isogeometric space on Ω is defined as

$$\mathcal{S}_h = \mathcal{S}_h(\Omega) := \operatorname{span}\left\{ B_{\mathbf{i}} := \widehat{B}_{\mathbf{i}} \circ \mathbf{F}^{-1} \ : \ \mathbf{i} \in \mathbf{I} \right\}.$$

Corollary 1. *The family $\{\varphi_{\mathbf{i}}\}_{\mathbf{i}\in\mathbf{I}}$, defined as*

$$\varphi_{\mathbf{i}}(u) := \widehat{\varphi}_{\mathbf{i}}(u \circ \mathbf{F}), \qquad \forall\, \mathbf{i} \in \mathbf{I},$$

is a dual basis for $\mathcal{S}_h$. Moreover, there exists a positive constant C, independent of h, satisfying

$$|\varphi_{\mathbf{i}}(u)| \le Ch^{-\frac{d}{2}} \|u\|_{L^2(\mathbf{F}(Q'_{\mathbf{i}}))}, \qquad \forall\, u \in L^2(\Omega) \text{ and } \forall\, \mathbf{i} \in \mathbf{I}.$$

Proof. The inequality is obtained from Theorem 1 by a standard change of variables. □

Proposition 1. *There exists a positive constant C, independent of h and p, such that*

$$\|u\|_{L^2(\boldsymbol{F}(Q_{\mathbf{i}}))} \le Ch^{\frac{d}{2}} \max_{\mathbf{j}\in\mathcal{I}_{\mathbf{i}}} |\varphi_{\mathbf{j}}(u)|, \qquad \forall\, u \in L^2(\Omega) \text{ and } \forall\, \mathbf{i} \in \mathbf{I}_e.$$

Proof. Using the extension to d-variate isogeometric functions of the partition of unity property (2.1), it holds

$$\begin{aligned}\|u\|^2_{L^2(\boldsymbol{F}(Q_{\mathbf{i}}))} &= \int_{\boldsymbol{F}(Q_{\mathbf{i}})} \left(\sum_{\mathbf{i}\in\mathcal{I}_{\mathbf{i}}} \varphi_{\mathbf{i}}(u) B_{\mathbf{i}}\right)^2 \leq \int_{\boldsymbol{F}(Q_{\mathbf{i}})} \left(\max_{\mathbf{j}\in\mathcal{I}_{\mathbf{i}}} |\varphi_{\mathbf{j}}(u)| \sum_{\mathbf{j}\in\mathcal{I}_{\mathbf{i}}} B_{\mathbf{i}}\right)^2 \\ &= |\boldsymbol{F}(Q_{\mathbf{i}})| \max_{\mathbf{j}\in\mathcal{I}_{\mathbf{i}}} |\varphi_{\mathbf{j}}(u)|^2 \leq C h^d \max_{\mathbf{j}\in\mathcal{I}_{\mathbf{i}}} |\varphi_{\mathbf{j}}(u)|^2.\end{aligned}$$

□

By introducing a co-lexicographical reordering of the basis functions, with a minor abuse of notation we will also write in what follows

$$\mathcal{S}_h = \operatorname{span}\{B_{\mathbf{i}} : \mathbf{i}\in\mathbf{I}\} = \operatorname{span}\{B_i\}_{i=1}^{N_{\text{dof}}}. \tag{2.4}$$

2.3 Isogeometric spaces on a multipatch domain

We follow the notation of [72]. A multipatch domain $\Omega \subset \mathbb{R}^d$ is an open set, defined as the union of N_{patch} subdomains,

$$\overline{\Omega} = \bigcup_{r=1}^{N_{\text{patch}}} \overline{\Omega^{(r)}}, \tag{2.5}$$

where the subdomains $\Omega^{(r)} = \boldsymbol{F}^{(r)}(\widehat{\Omega})$ are referred to as patches and are assumed to be disjoint. Each $\boldsymbol{F}^{(r)}$ is a different spline parametrization. In the following, the superindex (r) will identify entities that refer to $\Omega^{(r)}$. Then, following the same construction as above, we introduce, for each patch $\Omega^{(r)}$, B-spline spaces

$$\widehat{\mathcal{S}}_h^{(r)} := \operatorname{span}\left\{\widehat{B}_i^{(r)} : i = 1,\dots,N_{\text{dof}}^{(r)}\right\}$$

and isogeometric spaces

$$\mathcal{S}_h^{(r)} := \operatorname{span}\left\{B_i^{(r)} : i = 1,\dots,N_{\text{dof}}^{(r)}\right\}.$$

We assume for simplicity that the degree p is the same for all patches. For the definition of the isogeometric space in the whole Ω, we further impose continuity at the interfaces between patches, that is

$$V_h := \left\{v \in C^0(\Omega) : v|_{\Omega^{(r)}} \in \mathcal{S}_h^{(r)} \text{ for } r = 1,\dots,N_{\text{patch}}\right\}. \tag{2.6}$$

To construct a basis for space V_h, we introduce a suitable conformity assumption. For all $r, s \in \{1,\dots,N_{\text{patch}}\}$, with $r \neq s$, let $\Gamma_{rs} = \partial\Omega^{(r)} \cap \partial\Omega^{(s)}$ be the interface between the patches $\Omega^{(r)}$ and $\Omega^{(s)}$.

Assumption 2. *We assume:*

1. *Γ_{rs} is either a vertex or the image of a full edge or the image of a full face for both parametric domains.*
2. *For each $B_{\mathbf{i}}^{(r)} \in \mathcal{S}_h^{(r)}$ such that $\operatorname{supp}(B_{\mathbf{i}}^{(r)}) \cap \Gamma_{rs} \neq \emptyset$, there exists a function $B_{\mathbf{j}}^{(s)} \in \mathcal{S}_h^{(s)}$ such that $B_{\mathbf{i}}^{(r)}|_{\Gamma_{rs}} = B_{\mathbf{j}}^{(s)}|_{\Gamma_{rs}}$.*

We define, for each patch $\Omega^{(r)}$, an application

$$G^{(r)} : \{1, \dots, N_{\text{dof}}^{(r)}\} \to \mathcal{J} = \{1, \dots, \dim(V_h)\},$$

in such a way that $G^{(r)}(i) = G^{(s)}(j)$ if and only if $\Gamma_{rs} \neq \emptyset$ and $B_i^{(r)}|_{\Gamma_{rs}} = B_j^{(s)}|_{\Gamma_{rs}}$. Moreover, we define, for each global index $l \in \mathcal{J}$, the set of pairs $\mathcal{J}_l := \{(r, i) : G^{(r)}(i) = l\}$, which collects the local indices of patchwise contributions to the global function, and the scalar

$$n_l := \#\mathcal{J}_l, \tag{2.7}$$

that expresses the patch multiplicity for the global index l. Furthermore, let

$$N_{\text{adj}} := \max\{n_l : l \in \mathcal{J}\} \tag{2.8}$$

be the maximum number of adjacent patches (i.e., whose closure has non-empty intersection). We define, for each $l \in \mathcal{J}$, the global basis function

$$B_l(\boldsymbol{x}) := \begin{cases} B_i^{(r)}(\boldsymbol{x}) & \text{if } \boldsymbol{x} \in \overline{\Omega^{(r)}} \text{ and } (r, i) \in \mathcal{J}_l, \\ 0 & \text{otherwise,} \end{cases} \tag{2.9}$$

which is continuous due to Assumption 2. Then

$$V_h = \text{span}\{B_l : l \in \mathcal{J}\}. \tag{2.10}$$

The set $\{B_l : l \in \mathcal{J}\}$ where B_l is defined as in (2.9), represents a basis for V_h. Finally, we also introduce the index set $\mathcal{J}^{(r)} \subset \mathcal{J}$ such that $l \in \mathcal{J}^{(r)}$ if and only if $l = G^{(r)}(i)$ for some i. Clearly $\#\mathcal{J}^{(r)} = N_{\text{dof}}^{(r)}$ and $\mathcal{J}^{(r)}$ can be used directly as index set for $\widehat{\mathcal{S}}_h^{(r)}$ and $\mathcal{S}_h^{(r)}$, with minor abuse of notation.

2.4 Kronecker product

The Kronecker product between two matrices $\mathbf{A} \in \mathbb{C}^{n_1 \times n_2}$ and $\mathbf{B} \in \mathbb{C}^{n_3 \times n_4}$ is defined as

$$\mathbf{A} \otimes \mathbf{B} := \begin{bmatrix} [\mathbf{A}]_{1,1}\mathbf{B} & \dots & [\mathbf{A}]_{1,n_2}\mathbf{B} \\ \vdots & \ddots & \vdots \\ [\mathbf{A}]_{n_1,1}\mathbf{B} & \dots & [\mathbf{A}]_{n_1,n_2}\mathbf{B} \end{bmatrix} \in \mathbb{C}^{n_1 n_3 \times n_2 n_4},$$

where the ij-th entry of the matrix $\mathbf{A}$ is denoted by $[\mathbf{A}]_{i,j}$. The most important properties of the Kronecker product that we will exploit in this work are the following:

- if $\mathbf{A}$, $\mathbf{B}$, $\mathbf{C}$ and $\mathbf{D}$ are matrices of conforming order, then it holds

$$(\mathbf{A} \otimes \mathbf{B}) \cdot (\mathbf{C} \otimes \mathbf{D}) = (\mathbf{AC}) \otimes (\mathbf{BD}); \tag{2.11}$$

- if $\mathbf{A}$ and $\mathbf{B}$ are non-singular, then

$$(\mathbf{A} \otimes \mathbf{B})^{-1} = \mathbf{A}^{-1} \otimes \mathbf{B}^{-1}. \tag{2.12}$$

Finally, we recall that the matrix-vector product can be efficiently computed for a matrix that has a Kronecker product structure. For this purpose we define, for $m = 1, \dots, d$, the m-mode product $\times_m$ of a tensor $\mathbf{X} \in \mathbb{C}^{n_1 \times \dots \times n_d}$ with a matrix $\mathbf{M} \in$

$\mathbb{C}^{k\times n_m}$ as a tensor of size $n_1 \times \cdots \times n_{m-1} \times k \times n_{m+1} \times \ldots n_d$ whose elements are

$$[\mathbf{X} \times_m \mathbf{M}]_{i_1,\ldots,i_d} = \sum_{j=1}^{n_m} [\mathbf{X}]_{i_1,,\ldots,i_{m-1},j,i_{m+1}\ldots,i_d} [\mathbf{M}]_{i_m,j}.$$

Then, given $\mathbf{M}_i \in \mathbb{C}^{k_i \times n_i}$ for $i = 1, \ldots, d$, it holds

$$(\mathbf{M}_d \otimes \cdots \otimes \mathbf{M}_1) \operatorname{vec}(\mathbf{X}) = \operatorname{vec}(\mathbf{X} \times_1 \mathbf{M}_1 \times_2 \cdots \times_d \mathbf{M}_d), \tag{2.13}$$

where the vectorization operator "vec" applied to a tensor stacks its entries into a column vector as

$$[\operatorname{vec}(\mathbf{X})]_j = [\mathbf{X}]_{i_1,\ldots,i_d},$$

for $i_l = 1, \ldots, n_l$, $l = 1, \ldots, d$ and

$$j = i_1 + \sum_{k=2}^{d} \left[(i_k - 1) \Pi_{l=1}^{k-1} n_l \right].$$

For more details on Kronecker product we refer to [47].

Chapter 3

Preconditioning of the Isogeometric Mass Matrix

The focus of this chapter is the solution of the linear systems associated with the isogeometric Galerkin mass matrix, for arbitrary degree and continuity of the spline approximation. In particular, we want to cover the case of high-degree and high-continuity spline approximation (the so-called isogeometric k-refinement) whose advantages are explored in, e.g., [27, 71, 61, 67, 11, 63]. Solving the mass matrix system is needed, for example:

- in explicit dynamic simulation, that is, when an explicit finite difference schemes in time is coupled to an isogeometric discretization in space, see e.g. [33]
- in PDE-constrained optimization problem [9]
- when the mass matrix is used as a smoother in a multigrid solver [39, 38]
- when the mass matrix is used as a preconditioner for the Schur complement of the Stokes problem [26]
- in general, when evaluations of L^2-projections are needed, for example in nearly-incompressible elasticity with the $\bar{B}$–$\bar{F}$ method [25], or in the mortar method for multipatch gluing [12], or in other applications like fast simulation of tumor evolution [53].

Due to the condition number of the mass matrix, that grows exponentially with respect to the spline degree (see [29]), finding efficient solvers is not a trivial task unless we are in the low degree case.

One of the first ideas that have been explored is to use collocation instead of a Galerkin formulation, since in this case the mass matrix (that is, the B-spline collocation matrix) is easier to invert (see [28, 2] and the references therein).

If we stay with the Galerkin formulation, the classical strategy of lumping and then inverting the mass matrix lacks accuracy and, as a preconditioner for an iterative solver, lacks robustness with respect to the spline degree. There are instead ad hoc constructions of sparse and approximated inverse of the mass matrix, see for example [68], or biorthogonal bases, see [76], designed with the aim of keeping accuracy. Approximated inverses or preconditioners of the mass matrix often use one key feature of multivariate splines: the tensor-product construction. Indeed $\widehat{\mathbf{M}}$, the Galerkin mass matrix on the reference patch $[0,1]^d$, is a Kronecker matrix of the form

$$\widehat{\mathbf{M}} = \widehat{\mathbf{M}}_d \otimes \ldots \otimes \widehat{\mathbf{M}}_1, \tag{3.1}$$

where the $\widehat{\mathbf{M}}_i$ are unidimensional parametric mass matrices. Inverting $\widehat{\mathbf{M}}$ above only requires the inversion of the factors $\widehat{\mathbf{M}}_i$. However, on a generic patch, due to the

geometry mapping, the structure above is lost, that is, the true isogeometric mass matrix $\mathbf{M}$ we are interested in is not a Kronecker matrix like $\widehat{\mathbf{M}}$. One could use $\widehat{\mathbf{M}}$ as a preconditioner for $\mathbf{M}$, but, depending on the geometry parametrization of the patch, the results are not always satisfactory. Then, [30] developed an extension of (3.1) that better approximate $\mathbf{M}$ and is suitable for a fast application, see also [75] for its parallel implementation. Another possibility is to seek for a low-rank approximation of $\mathbf{M}$, that is, approximate $\mathbf{M}$ as a sum of Kronecker matrices, see [55, 54, 37]. The recent paper [16] constructs an approximation of $\mathbf{M}^{-1}$ as $\widehat{\mathbf{M}}^{-1}\mathbf{M}_{\det(D\boldsymbol{F})^{-1}}\widehat{\mathbf{M}}^{-1}$, where $\mathbf{M}_{\det(D\boldsymbol{F})^{-1}}$ is a suitable weighted mass.

In our work, we also propose and study a preconditioner $\boldsymbol{\mathcal{M}}$ of the Galerkin mass matrix. The main feature of our approach is that, compared to previous results, it is very easy to implement but also extremely efficient and robust. On a single patch, we define $\boldsymbol{\mathcal{M}}$ as $\mathbf{D}^{\frac{1}{2}}\widehat{\mathbf{D}}^{-\frac{1}{2}}\widehat{\mathbf{M}}\widehat{\mathbf{D}}^{-\frac{1}{2}}\mathbf{D}^{\frac{1}{2}}$, where $\mathbf{D}$ and $\widehat{\mathbf{D}}$ are the diagonal matrices made with the diagonals of the true mass $\mathbf{M}$ and parametric mass $\widehat{\mathbf{M}}$, respectively. Therefore, we approximate $\mathbf{M}$ by the Kronecker $\widehat{\mathbf{M}}$ combined with a symmetric diagonal scaling. The computational cost of one application of the preconditioner is then just $O(pN_{\text{dof}})$ FLOPS, while each matrix-vector multiplication with $\mathbf{M}$ requires $O(p^dN_{\text{dof}})$ FLOPS, where p is the spline degree and N_{dof} is the number of degrees of freedom. For multipatch domains, we combine the preconditioner above on each patch with an Additive Schwarz method. We prove the robustness of the preconditioner with respect to the mesh size and, in the single patch case, we also show that $\kappa(\boldsymbol{\mathcal{M}}^{-\frac{1}{2}}\mathbf{M}\boldsymbol{\mathcal{M}}^{-\frac{1}{2}}) \to 1$ when $h \to 0$. Our numerical benchmarks show that the preconditioned problem behaves well also for large p and even in the case of typical singular parametrizations of the computational domain, which is a case not covered by the theory.

The rest of this chapter is organized as follows. In Section 3.1 we describe the proposed preconditioner on a single patch domain and we prove its h-robustness, while in Section 3.2 we generalize it to multipatch domains by means of the Additive Schwarz theory. We show how to efficiently apply the preconditioner and analyze its computational cost in Section 3.3. In Section 3.4 we report numerical results assessing the effectiveness of the proposed preconditioner, its good behaviour with respect to p and in case of singular parametrizations, and compare with the approach of [16]. Concluding remarks are wrapped up in Section 3.5.

3.1 Mass preconditioner on a patch

In this section we propose a preconditioner for the Galerkin mass matrix associated to a single patch domain, denoted Ω, that is

$$[\mathbf{M}]_{i,j} = \int_{\widehat{\Omega}} \widehat{B}_i \widehat{B}_j |\det(D\boldsymbol{F})|. \tag{3.2}$$

Generalizing, we will consider

$$[\mathbf{M}]_{i,j} = \int_{\widehat{\Omega}} \widehat{B}_i \widehat{B}_j \omega \tag{3.3}$$

for a weight ω that fulfils the following assumption.

Assumption 3. *We assume $\omega \in C^0([0,1]^d)$ and $\omega(\boldsymbol{x}) > 0$, for all $\boldsymbol{x} \in [0,1]^d$.*

Let

$$\omega_{\min} = \min_{\boldsymbol{x}\in[0,1]^d} \omega(\boldsymbol{x}),$$

that, thanks to Assumption 3, is strictly positive. Furthermore, thanks to Heine-Cantor theorem, the function ω is uniformly continuous, that is there exists a non-decreasing $\mu : [0,\infty) \to [0,\infty)$ such that

$$|\omega(\boldsymbol{x}_1) - \omega(\boldsymbol{x}_2)| \leq \mu(|\boldsymbol{x}_1 - \boldsymbol{x}_2|), \qquad \forall \boldsymbol{x}_1, \boldsymbol{x}_2 \in \widehat{\Omega} \tag{3.4}$$

and

$$\lim_{t \to 0^+} \mu(t) = 0. \tag{3.5}$$

As a preconditioner for the mass matrix $\mathbf{M}$, defined in (3.3), we consider

$$\boldsymbol{\mathcal{M}} := \mathbf{D}^{\frac{1}{2}} \widehat{\mathbf{D}}^{-\frac{1}{2}} \widehat{\mathbf{M}} \widehat{\mathbf{D}}^{-\frac{1}{2}} \mathbf{D}^{\frac{1}{2}}, \tag{3.6}$$

where

$$[\widehat{\mathbf{M}}]_{i,j} := \int_{\widehat{\Omega}} \widehat{B}_i \widehat{B}_j, \qquad \widehat{\mathbf{D}} := \operatorname{diag}\left(\widehat{\mathbf{M}}\right), \qquad \mathbf{D} := \operatorname{diag}\left(\mathbf{M}\right). \tag{3.7}$$

From now on, given $u \in \mathcal{S}_h$, we will denote by $\boldsymbol{u}$ the vector containing the coordinates of u with respect to spline basis.

Lemma 1. *There exist a constant $\widehat{C} > 0$, independent of h, such that*

$$\widehat{C} h^d \leq \lambda_{\min}(\widehat{\mathbf{M}}) \leq \lambda_{\max}(\widehat{\mathbf{M}}) \leq h^d, \tag{3.8}$$

where $\lambda_{\max}(\widehat{\mathbf{M}})$ and $\lambda_{\min}(\widehat{\mathbf{M}})$ are the maximum and minimum eigenvalue of $\widehat{\mathbf{M}}$.

Proof. Recalling Assumption 1, from the classical result [20, Theorem 5.1-5.2], for $d = 1$ we get

$$\frac{\alpha h}{4(p+1)^3 9^p} \sum_{i=1}^{m} v_i^2 \leq \left\| \sum_{i=1}^{m} v_i \widehat{b}_{i,p}(x) \right\|^2_{L^2(0,1)} \leq h \sum_{i=1}^{m} v_i^2$$

The bounds (3.8) follow by tensorization and applying the Courant-Fischer theorem. □

Corollary 2. *Under Assumption 3, there exist two positive constants C_1, C_2, independent of h, such that*

$$C_1 h^d \leq \lambda_{\min}(\mathbf{M}) \leq \lambda_{\max}(\mathbf{M}) \leq C_2 h^d. \tag{3.9}$$

Proof. We observe that

$$\begin{aligned} \lambda_{\min}(\mathbf{M}) &= \min_{\boldsymbol{v} \neq \mathbf{0}} \frac{\boldsymbol{v}^T \mathbf{M} \boldsymbol{v}}{\boldsymbol{v}^T \boldsymbol{v}} = \min_{\boldsymbol{v} \neq \mathbf{0}} \frac{\int_{\widehat{\Omega}} \left(\sum_{i=1}^{N_{\text{dof}}} \boldsymbol{v}_i \widehat{B}_i \right)^2 \omega}{\boldsymbol{v}^T \boldsymbol{v}} \\ &\geq \min_{\boldsymbol{v} \neq \mathbf{0}} \frac{\int_{\widehat{\Omega}} \left(\sum_{i=1}^{N_{\text{dof}}} \boldsymbol{v}_i \widehat{B}_i \right)^2}{\boldsymbol{v}^T \boldsymbol{v}} \inf_{\boldsymbol{x} \in \widehat{\Omega}} \omega(\boldsymbol{x}) = \lambda_{\min}(\widehat{\mathbf{M}}) \inf_{\boldsymbol{x} \in \widehat{\Omega}} \omega(\boldsymbol{x}) \end{aligned}$$

and similarly

$$\lambda_{\max}(\mathbf{M}) = \max_{\boldsymbol{v} \neq \mathbf{0}} \frac{\boldsymbol{v}^T \mathbf{M} \boldsymbol{v}}{\boldsymbol{v}^T \boldsymbol{v}} \leq \lambda_{\max}(\widehat{\mathbf{M}}) \sup_{\boldsymbol{x} \in \widehat{\Omega}} \omega(\boldsymbol{x}).$$

Thanks to Assumption 3, ω is bounded from below and above by two positive constants $\omega_{\min}$ and $\omega_{\max}$, thus exploiting Lemma 1, we obtain the thesis with $C_1 = \omega_{\min}\widehat{C}$ and $C_2 = \omega_{\max}$. □

Remark 1. *Thanks to Courant-Fischer theorem, the last inequality in* (3.9) *can be rewritten as follows*

$$\|u\|^2_{L^2(\Omega)} \leq C_2 h^d \sum_{\mathbf{i}\in\mathbf{I}} |\varphi_{\mathbf{i}}(u)|^2, \qquad \forall u \in \mathcal{S}_h, \tag{3.10}$$

where $\{\varphi_{\mathbf{i}}\}_{\mathbf{i}\in\mathbf{I}}$ *denotes the dual basis introduced in Corollary 1.*

Corollary 3. *Under Assumption 3, there exist two positive constants* $\widetilde{C}_1, \widetilde{C}_2$*, independent of* h*, such that*

$$\widetilde{C}_1 h^d \leq \lambda_{\min}(\boldsymbol{\mathcal{M}}) \leq \lambda_{\max}(\boldsymbol{\mathcal{M}}) \leq \widetilde{C}_2 h^d.$$

Proof. It holds

$$\begin{aligned}\lambda_{\min}(\boldsymbol{\mathcal{M}}) &= \lambda_{\min}(\mathbf{D}^{\frac{1}{2}}\widehat{\mathbf{D}}^{-\frac{1}{2}}\widehat{\mathbf{M}}\widehat{\mathbf{D}}^{-\frac{1}{2}}\mathbf{D}^{\frac{1}{2}}) \geq \lambda_{\min}(\mathbf{D})\lambda_{\min}(\widehat{\mathbf{M}})\lambda_{\min}(\widehat{\mathbf{D}}^{-1}) \\ &= \frac{\lambda_{\min}(\mathbf{D})\lambda_{\min}(\widehat{\mathbf{M}})}{\lambda_{\max}(\widehat{\mathbf{D}})}\end{aligned} \tag{3.11}$$

and similarly

$$\lambda_{\max}(\boldsymbol{\mathcal{M}}) \leq \frac{\lambda_{\max}(\mathbf{D})\lambda_{\max}(\widehat{\mathbf{M}})}{\lambda_{\min}(\widehat{\mathbf{D}})} \tag{3.12}$$

Having that the matrices $\mathbf{D}$ and $\widehat{\mathbf{D}}$ are diagonal, their eigenvalues correspond to their diagonal entries. We have

$$[\mathbf{D}]_{i,i} = [\mathbf{M}]_{i,i} = \boldsymbol{e}_i^T \mathbf{M} \boldsymbol{e}_i \qquad \text{and} \qquad [\widehat{\mathbf{D}}]_{i,i} = [\widehat{\mathbf{M}}]_{i,i} = \boldsymbol{e}_i^T \widehat{\mathbf{M}} \boldsymbol{e}_i,$$

where $\boldsymbol{e}_i$ denotes the i-th vector of the standard basis. Thus, it holds

$$\lambda_{\min}(\mathbf{M}) \leq [\mathbf{D}]_{i,i} \leq \lambda_{\max}(\mathbf{M}) \qquad \text{and} \qquad \lambda_{\min}(\widehat{\mathbf{M}}) \leq [\widehat{\mathbf{D}}]_{i,i} \leq \lambda_{\max}(\widehat{\mathbf{M}}). \tag{3.13}$$

In this way, equation (3.11) becomes

$$\lambda_{\min}(\boldsymbol{\mathcal{M}}) \geq \frac{\lambda_{\min}(\mathbf{M})\lambda_{\min}(\widehat{\mathbf{M}})}{\lambda_{\max}(\widehat{\mathbf{M}})}, \tag{3.14}$$

while equation (3.12) becomes

$$\lambda_{\max}(\boldsymbol{\mathcal{M}}) \leq \frac{\lambda_{\max}(\mathbf{M})\lambda_{\max}(\widehat{\mathbf{M}})}{\lambda_{\min}(\widehat{\mathbf{M}})}. \tag{3.15}$$

Combining (3.11) and (3.14) with Lemma 1 and Corollary 2, it follows that there exists a constant $\widetilde{C}_1$, independent of h, such that

$$\lambda_{\min}(\boldsymbol{\mathcal{M}}) \geq \widetilde{C}_1 h^d.$$

Similarly, thanks to (3.12) and (3.15), there exists a constant $\widetilde{C}_2$, independent of h, such that

$$\lambda_{\max}(\boldsymbol{\mathcal{M}}) \leq \widetilde{C}_2 h^d.$$

□

By using the definition

$$\kappa(\mathbf{A}) := \frac{\lambda_{\max}(\mathbf{A})}{\lambda_{\min}(\mathbf{A})}, \tag{3.16}$$

for a symmetric, positive definite matrix $\mathbf{A}$, the following result holds.

Theorem 2. *Under Assumption 3, there exists a constant C, independent of h, such that*

$$\kappa(\boldsymbol{\mathcal{M}}^{-\frac{1}{2}}\mathbf{M}\boldsymbol{\mathcal{M}}^{-\frac{1}{2}}) \leq C.$$

Proof. Recalling Courant-Fischer theorem, it follows

$$\lambda_{\min}(\boldsymbol{\mathcal{M}}^{-\frac{1}{2}}\mathbf{M}\boldsymbol{\mathcal{M}}^{-\frac{1}{2}}) = \min_{\boldsymbol{v}\neq\mathbf{0}} \frac{\boldsymbol{v}^T\mathbf{M}\boldsymbol{v}}{\boldsymbol{v}^T\boldsymbol{\mathcal{M}}\boldsymbol{v}} \geq \frac{\lambda_{\min}(\mathbf{M})}{\lambda_{\max}(\boldsymbol{\mathcal{M}})}$$

and similarly

$$\lambda_{\max}(\boldsymbol{\mathcal{M}}^{-\frac{1}{2}}\mathbf{M}\boldsymbol{\mathcal{M}}^{-\frac{1}{2}}) = \max_{\boldsymbol{v}\neq\mathbf{0}} \frac{\boldsymbol{v}^T\mathbf{M}\boldsymbol{v}}{\boldsymbol{v}^T\boldsymbol{\mathcal{M}}\boldsymbol{v}} \leq \frac{\lambda_{\max}(\mathbf{M})}{\lambda_{\min}(\boldsymbol{\mathcal{M}})}.$$

The thesis follows from Corollary (2), Corollary (3) and from (3.16). □

The previous result can be improved as follows.

Theorem 3. *Under Assumption 3, it holds*

$$\lim_{h\to 0} \kappa(\boldsymbol{\mathcal{M}}^{-\frac{1}{2}}\mathbf{M}\boldsymbol{\mathcal{M}}^{-\frac{1}{2}}) = 1. \tag{3.17}$$

Proof. Recalling Courant-Fischer theorem, it follows

$$\begin{aligned}\lambda_{\min}(\boldsymbol{\mathcal{M}}^{-\frac{1}{2}}\mathbf{M}\boldsymbol{\mathcal{M}}^{-\frac{1}{2}}) &= \min_{\boldsymbol{v}\neq\mathbf{0}} \frac{\boldsymbol{v}^T\mathbf{M}\boldsymbol{v}}{\boldsymbol{v}^T\boldsymbol{\mathcal{M}}\boldsymbol{v}} \\ &= \min_{\boldsymbol{w}\neq\mathbf{0}} \frac{\boldsymbol{w}^T\mathbf{D}^{-\frac{1}{2}}\widehat{\mathbf{D}}^{\frac{1}{2}}\mathbf{M}\widehat{\mathbf{D}}^{\frac{1}{2}}\mathbf{D}^{-\frac{1}{2}}\boldsymbol{w}}{\boldsymbol{w}^T\widehat{\mathbf{M}}\boldsymbol{w}} = \min_{\boldsymbol{w}\neq\mathbf{0}} \frac{\boldsymbol{w}^T\widetilde{\mathbf{M}}\boldsymbol{w}}{\boldsymbol{w}^T\widehat{\mathbf{M}}\boldsymbol{w}}\end{aligned} \tag{3.18}$$

and similarly

$$\lambda_{\max}(\boldsymbol{\mathcal{M}}^{-\frac{1}{2}}\mathbf{M}\boldsymbol{\mathcal{M}}^{-\frac{1}{2}}) = \max_{\boldsymbol{w}\neq\mathbf{0}} \frac{\boldsymbol{w}^T\widetilde{\mathbf{M}}\boldsymbol{w}}{\boldsymbol{w}^T\widehat{\mathbf{M}}\boldsymbol{w}}, \tag{3.19}$$

where we have defined $\widetilde{\mathbf{M}} := \mathbf{D}^{-\frac{1}{2}}\widehat{\mathbf{D}}^{\frac{1}{2}}\mathbf{M}\widehat{\mathbf{D}}^{\frac{1}{2}}\mathbf{D}^{-\frac{1}{2}}$.
The entries of the matrix $\widetilde{\mathbf{M}}$ can be rewritten as

$$[\widetilde{\mathbf{M}}]_{i,j} = [\mathbf{D}^{-\frac{1}{2}}\widehat{\mathbf{D}}^{\frac{1}{2}}\mathbf{M}\widehat{\mathbf{D}}^{\frac{1}{2}}\mathbf{D}^{-\frac{1}{2}}]_{i,j} = \frac{\|\widehat{B}_i\|_{L^2(\widehat{\Omega})}\|\widehat{B}_j\|_{L^2(\widehat{\Omega})}}{\|\sqrt{\omega}\widehat{B}_i\|_{L^2(\widehat{\Omega})}\|\sqrt{\omega}\widehat{B}_j\|_{L^2(\widehat{\Omega})}} \int_{\widehat{\Omega}} \omega\widehat{B}_i\widehat{B}_j.$$

We observe that for all $i \in \{1\dots, N_{\text{dof}}\}$, it holds

$$[\widetilde{\mathbf{M}}]_{i,i} = \frac{\|\widehat{B}_i\|^2_{L^2(\widehat{\Omega})}}{\|\sqrt{\omega}\widehat{B}_i\|^2_{L^2(\widehat{\Omega})}} \int_{\widehat{\Omega}} \omega\widehat{B}_i^2 = \|\widehat{B}_i\|^2_{L^2(\widehat{\Omega})} = [\widehat{\mathbf{M}}]_{i,i}.$$

Let us now consider $i, j \in \{1 \dots, N_{\text{dof}}\}$, with $i \neq j$. From equation (3.4), it follows

$$\omega(\boldsymbol{x}_1) \leq \omega(\boldsymbol{x}_2) + \mu(|\boldsymbol{x}_1 - \boldsymbol{x}_2|), \quad \forall\, \boldsymbol{x}_1, \boldsymbol{x}_2 \in \widehat{\Omega}.$$

As a consequence, by observing that $\operatorname{diam}\left(\operatorname{supp}(\widehat{B}_i) \cap \operatorname{supp}(\widehat{B}_j)\right) \leq h(p+1)\sqrt{d}$, for all $i, j = 1, \dots, N_{\text{dof}}$ with $i \neq j$, and denoting

$$\boldsymbol{x}_{ij} := \operatorname{argmin}\left\{\omega(\boldsymbol{x}) : \boldsymbol{x} \in \operatorname{supp}(\widehat{B}_i) \cap \operatorname{supp}(\widehat{B}_j)\right\},$$

we obtain

$$\omega(\boldsymbol{x}_{ij}) \int_{\widehat{\Omega}} \widehat{B}_i \widehat{B}_j \leq \int_{\widehat{\Omega}} \omega \widehat{B}_i \widehat{B}_j \leq \left(\omega(\boldsymbol{x}_{ij}) + \mu(h(p+1)\sqrt{d})\right) \int_{\widehat{\Omega}} \widehat{B}_i \widehat{B}_j. \tag{3.20}$$

Similarly, for all $i, j = 1, \dots, N_{\text{dof}}$ with $i \neq j$ and such that $\operatorname{supp}(\widehat{B}_i) \cap \operatorname{supp}(\widehat{B}_j) \neq \emptyset$, it holds

$$\begin{aligned} \omega(\boldsymbol{x}_{ij}) \|\widehat{B}_i\|_{L^2(\widehat{\Omega})} \|\widehat{B}_j\|_{L^2(\widehat{\Omega})} &\leq \|\sqrt{\omega}\widehat{B}_i\|_{L^2(\widehat{\Omega})} \|\sqrt{\omega}\widehat{B}_j\|_{L^2(\widehat{\Omega})} \\ &\leq \left(\omega(\boldsymbol{x}_{ij}) + \mu(h(p+1)\sqrt{d})\right) \|\widehat{B}_i\|_{L^2(\widehat{\Omega})} \|\widehat{B}_j\|_{L^2(\widehat{\Omega})}. \end{aligned} \tag{3.21}$$

Thus, by combining inequalities (3.20) and (3.21), we have the following bounds for the entries of $\widetilde{\mathbf{M}}$:

$$\begin{aligned} [\widetilde{\mathbf{M}}]_{i,j} =& \frac{\|\widehat{B}_i\|_{L^2(\widehat{\Omega})} \|\widehat{B}_j\|_{L^2(\widehat{\Omega})}}{\|\sqrt{\omega}\widehat{B}_i\|_{L^2(\widehat{\Omega})} \|\sqrt{\omega}\widehat{B}_j\|_{L^2(\widehat{\Omega})}} \int_{\widehat{\Omega}} \omega \widehat{B}_i \widehat{B}_j \\ \leq& \frac{\omega(\boldsymbol{x}_{ij}) + \mu(h(p+1)\sqrt{d})}{\omega(\boldsymbol{x}_{ij})} \int_{\widehat{\Omega}} \widehat{B}_i \widehat{B}_j, \\ [\widetilde{\mathbf{M}}]_{i,j} =& \frac{\|\widehat{B}_i\|_{L^2(\widehat{\Omega})} \|\widehat{B}_j\|_{L^2(\widehat{\Omega})}}{\|\sqrt{\omega}\widehat{B}_i\|_{L^2(\widehat{\Omega})} \|\sqrt{\omega}\widehat{B}_j\|_{L^2(\widehat{\Omega})}} \int_{\widehat{\Omega}} \omega \widehat{B}_i \widehat{B}_j \\ \geq& \frac{\omega(\boldsymbol{x}_{ij})}{\omega(x_{ij}) + \mu(h(p+1)\sqrt{d})} \int_{\widehat{\Omega}} \widehat{B}_i \widehat{B}_j. \end{aligned} \tag{3.22}$$

Having defined

$$\sigma := \frac{\mu(h(p+1)\sqrt{d})}{\omega_{\min}},$$

we observe that

$$\lim_{h \to 0} \sigma = 0 \tag{3.23}$$

and

$$\begin{aligned} \frac{\omega(\boldsymbol{x}_{ij}) + \mu(h(p+1)\sqrt{d})}{\omega(\boldsymbol{x}_{ij})} &= 1 + \frac{\mu(h(p+1)\sqrt{d})}{\omega(\boldsymbol{x}_{ij})} \leq 1 + \sigma, \\ \frac{\omega(\boldsymbol{x}_{ij})}{\omega(\boldsymbol{x}_{ij}) + \mu(h(p+1)\sqrt{d})} &= 1 - \frac{\mu(h(p+1)\sqrt{d})}{\omega(\boldsymbol{x}_{ij}) + \mu(h(p+1)\sqrt{d})} \geq 1 - \sigma. \end{aligned} \tag{3.24}$$

Collecting (3.2), (3.22) and (3.24), we can bound the entry-wise distance between the matrices $\widetilde{\mathbf{M}}$ and $\widehat{\mathbf{M}}$ as follows

$$-\sigma[\widehat{\mathbf{M}}]_{i,j} \leq [\widetilde{\mathbf{M}}]_{i,j} - [\widehat{\mathbf{M}}]_{i,j} \leq \sigma[\widehat{\mathbf{M}}]_{i,j}. \tag{3.25}$$

For all $\boldsymbol{w} \neq \boldsymbol{0}$, it holds

$$\frac{\boldsymbol{w}^T\widetilde{\mathbf{M}}\boldsymbol{w}}{\boldsymbol{w}^T\widehat{\mathbf{M}}\boldsymbol{w}} = \frac{\boldsymbol{w}^T(\widetilde{\mathbf{M}}+\widehat{\mathbf{M}}-\widehat{\mathbf{M}})\boldsymbol{w}}{\boldsymbol{w}^T\widehat{\mathbf{M}}\boldsymbol{w}} = 1 + \frac{\boldsymbol{w}^T(\widetilde{\mathbf{M}}-\widehat{\mathbf{M}})\boldsymbol{w}}{\boldsymbol{w}^T\widehat{\mathbf{M}}\boldsymbol{w}}. \tag{3.26}$$

Exploiting equation (3.25), it follows

$$\begin{aligned}
\sup_{\boldsymbol{w}\neq\boldsymbol{0}} \frac{\boldsymbol{w}^T(\widetilde{\mathbf{M}}-\widehat{\mathbf{M}})\boldsymbol{w}}{\boldsymbol{w}^T\widehat{\mathbf{M}}\boldsymbol{w}} &= \sup_{\boldsymbol{w}\neq\boldsymbol{0}} \frac{\sum_{i,j=1}^N \boldsymbol{w}_i\boldsymbol{w}_j([\widetilde{\mathbf{M}}]_{i,j}-[\widehat{\mathbf{M}}]_{i,j})}{\boldsymbol{w}^T\widehat{\mathbf{M}}\boldsymbol{w}} \\
&\leq \sup_{\boldsymbol{w}\neq\boldsymbol{0}} \frac{\sum_{i,j=1}^N |\boldsymbol{w}_i\boldsymbol{w}_j||[\widetilde{\mathbf{M}}]_{i,j}-[\widehat{\mathbf{M}}]_{i,j}|}{\boldsymbol{w}^T\widehat{\mathbf{M}}\boldsymbol{w}} \\
&\leq \sup_{\boldsymbol{w}\neq\boldsymbol{0}} \frac{\sigma\sum_{i,j=1}^N |\boldsymbol{w}_i\boldsymbol{w}_j|[\widehat{\mathbf{M}}]_{i,j}}{\boldsymbol{w}^T\widehat{\mathbf{M}}\boldsymbol{w}} \\
&\leq \sigma\frac{\sup_{\boldsymbol{w}\neq\boldsymbol{0}} \frac{|\boldsymbol{w}|^T[\widehat{\mathbf{M}}]|\boldsymbol{w}|}{\boldsymbol{w}^T\boldsymbol{w}}}{\inf_{\boldsymbol{w}\neq\boldsymbol{0}} \frac{\boldsymbol{w}^T[\widehat{\mathbf{M}}]\boldsymbol{w}}{\boldsymbol{w}^T\boldsymbol{w}}} \leq \sigma\frac{\lambda_{\max}(\widehat{\mathbf{M}})}{\lambda_{\min}(\widehat{\mathbf{M}})}
\end{aligned} \tag{3.27}$$

where, in the last step, we have used the property that

$$\sup \frac{|\boldsymbol{w}|^T\widehat{\mathbf{M}}|\boldsymbol{w}|}{\boldsymbol{w}^T\boldsymbol{w}} = \sup \frac{\boldsymbol{w}^T\widehat{\mathbf{M}}\boldsymbol{w}}{\boldsymbol{w}^T\boldsymbol{w}},$$

where indeed the last sup is obtained for a $\boldsymbol{w}$ with non-negative entries, due to the fact that $\widehat{\mathbf{M}}$ has non-negative entries. Similarly

$$\inf_{\boldsymbol{w}\neq\boldsymbol{0}} \frac{\boldsymbol{w}^T(\widetilde{\mathbf{M}}-\widehat{\mathbf{M}})\boldsymbol{w}}{\boldsymbol{w}^T\widehat{\mathbf{M}}\boldsymbol{w}} \geq \inf_{\boldsymbol{w}\neq\boldsymbol{0}} \frac{-\sigma\sum_{i,j=1}^N |\boldsymbol{w}_i\boldsymbol{w}_j|[\widehat{\mathbf{M}}]_{i,j}}{\boldsymbol{w}^T\widehat{\mathbf{M}}\boldsymbol{w}} \tag{3.28}$$

$$\geq -\sigma \sup_{\boldsymbol{w}\neq\boldsymbol{0}} \frac{\sum_{i,j=1}^N |\boldsymbol{w}_i\boldsymbol{w}_j|[\widehat{\mathbf{M}}]_{i,j}}{\boldsymbol{w}^T\widehat{\mathbf{M}}\boldsymbol{w}} \geq -\sigma\frac{\lambda_{\max}(\widehat{\mathbf{M}})}{\lambda_{\min}(\widehat{\mathbf{M}})}. \tag{3.29}$$

From (3.26), (3.27) and (3.28) we get

$$1 - \sigma\kappa(\widehat{\mathbf{M}}) \leq \frac{\boldsymbol{w}^T\widetilde{\mathbf{M}}\boldsymbol{w}}{\boldsymbol{w}^T\widehat{\mathbf{M}}\boldsymbol{w}} \leq 1 + \sigma\kappa(\widehat{\mathbf{M}}), \qquad \forall \boldsymbol{w} \neq \boldsymbol{0}. \tag{3.30}$$

Finally, combining Lemma 1, (3.16), (3.5), (3.18), (3.19), (3.23) and (3.30) we obtain

$$\lim_{h\to 0} \kappa(\boldsymbol{\mathcal{M}}^{-\frac{1}{2}}\mathbf{M}\boldsymbol{\mathcal{M}}^{-\frac{1}{2}}) \leq \lim_{h\to 0} \frac{1+C\sigma}{1-C\sigma} = 1.$$

□

Remark 2. *By applying Theorem 3 to the constant coefficient mass matrix* (3.2)*, if we assume that* $\boldsymbol{F} \in C^1([0,1]^d)$ *and that* $\det(D\boldsymbol{F}) > 0$ *for all* $\boldsymbol{x} \in [0,1]^d$*, then the preconditioned matrix fulfils* (3.17)*.*

Remark 3. *Theorem 3 states that if we define*

$$\mu(h) := \kappa(\boldsymbol{\mathcal{M}}^{-\frac{1}{2}}\mathbf{M}\boldsymbol{\mathcal{M}}^{-\frac{1}{2}}) - 1,$$

then $\mu(h) = o(1)$ *as* $h \to 0$*. Clearly, the function* μ *may depend on other parameters beside the mesh size, in particular it may depend on the spline degree* p *and the*

parametrization $\boldsymbol{F}$. However, in all problems considered in Section 3.4 our numerical tests indicate that μ is linear with respect to p and mildly depends on $\boldsymbol{F}$, even when the geometry parametrization is singular.

3.2 Mass preconditioner on multipatch domain

We now turn to examine a preconditioner for the mass matrix arising from multipatch domains, that is

$$[\mathbf{M}]_{i,j} = \int_{\Omega} B_i B_j, \qquad B_i, B_j \in \{B_l : l \in \mathcal{J}\}, \tag{3.31}$$

where Ω is formed by the union of patches $\Omega^{(r)}$, see definition (2.5). We combine the single patch preconditioner, introduced in (3.6), with an Additive Schwarz method. Let us define a family of local spaces

$$V_h^{(r)} := \operatorname{span}\left\{B_l : l \in \mathcal{J}^{(r)}\right\}, \qquad r = 1, \dots, N_{\text{patch}}, \tag{3.32}$$

with $\mathcal{J}^{(r)}$ defined as in Section 2.3. Therefore, $V_h^{(r)}$ is the subspace of V_h spanned by the B-splines basis function whose support intersect $\Omega^{(r)}$. Moreover, following the notation of [69], we consider restriction operators $R^{(r)} : V_h \to V_h^{(r)}$ with $r = 1, \dots, N_{\text{patch}}$, defined by

$$R^{(r)}\left(\sum_{l \in \mathcal{J}} u_l B_l\right) = \sum_{l \in \mathcal{J}^{(r)}} u_l B_l.$$

Their transpose, in the basis representation, ${R^{(r)}}^T : V_h^{(r)} \to V_h$ correspond, in our case, to the inclusion of $V_h^{(r)}$ into V_h. We denote with $\mathbf{R}^{(r)}$ and $\mathbf{R}^{(r)^T}$ the rectangular matrices associated to $R^{(r)}$ and ${R^{(r)}}^T$, respectively. From now on, given $u^{(r)} \in V_h^{(r)}$, we will denote by $\boldsymbol{u}^{(r)}$ the vector of its coordinates with respect to the basis $\{B_l : l \in \mathcal{J}^{(r)}\}$ and define the family of bilinear forms $a^{(r)} : V_h^{(r)} \times V_h^{(r)} \to \mathbb{R}$, for $r = 1, \dots, N_{\text{patch}}$, as

$$a^{(r)}(u^{(r)}, v^{(r)}) := {\boldsymbol{v}^{(r)}}^T \boldsymbol{\mathcal{M}}^{(r)} \boldsymbol{u}^{(r)}, \qquad u^{(r)}, v^{(r)} \in V_h^{(r)}, \tag{3.33}$$

with

$$\boldsymbol{\mathcal{M}}^{(r)} := {\mathbf{D}^{(r)}}^{\frac{1}{2}} {\widehat{\mathbf{D}}^{(r)}}^{-\frac{1}{2}} \widehat{\mathbf{M}}^{(r)} {\widehat{\mathbf{D}}^{(r)}}^{-\frac{1}{2}} {\mathbf{D}^{(r)}}^{\frac{1}{2}}, \tag{3.34}$$

where we have set

$$[\widehat{\mathbf{M}}^{(r)}]_{i,j} := \int_{\widehat{\Omega}} \widehat{B}_i^{(r)} \widehat{B}_j^{(r)}, \quad \widehat{\mathbf{D}}^{(r)} := \operatorname{diag}\left(\widehat{\mathbf{M}}^{(r)}\right), \quad \mathbf{D}^{(r)} := \operatorname{diag}\left(\mathbf{M}^{(r)}\right), \tag{3.35}$$

with the assumption that the basis functions $\{\widehat{B}_i^{(r)}\}_{i=1}^{N_{\text{dof}}^{(r)}}$ and $\{B_i^{(r)}\}_{i=1}^{N_{\text{dof}}^{(r)}}$ are ordered as described at the end of Section 2.3. We underline that the bilinear forms $\{a^{(r)}\}$ are symmetric and positive definite. The Additive Schwarz Preconditioner (inverse) is defined as

$$\boldsymbol{\mathcal{M}}_{\text{ad}}^{-1} := \sum_{r=1}^{N_{\text{patch}}} \mathbf{R}^{(r)^T} {\boldsymbol{\mathcal{M}}^{(r)}}^{-1} \mathbf{R}^{(r)}. \tag{3.36}$$

The following Lemma follows straightforwardly from [69, Theorem 2.7] and provides a bound on the condition number of the multipatch mass matrix (3.31) preconditioned by (3.36).

Lemma 2. *Let the following three hypothesis be satisfied:*

- *(*Stable Decomposition*) There exists a constant $C_{\mathrm{SD}} > 0$, such that every $u \in V_h$ admits a decomposition*

$$u = \sum_{r=1}^{N_{\mathrm{patch}}} u^{(r)}, \qquad \text{with } u^{(r)} \in V_h^{(r)},$$

that satisfies

$$\sum_{r=1}^{N_{\mathrm{patch}}} a^{(r)}(u^{(r)}, u^{(r)}) \leq C_{\mathrm{SD}} \|u\|^2_{L^2(\Omega)}.$$

- *(*Strengthened Cauchy-Schwarz Inequalities*) There exist constants $0 \leq \epsilon_{rs} \leq 1$, for $1 \leq r, s \leq N_{\mathrm{patch}}$, such that*

$$|(u^{(r)}, u^{(s)})_{L^2(\Omega)}| \leq \epsilon_{rs} \|u^{(r)}\|_{L^2(\Omega)} \|u^{(s)}\|_{L^2(\Omega)},$$

for $u^{(r)} \in V_h^{(r)}$ and $u^{(s)} \in V_h^{(s)}$.

- *(*Local Stability*) There exists $C_{\mathrm{LS}} > 0$, such that for all $r = 1, \ldots, N_{\mathrm{patch}}$,*

$$\|u^{(r)}\|^2_{L^2(\Omega)} \leq C_{\mathrm{LS}} a^{(r)}(u^{(r)}, u^{(r)}), \qquad \forall\, u^{(r)} \in V_h^{(r)}.$$

Then the condition number of the preconditioned operator satisfies

$$\kappa\left(\boldsymbol{\mathcal{M}}_{ad}^{-\frac{1}{2}} \mathbf{M} \boldsymbol{\mathcal{M}}_{ad}^{-\frac{1}{2}}\right) \leq C_{\mathrm{SD}} C_{\mathrm{LS}} \rho(\mathcal{E}),$$

where $\rho(\mathcal{E})$ represents the spectral radius of the matrix $\mathcal{E} = \{\epsilon_{rs}\}$.

Assumption 4. *Let $\boldsymbol{F}^{(r)} \in C^1([0,1]^d)$ and assume that for all $\boldsymbol{x} \in [0,1]^d$, $\det(D\boldsymbol{F}^{(r)}) > 0$, for all $r = 1, \ldots, N_{\mathrm{patch}}$.*

We are now able to present the main result of this section.

Theorem 4. *Under Assumption 4, there exists a constant C, independent of h and N_{adj}, verifying*

$$\kappa\left(\boldsymbol{\mathcal{M}}_{ad}^{-\frac{1}{2}} \mathbf{M} \boldsymbol{\mathcal{M}}_{ad}^{-\frac{1}{2}}\right) \leq C N_{\mathrm{adj}}^2,$$

where N_{adj}, defined in (2.8), denotes the maximum number of adjacent patches.

Proof. We show that the hypothesis of Lemma 2 hold with C_{SD} and C_{LS} independent of h and $\rho(\mathcal{E}) \leq N_{\mathrm{adj}}$.

Part I: Stable Decomposition. The argument we use is similar to the one presented in [73, Lemma 4.1]. Given $u \in V_h$, with

$$u = \sum_{l \in \mathcal{J}} u_l B_l,$$

we define $u^{(r)} \in V_h^{(r)}$ as

$$u^{(r)} := \sum_{l \in \mathcal{J}^{(r)}} \frac{u_l}{n_l} B_l, \qquad\qquad r = 1, \dots, N_{\text{patch}},$$

where n_l is defined in (2.7). It is straightforward to see that

$$\sum_{r=1}^{N_{\text{patch}}} u^{(r)} = u.$$

Recalling definitions (3.33), (3.34) and (3.35) and introducing

$$[\mathbf{M}^{(r)}]_{i,j} := \int_{\Omega^{(r)}} B_i^{(r)} B_j^{(r)},$$

we have

$$\begin{aligned}
\sum_{r=1}^{N_{\text{patch}}} a^{(r)}(u^{(r)}, u^{(r)}) &= \sum_{r=1}^{N_{\text{patch}}} \boldsymbol{u}^{(r)^T} \boldsymbol{\mathcal{M}}^{(r)} \boldsymbol{u}^{(r)} \\
&= \sum_{r=1}^{N_{\text{patch}}} \frac{\boldsymbol{u}^{(r)^T} \boldsymbol{\mathcal{M}}^{(r)} \boldsymbol{u}^{(r)}}{\boldsymbol{u}^{(r)^T} \mathbf{M}^{(r)} \boldsymbol{u}^{(r)}} \boldsymbol{u}^{(r)^T} \mathbf{M}^{(r)} \boldsymbol{u}^{(r)} \\
&\leq \sum_{r=1}^{N_{\text{patch}}} \frac{\boldsymbol{u}^{(r)^T} \boldsymbol{\mathcal{M}}^{(r)} \boldsymbol{u}^{(r)}}{\boldsymbol{u}^{(r)^T} \mathbf{M}^{(r)} \boldsymbol{u}^{(r)}} \| u^{(r)}{}_{|\Omega^{(r)}} \|^2_{L^2(\Omega^{(r)})} \\
&\leq \left(\max_{r=1,\dots,N_{\text{patch}}} \frac{\boldsymbol{u}^{(r)^T} \boldsymbol{\mathcal{M}}^{(r)} \boldsymbol{u}^{(r)}}{\boldsymbol{u}^{(r)^T} \mathbf{M}^{(r)} \boldsymbol{u}^{(r)}} \right) \sum_{r=1}^{N_{\text{patch}}} \| u^{(r)}{}_{|\Omega^{(r)}} \|^2_{L^2(\Omega^{(r)})}.
\end{aligned} \tag{3.37}$$

Combining Corollary 2 and Corollary 3, we obtain a constant $C_{\max}$, independent of h, such that

$$\frac{\boldsymbol{u}^{(r)^T} \boldsymbol{\mathcal{M}}^{(r)} \boldsymbol{u}^{(r)}}{\boldsymbol{u}^{(r)^T} \mathbf{M}^{(r)} \boldsymbol{u}^{(r)}} \leq C_{\max}, \qquad \forall u^{(r)} \in V_h^{(r)}, \, \forall r = 1, \dots, N_{\text{patch}}. \tag{3.38}$$

By observing that $n_l \geq 1$, for all l, it follows

$$\left| \frac{u_l}{n_l} \right| \leq |u_l|$$

and thus

$$\left| \varphi_{\mathbf{i}}(u^{(r)}_{|\Omega^{(r)}}) \right| \leq \left| \varphi_{\mathbf{i}}(u_{|\Omega^{(r)}}) \right|, \qquad\qquad \forall \mathbf{i} \in \mathbf{I}^{(r)}, \tag{3.39}$$

where $\{\varphi_{\mathbf{i}}\}_{\mathbf{i} \in \mathbf{I}^{(r)}}$ denotes the dual basis introduced in Corollary (1), relative to the isogeometric space defined on the patch $\Omega^{(r)}$. Using Corollary 1, (3.39) and (3.10) in the patch $\Omega^{(r)}$ and the adjacent ones $\Omega^{(s)}$, there exist constants C_1, C_2, C_3, independent

of h and N_{adj}, such that

$$\begin{aligned}\|u^{(r)}\|^2_{L^2(\Omega^{(r)})} &\leq C_1 h^d \sum_{\mathbf{i}\in\mathbf{I}^{(r)}} \varphi_{\mathbf{i}}(u^{(r)})^2 \leq C_1 h^d \sum_{\mathbf{i}\in\mathbf{I}^{(r)}} \varphi_{\mathbf{i}}(u_{|\Omega^{(r)}})^2 \\ &\leq C_2 \sum_{\mathbf{i}\in\mathbf{I}^{(r)}} \|u_{|\Omega^{(r)}}\|^2_{L^2(\boldsymbol{F}^{(r)}(Q'_{\mathbf{i}}))} \leq C_3 \|u\|^2_{L^2(\Omega^{(r)})}\end{aligned}$$

Finally, summing over all $r \in \{1, \dots, N_{\text{patch}}\}$, it holds

$$\sum_{r=1}^{N_{\text{patch}}} \|u^{(r)}\|^2_{L^2(\Omega^{(r)})} \leq C_3 \|u\|^2_{L^2(\Omega)}. \tag{3.40}$$

Combining (3.37), (3.38) and (3.40), we obtain

$$C_{\text{SD}} \leq C_3 C_{\max}. \tag{3.41}$$

Part II: Strengthened Cauchy-Schwarz Inequalities. Cauchy-Schwarz inequality, assures us that $\epsilon_{rs} \leq 1$, for all $1 \leq r, s \leq N_{\text{patch}}$. Furthermore, for each $r \in \{1, \dots N_{\text{patch}}\}$, there are at most N_{adj} indices $s \in \{1, \dots N_{\text{patch}}\}$ such that there exists two basis functions $B_{l_1} \in \{B_l : l \in \mathcal{J}^{(r)}\}$ and $B_{l_2} \in \{B_l : l \in \mathcal{J}^{(s)}\}$ with $\text{supp}(B_{l_1}) \cap \text{supp}(B_{l_2}) \neq \emptyset$. As a consequence, in every row of the matrix $\mathcal{E} = \{\epsilon_{rs}\}$ there are at most N_{adj} non-zero entries. Combining these facts, we can conclude that the spectral radius of $\mathcal{E}$ satisfies:

$$\rho(\mathcal{E}) \leq N_{\text{adj}}. \tag{3.42}$$

Part III: Local Stability. Using (3.10) in the patch $\Omega^{(r)}$ and the adjacent ones $\Omega^{(s)}$, there exists a constant C, independent of h and N_{adj}, such that

$$\begin{aligned}\|u^{(r)}\|^2_{L^2(\Omega)} &= \sum_{s\,:\overline{\Omega^{(r)}}\cap\overline{\Omega^{(s)}}\neq\emptyset} \|u^{(r)}_{|\Omega^{(s)}}\|^2_{L^2(\Omega^{(s)})} \\ &\leq C N_{\text{adj}} h^d \sum_{\mathbf{i}\in\mathbf{I}^{(r)}} (u^{(r)}_{\mathbf{i}})^2 = C N_{\text{adj}} h^d (\boldsymbol{u}^{(r)})^T \boldsymbol{u}^{(r)}.\end{aligned}$$

It holds

$$\begin{aligned}h^d (\boldsymbol{u}^{(r)})^T \boldsymbol{u}^{(r)} &= h^d \frac{(\boldsymbol{u}^{(r)})^T (\boldsymbol{u}^{(r)})}{(\boldsymbol{u}^{(r)})^T \boldsymbol{\mathcal{M}}^{(r)} \boldsymbol{u}^{(r)}} (\boldsymbol{u}^{(r)})^T \boldsymbol{\mathcal{M}}^{(r)} \boldsymbol{u}^{(r)} \\ &\leq \frac{h^d}{\lambda_{\min}(\boldsymbol{\mathcal{M}}^{(r)})} a^{(r)}(u^{(r)}, u^{(r)}).\end{aligned} \tag{3.43}$$

Using (3.43) and Corollary 3, finally yields local stability:

$$\|u^{(r)}\|^2_{L^2(\Omega)} \leq C N_{\text{adj}} a^{(r)}(u^{(r)}, u^{(r)}), \tag{3.44}$$

with another constant C, independent of h and N_{adj}.

Finally, by applying Lemma 2 with the estimates provided in (3.41), (3.42) and (3.44), we obtain that there exists a constant C, independent of h, verifying

$$\kappa\left(\boldsymbol{\mathcal{M}}_{\text{ad}}^{-\frac{1}{2}} \mathbf{M} \boldsymbol{\mathcal{M}}_{\text{ad}}^{-\frac{1}{2}}\right) \leq C N_{\text{adj}}^2.$$

□

3.3 Preconditioners application and cost

The mass matrices and the preconditioners introduced in this paper are symmetric and positive definite. We then adopt the Preconditioned Conjugate Gradient method (PCG) to solve the associated linear systems. For evaluating the computational cost of PCG, we recall that for each iteration, the two most expensive steps are: the solution of a linear system associated to the preconditioner and the computation of the residual, through a matrix-vector with $\mathbf{M}$. We recall that all the univariate matrices have dimension m. Then, the single patch mass matrix has dimension $N_{\text{dof}} = m^d$, while for the multipatch one we have $N_{\text{dof}} \approx N_{\text{patch}} m^d$.

3.3.1 Single patch preconditioner

The application of the single patch preconditioner is the solution of a linear system associated to

$$\boldsymbol{\mathcal{M}} = \mathbf{D}^{\frac{1}{2}} \widehat{\mathbf{D}}^{-\frac{1}{2}} \widehat{\mathbf{M}} \widehat{\mathbf{D}}^{-\frac{1}{2}} \mathbf{D}^{\frac{1}{2}}.$$

Thanks to (2.11), it holds

$$\widehat{\mathbf{D}} = \operatorname{diag}(\widehat{\mathbf{M}}_d \otimes \cdots \otimes \widehat{\mathbf{M}}_1) = \widehat{\mathbf{D}}_d \otimes \cdots \otimes \widehat{\mathbf{D}}_1,$$

where we have set $\widehat{\mathbf{D}}_i = \operatorname{diag}(\widehat{\mathbf{M}}_i)$, for $i = 1, \dots, d$, and

$$\widehat{\mathbf{D}}^{-\frac{1}{2}} \widehat{\mathbf{M}} \widehat{\mathbf{D}}^{-\frac{1}{2}} = \widehat{\mathbf{D}}_d^{-\frac{1}{2}} \widehat{\mathbf{M}}_d \widehat{\mathbf{D}}_d^{-\frac{1}{2}} \otimes \cdots \otimes \widehat{\mathbf{D}}_1^{-\frac{1}{2}} \widehat{\mathbf{M}}_1 \widehat{\mathbf{D}}_1^{-\frac{1}{2}}.$$

By exploiting (2.12), the inverse of $\boldsymbol{\mathcal{M}}$ may be expressed as

$$\begin{aligned} \boldsymbol{\mathcal{M}}^{-1} &= \left(\mathbf{D}^{\frac{1}{2}} \widehat{\mathbf{D}}^{-\frac{1}{2}} \widehat{\mathbf{M}} \widehat{\mathbf{D}}^{-\frac{1}{2}} \mathbf{D}^{\frac{1}{2}} \right)^{-1} \\ &= \mathbf{D}^{-\frac{1}{2}} \left(\widehat{\mathbf{D}}_d^{-\frac{1}{2}} \widehat{\mathbf{M}}_d \widehat{\mathbf{D}}_d^{-\frac{1}{2}} \right)^{-1} \otimes \cdots \otimes \left(\widehat{\mathbf{D}}_1^{-\frac{1}{2}} \widehat{\mathbf{M}}_1 \widehat{\mathbf{D}}_1^{-\frac{1}{2}} \right)^{-1} \mathbf{D}^{-\frac{1}{2}}. \end{aligned}$$

Therefore, the solution of a linear system associated to $\boldsymbol{\mathcal{M}}$ can be summarized as follows.

Algorithm 1 Single patch

1: Assemble the matrices $\widehat{\mathbf{D}}_i^{-\frac{1}{2}} \widehat{\mathbf{M}}_i \widehat{\mathbf{D}}_i^{-\frac{1}{2}}$, for $i = 1, \dots, d$.
2: Compute the diagonal scaling $\widetilde{\boldsymbol{z}} = \mathbf{D}^{-\frac{1}{2}} \boldsymbol{z}$.
3: Solve the linear system $\left(\widehat{\mathbf{D}}_d^{-\frac{1}{2}} \widehat{\mathbf{M}}_d \widehat{\mathbf{D}}_d^{-\frac{1}{2}} \otimes \cdots \otimes \widehat{\mathbf{D}}_1^{-\frac{1}{2}} \widehat{\mathbf{M}}_1 \widehat{\mathbf{D}}_1^{-\frac{1}{2}} \right) \widetilde{\boldsymbol{y}} = \widetilde{\boldsymbol{z}}$.
4: Compute the diagonal scaling $\boldsymbol{y} = \mathbf{D}^{-\frac{1}{2}} \widetilde{\boldsymbol{y}}$.

Step 1 represents the preconditioner setup. The matrices $\widehat{\mathbf{D}}_i^{-\frac{1}{2}} \widehat{\mathbf{M}}_i \widehat{\mathbf{D}}_i^{-\frac{1}{2}}$ need to be constructed only once, before starting the PCG solver. The overall cost of this step is $C(p)dm$ FLOPs, where $C(p)$ denotes a constant that depends on p and depends on how the matrices $\widehat{\mathbf{M}}_i$ are computed: Gauss quadrature is the least efficient approach and in such a case $C(p) = O(p^3)$. However this cost can be considered negligible in practice (for examples, in all the tests we present in Section 3.4, where $p \ll m$), since

$m = N_{\text{dof}}^{1/d}$ and Steps 2-4 have a cost which is proportional to N_{dof}. Furthermore, Steps 2-4 need to be performed at each iteration. Both Steps 2 and 4 consist in the product of a diagonal matrix by a vector, thus their cost is $2N_{\text{dof}}$ FLOPs. Thanks to (2.13) and recalling that univariate mass matrices are symmetric banded matrices with bandwidth p, Step 3 costs roughly $2d(2p+1)N_{\text{dof}} = O(pN_{\text{dof}})$ FLOPs. To sum up, we get that the application of Algorithm 1 requires roughly $2\left(d(2p+1)+1\right)N_{\text{dof}} = O(pN_{\text{dof}})$ FLOPs. We emphasize that the cost of our preconditioner is proportional to N_{dof}, and depends linearly with respect to p. Moreover, this cost is even smaller than that required for the residual computation PCG (or any iterative solver). Indeed, having in mind that the computational cost of a matrix-vector product is twice the number of non-zero entries of that matrix and that for the isogeometric mass matrix this number is at most $(2p+1)^d N_{\text{dof}}$, it follows that the residual computation requires $2(2p+1)^d N_{\text{dof}} = O(p^d N_{\text{dof}})$ FLOPs.

3.3.2 Multipatch preconditioner

The application of $\boldsymbol{\mathcal{M}}_{\text{ad}}^{-1}$, provided in (3.36), involves, for $r \in \{1, \dots, N_{\text{patch}}\}$, the application of the operators $R^{(r)}$ and $R^{(r)^T}$, whose cost is negligible, and the application of $\left(\boldsymbol{\mathcal{M}}^{(r)}\right)^{-1}$, whose cost has been analyzed in the previous section. In conclusion, the cost of application of $\boldsymbol{\mathcal{M}}_{\text{ad}}^{-1}$ is $O(p\sum_{r=1}^{N_{\text{patch}}} N_{\text{dof}}^{(r)}) = O(pN_{\text{dof}})$.

3.4 Numerical Tests

In this section we show the performance of the preconditioners presented in this paper. In our simulations, we consider only sequential executions and we force the use of a single computational thread in a Intel Core i7-5820K processor, running at 3.30 GHz and with 64 GB of RAM. All the tests are performed with Matlab R2015a and GeoPDEs toolbox [70]. The linear system is solved by PCG, with tolerance equal to 10^{-8} and with the null vector as initial guess. We denote by n_{sub} the number of subdivisions, which are the same in each parametric direction and in each patch. Moreover, we underline that we only consider splines of maximal regularity. The symbol "*" denotes the impossibility of formation of the matrix $\mathbf{M}$, due to memory requirements.

For assessing the performance of the preconditioners, we consider the problem of finding the L^2-projection of a given function f, on different domains, see Figures 3.1 and 3.2. For bidimensional problems, the given function is $f(x,y) = \cos(\pi x)\cos(\pi y)$, while for the tridimensional ones, we have set $f(x,y,z) = \cos(\pi x)\cos(\pi y)\cos(\pi z)$.

3.4.1 Single Patch domains

As examples of regularly parametrized single patch domains, we consider a bidimensional kite and a tridimensional blade (see Figures 3.1a and 3.2a). For the kite domain, we compute the condition number of the unpreconditioned and preconditioned mass matrix for different values of h and p and report them in Tables 3.1 and 3.2, respectively. By comparing these numbers, we can see that the condition number is dramatically reduced by our preconditioning strategy. In particular, as predicted by Theorem 3, the condition number of preconditioned matrices converges to 1 as the mesh-size h goes to 0. Tables 3.3 and 3.4 show the number of iterations and computation time spent by PCG for the kite and the blade domain, respectively. We

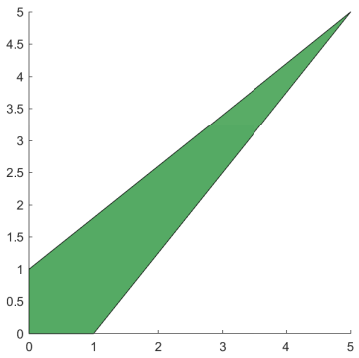

(A) Kite.

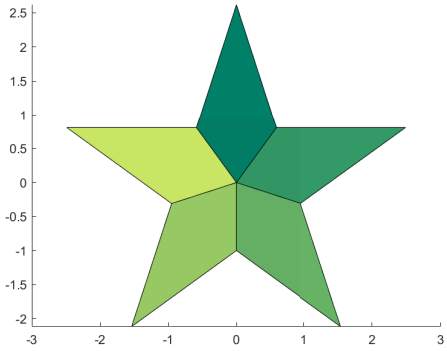

(B) Multipatch Star.

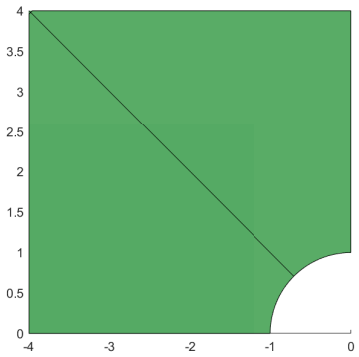

(C) Holed plate.

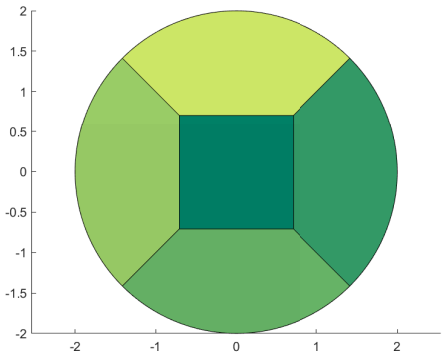

(D) Multipatch Disc.

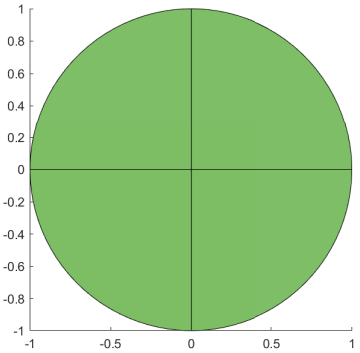

(E) Disc with one singularity.

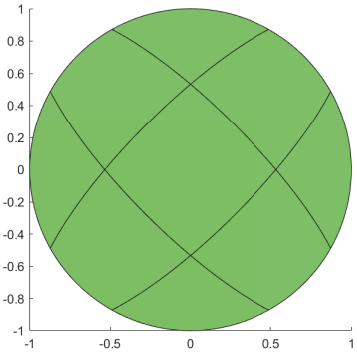

(F) Disc with four singularities.

FIGURE 3.1: Bidimensional domains.

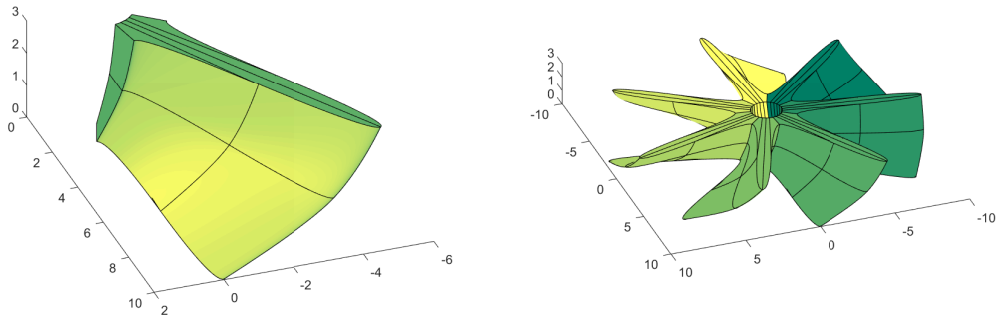

(A) Blade. (B) Multipatch Fan.

FIGURE 3.2: Tridimensional domains.

n_{sub}	$p=2$	$p=3$	$p=4$	$p=5$	$p=6$
16	$5.540 \cdot 10^2$	$2.980 \cdot 10^3$	$1.673 \cdot 10^4$	$9.892 \cdot 10^4$	$6.106 \cdot 10^5$
32	$7.040 \cdot 10^2$	$4.063 \cdot 10^3$	$2.435 \cdot 10^4$	$1.523 \cdot 10^5$	$9.853 \cdot 10^5$
64	$8.150 \cdot 10^2$	$4.929 \cdot 10^3$	$3.082 \cdot 10^4$	$2.002 \cdot 10^5$	$1.340 \cdot 10^6$
128	$8.900 \cdot 10^2$	$5.536 \cdot 10^3$	$3.555 \cdot 10^4$	$2.366 \cdot 10^5$	$1.617 \cdot 10^6$

TABLE 3.1: Condition number of mass matrix for kite.

emphasize that the number of iterations is always very low and even decreases when h is reduced.

The case of singularly parametrized domains is beyond the theory of Section 3.1 (Assumption 3 does not hold). Nevertheless, we test numerically this situation on three examples: a holed plate with a singular point in the top left vertex (see Figure 3.1c); a disc with a singularity in the center (Figure 3.1e) and a disc with four singularities on the boundary (Figure 3.1f). In all the three examples the condition number is always close to 1 and, even though it does not converge to 1 as in the non-singular case, it does not grow as h goes to 0. Accordingly, the number of PCG iterations is very low (see Tables 3.6, 3.8 and 3.10).

We are interested in studying the dependence on p of the condition number of the preconditioned system. For this purpose, we follow Remark 3 and define $\mu := \kappa\left(\boldsymbol{\mathcal{M}}^{-\frac{1}{2}}\mathbf{M}\boldsymbol{\mathcal{M}}^{-\frac{1}{2}}\right) - 1$. For all the problems considered so far, the numerical results show that μ grows roughly linearly with respect to p. This phenomenon can be clearly seen in Figure 3.3a. The crucial consequence of this fact is that the number of PCG iterations is almost independent of p. This is confirmed by the results already shown in Tables 3.3, 3.4, 3.6, 3.8 and 3.10.

We now compare our preconditioner $\boldsymbol{\mathcal{M}}$ as defined in (3.6) with the preconditioner

n_{sub}	$p=2$	$p=3$	$p=4$	$p=5$	$p=6$
16	1.056	1.077	1.103	1.129	1.157
32	1.034	1.047	1.062	1.078	1.094
64	1.019	1.027	1.035	1.045	1.054
128	1.010	1.015	1.019	1.024	1.030

TABLE 3.2: Condition number of preconditioned mass matrix for kite.

n_{sub}	$p = 2$	$p = 3$	$p = 4$	$p = 5$	$p = 6$
16	4 / 0.00134	4 / 0.00141	4 / 0.00152	4 / 0.00167	4 / 0.00184
32	3 / 0.00191	3 / 0.00203	3 / 0.00225	4 / 0.00316	4 / 0.00352
64	3 / 0.00465	3 / 0.00525	3 / 0.00578	3 / 0.00675	3 / 0.00812
128	3 / 0.0155	3 / 0.0181	3 / 0.0213	3 / 0.0255	3 / 0.0310

TABLE 3.3: Iterations and time spent by PCG for kite.

n_{sub}	$p = 2$	$p = 3$	$p = 4$	$p = 5$	$p = 6$
16	6 / 0.0137	6 / 0.0315	6 / 0.0654	6 / 0.137	7 / 0.274
32	5 / 0.0821	5 / 0.154	5 / 0.299	5 / 0.608	6 / 1.27
64	4 / 0.499	4 / 1.01	4 / 1.75	4 / 3.49	4 / 6.37

TABLE 3.4: Iterations and time spent by PCG for blade.

n_{sub}	$p = 2$	$p = 3$	$p = 4$	$p = 5$	$p = 6$
16	1.692	1.861	2.018	2.173	2.330
32	1.696	1.866	2.024	2.177	2.330
64	1.699	1.869	2.028	2.182	2.334
128	1.700	1.871	2.029	2.184	2.336

TABLE 3.5: Condition number of preconditioned mass matrix for holed plate.

n_{sub}	$p = 2$	$p = 3$	$p = 4$	$p = 5$	$p = 6$
16	6 / 0.00181	7 / 0.00227	7 / 0.00248	7 / 0.00275	7 / 0.00311
32	6 / 0.00335	6 / 0.00370	6 / 0.00414	6 / 0.00466	6 / 0.00528
64	5 / 0.00734	6 / 0.00968	6 / 0.0108	6 / 0.0124	6 / 0.0151
128	5 / 0.0250	5 / 0.0287	5 / 0.0343	5 / 0.0405	5 / 0.0488

TABLE 3.6: Iterations and time spent by PCG for holed plate.

n_{sub}	$p = 2$	$p = 3$	$p = 4$	$p = 5$	$p = 6$
16	1.093	1.170	1.249	1.323	1.395
32	1.090	1.159	1.230	1.305	1.381
64	1.082	1.148	1.212	1.276	1.339
128	1.077	1.140	1.200	1.259	1.317

TABLE 3.7: Condition number of preconditioned mass matrix for disc with one singularity.

n_{sub}	$p = 2$	$p = 3$	$p = 4$	$p = 5$	$p = 6$
16	5 / 0.00156	5 / 0.00172	5 / 0.00192	6 / 0.00259	5 / 0.00259
32	4 / 0.00198	5 / 0.00274	5 / 0.00305	5 / 0.00355	5 / 0.00416
64	4 / 0.00435	4 / 0.00498	5 / 0.00693	5 / 0.00815	5 / 0.00951
128	4 / 0.0125	4 / 0.0146	4 / 0.0175	4 / 0.0220	5 / 0.0330

TABLE 3.8: Iterations and time spent by PCG for disc with one singularity.

n_{sub}	$p=2$	$p=3$	$p=4$	$p=5$	$p=6$
16	1.167	1.252	1.350	1.459	1.575
32	1.161	1.241	1.341	1.450	1.564
64	1.158	1.237	1.338	1.447	1.559
128	1.156	1.236	1.336	1.444	1.556

TABLE 3.9: Condition number of preconditioned mass matrix for disc with four singularities.

n_{sub}	$p=2$	$p=3$	$p=4$	$p=5$	$p=6$
16	5 / 0.00157	5 / 0.00172	6 / 0.00203	6 / 0.00229	6 / 0.00245
32	5 / 0.00282	5 / 0.00310	5 / 0.00329	5 / 0.00368	6 / 0.00478
64	4 / 0.00575	4 / 0.00648	5 / 0.00858	5 / 0.00983	5 / 0.0117
128	4 / 0.0191	4 / 0.0223	4 / 0.0264	4 / 0.0315	4 / 0.0378

TABLE 3.10: Iterations and time spent by PCG for disc with four singularities.

proposed by Chan and Evans in [16], that we denote by $\boldsymbol{\mathcal{M}}_{CE}$. This preconditioner has some similarity with the one we propose and, moreover, is one of the best performing to our knowledge. The application of $\boldsymbol{\mathcal{M}}_{CE}$ is, by definition, a multiplication by

$$\boldsymbol{\mathcal{M}}_{CE}^{-1} = \widehat{\mathbf{M}}^{-1}\mathbf{M}_{\det(D\boldsymbol{F})^{-1}}\widehat{\mathbf{M}}^{-1},$$

where $\mathbf{M}_{\det(D\boldsymbol{F})^{-1}}$ is a weighted mass matrix as (3.3) with $\omega = \det(D\boldsymbol{F})^{-1}$. Table 3.11 reports on the condition number of the preconditioned mass matrix, by $\boldsymbol{\mathcal{M}}$ and $\boldsymbol{\mathcal{M}}_{CE}$. For a more in-depth analysis of the efficiency of the two methods, we need to consider that one iteration of $\boldsymbol{\mathcal{M}}_{CE}$-PCG costs roughly as two iterations of $\boldsymbol{\mathcal{M}}$-PCG. This is because in the latter case the cost is concentrated in the matrix-vector product with $\mathbf{M}$ and the solution of a system with $\widehat{\mathbf{M}}$, while in the former case two such products (one with $\mathbf{M}$ and one with $\mathbf{M}_{\det(D\boldsymbol{F})^{-1}}$) and two such solutions are needed.

It is well-known that when Conjugate Gradient (CG) is used to solve a linear system $\mathbf{A}x = \mathbf{b}$, with $\mathbf{A}$ symmetric and positive definite, it holds

$$\frac{\|\mathbf{e}_k\|_{\mathbf{A}}}{\|\mathbf{e}_0\|_{\mathbf{A}}} \leq 2\left(\frac{\sqrt{\kappa(\mathbf{A})}-1}{\sqrt{\kappa(\mathbf{A})}+1}\right)^k, \qquad k = 1, 2, \ldots,$$

where $\mathbf{e}_k$ is the error relative to the $k-$th iteration, and $\|\mathbf{e}_k\|_{\mathbf{A}} := \sqrt{\mathbf{e}_k^T\mathbf{A}\mathbf{e}_k}$ for $k \geq 0$. Thus, at each iteration of CG , the upper bound on the relative error is reduced by a factor

$$q(\mathbf{A}) := \frac{\sqrt{\kappa(\mathbf{A})}-1}{\sqrt{\kappa(\mathbf{A})}+1} < 1.$$

In our case, $\mathbf{A}$ is the preconditioned mass matrix. Then, we use this principle in order to compare the effectiveness of $\boldsymbol{\mathcal{M}}$ and $\boldsymbol{\mathcal{M}}_{CE}$. Since one iteration of $\boldsymbol{\mathcal{M}}_{CE}$-PCG costs twice as one iterations of $\boldsymbol{\mathcal{M}}$-PCG, we compare $q(\boldsymbol{\mathcal{M}}_{CE}^{-\frac{1}{2}}\mathbf{M}\boldsymbol{\mathcal{M}}_{CE}^{-\frac{1}{2}})$ with the factor by which the error bound is reduced after 2 iterations of $\boldsymbol{\mathcal{M}}$-PCG, which is $q(\boldsymbol{\mathcal{M}}^{-\frac{1}{2}}\mathbf{M}\boldsymbol{\mathcal{M}}^{-\frac{1}{2}})^2$. The results are shown in Table 3.12. In all cases, the bound-reducing factor is significantly small, confirming that both approaches lead to fast

domain	$\kappa(\boldsymbol{\mathcal{M}}_{CE}^{-\frac{1}{2}}\mathbf{M}\boldsymbol{\mathcal{M}}_{CE}^{-\frac{1}{2}})$	$\kappa(\boldsymbol{\mathcal{M}}^{-\frac{1}{2}}\mathbf{M}\boldsymbol{\mathcal{M}}^{-\frac{1}{2}})$
kite	1.049	1.157
blade	1.202	1.538
holed plate	1.051	1.216
disc (e)	3.652	1.395
disc (f)	3.185	1.575

TABLE 3.11: Condition number of preconditioned mass matrix for $n_{\text{sub}} = 16$ and $p = 6$: comparison between $\boldsymbol{\mathcal{M}}$ and $\boldsymbol{\mathcal{M}}_{CE}$.

domain	$q(\boldsymbol{\mathcal{M}}_{CE}^{-\frac{1}{2}}\mathbf{M}\boldsymbol{\mathcal{M}}_{CE}^{-\frac{1}{2}})$	$q(\boldsymbol{\mathcal{M}}^{-\frac{1}{2}}\mathbf{M}\boldsymbol{\mathcal{M}}^{-\frac{1}{2}})^2$
kite	$1.20 \cdot 10^{-2}$	$1.33 \cdot 10^{-3}$
blade	$4.60 \cdot 10^{-2}$	$1.15 \cdot 10^{-2}$
holed plate	$1.24 \cdot 10^{-2}$	$2.39 \cdot 10^{-3}$
disc (e)	$3.13 \cdot 10^{-1}$	$6.89 \cdot 10^{-3}$
disc (f)	$2.82 \cdot 10^{-1}$	$1.28 \cdot 10^{-2}$

TABLE 3.12: Comparison between $q(\boldsymbol{\mathcal{M}}_{CE}^{-\frac{1}{2}}\mathbf{M}\boldsymbol{\mathcal{M}}_{CE}^{-\frac{1}{2}})$ and $q(\boldsymbol{\mathcal{M}}^{-\frac{1}{2}}\mathbf{M}\boldsymbol{\mathcal{M}}^{-\frac{1}{2}})^2$ for $n_{\text{sub}} = 16$ and $p = 6$.

solvers, with an advantage for $\boldsymbol{\mathcal{M}}$ in all the considered problems and especially in the case of the singular parametrizations considered.

3.4.2 Multipatch domains

Finally, in order to evaluate the performance of our Additive Schwarz preconditioner, we consider three domains: a multipatch five-pointed star (Figure 3.1b), a multipatch disc (Figure 3.1d) and a multipatch fan (Figure 3.2b), obtained by gluing together 7 blade-shaped patches like the one represented in Figure 3.2a.

As in the single patch case, we compare the condition number of the original mass matrix (Tables 3.13 and 3.16) with that of the preconditioned one (Tables 3.14 and 3.17). In all cases, the preconditioner greatly reduces the condition number of the matrix, robustly with respect to h. Moreover, the growth of the condition number with respect to the spline degree p seems to be linear (see Figure 3.3b). This is reflected also in the number of iterations needed by PCG to reach the given tolerance, see Tables 3.18 and 3.19.

3.5 Conclusions

In this chapter, we have presented a simple and efficient preconditioner for mass matrices arising in isogeometric analysis. The main idea for the single patch case is to

n_{sub}	$p = 2$	$p = 3$	$p = 4$	$p = 5$	$p = 6$
16	$1.326 \cdot 10^2$	$9.994 \cdot 10^2$	$6.848 \cdot 10^3$	$4.611 \cdot 10^4$	$3.160 \cdot 10^5$
32	$1.503 \cdot 10^2$	$1.156 \cdot 10^3$	$8.104 \cdot 10^3$	$5.565 \cdot 10^4$	$3.845 \cdot 10^5$
64	$1.618 \cdot 10^2$	$1.258 \cdot 10^3$	$8.935 \cdot 10^3$	$6.217 \cdot 10^4$	$4.351 \cdot 10^5$

TABLE 3.13: Condition number of mass matrix for multipatch star.

n_{sub}	$p = 2$	$p = 3$	$p = 4$	$p = 5$	$p = 6$
16	39.69	48.05	56.17	64.03	71.62
32	39.80	48.23	56.42	64.32	71.95
64	39.86	48.33	56.55	64.48	72.13

TABLE 3.14: Condition number of preconditioned mass matrix for multipatch star.

n_{sub}	$p = 2$	$p = 3$	$p = 4$	$p = 5$	$p = 6$
16	13 / 0.0111	14 / 0.0134	14 / 0.0145	15 / 0.0175	15 / 0.0198
32	12 / 0.0251	12 / 0.0276	13 / 0.0320	13 / 0.0375	14 / 0.0488
64	10 / 0.0647	12 / 0.0892	12 / 0.102	12 / 0.119	12 / 0.141
128	9 / 0.221	11 / 0.303	11 / 0.348	11 / 0.393	12 / 0.502

TABLE 3.15: Iterations and time spent by PCG for multipatch star.

n_{sub}	$p = 2$	$p = 3$	$p = 4$	$p = 5$	$p = 6$
16	$2.098 \cdot 10^2$	$1.550 \cdot 10^3$	$1.049 \cdot 10^4$	$7.007 \cdot 10^4$	$4.761 \cdot 10^5$
32	$2.585 \cdot 10^2$	$1.970 \cdot 10^3$	$1.374 \cdot 10^4$	$9.360 \cdot 10^4$	$6.399 \cdot 10^5$
64	$2.949 \cdot 10^2$	$2.291 \cdot 10^3$	$1.637 \cdot 10^4$	$1.143 \cdot 10^5$	$7.994 \cdot 10^5$

TABLE 3.16: Condition number of mass matrix for multipatch disc.

n_{sub}	$p = 2$	$p = 3$	$p = 4$	$p = 5$	$p = 6$
16	13.88	16.02	18.03	19.92	21.70
32	13.99	16.16	18.18	20.08	21.87
64	14.06	16.24	18.28	20.18	21.98

TABLE 3.17: Condition number of preconditioned mass matrix for multipatch disc.

n_{sub}	$p = 2$	$p = 3$	$p = 4$	$p = 5$	$p = 6$
16	14 / 0.0125	15 / 0.0147	17 / 0.0180	17 / 0.0203	18 / 0.0240
32	14 / 0.0310	15 / 0.0365	16 / 0.0424	17 / 0.0513	17 / 0.0617
64	14 / 0.0995	14 / 0.114	16 / 0.145	16 / 0.170	16 / 0.196
128	14 / 0.380	14 / 0.421	15 / 0.496	16 / 0.606	16 / 0.704

TABLE 3.18: Iterations and time spent by PCG for multipatch disc.

n_{sub}	$p = 2$	$p = 3$	$p = 4$	$p = 5$	$p = 6$
16	12 / 0.205	13 / 0.436	13 / 0.844	14 / 1.96	15 / 3.76
32	10 / 1.11	10 / 2.04	12 / 4.50	12 / 9.02	12 / 16.0
64	9 / 7.70	9 / 13.2	10 / 27.7	*	*

TABLE 3.19: Iterations and time spent by PCG for multipatch fan. In the cases denoted by "*", we were not able to assemble the mass matrix due to memory limitations.

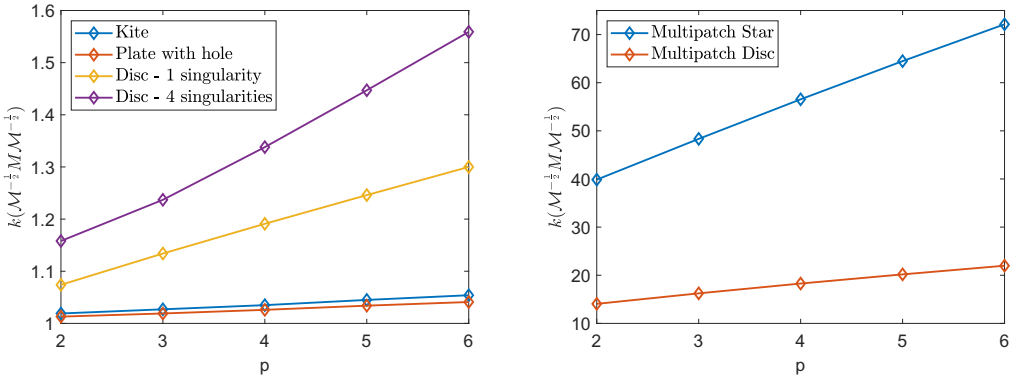

(A) Single patch domains (B) Multipatch domains

FIGURE 3.3: Condition number of preconditioned mass matrix ($n_{\text{sub}} = 64$).

exploit the Kronecker product structure of parametric mass matrix on the reference domain, combined with a diagonal scaling to correctly incorporate the effect of the geometry parametrization. In order to deal with multipatch domains, we have used the single patch strategy in an Additive Schwarz preconditioner. The preconditioner has an application cost of $O(pN_{\text{dof}})$ FLOPs, and is well suited for parallelization. We have proved that the single-patch preconditioner converges, as the mesh-size h goes to 0, to the exact mass, and that robustness with respect to h is preserved in the multipatch case. Numerical tests reflect the theoretical results and show a very good behaviour also with respect to the spline degree p.

Chapter 4

Explicit high-order generalized-α methods

Chung and Hulbert in [17] introduced the generalized-α method for solving hyperbolic equations arising in structural dynamics. The method has second-order accuracy in time, unconditional stability and user-control on the high-frequency numerical dissipation. Consequently, the method has been widely used for various applications. In [21], Behnoudfar, Calo and Deng propose a k-step form of the generalized-α method that delivers $2k$ accuracy in time for problems of second derivatives in time. The main idea of their generalization is to add higher-order terms as the residuals obtained by solving auxiliary systems as well as adopting higher-order terms in Taylor expansions used in the generalized-α method. More precisely, to gain $2k$-th order of accuracy, they build an algorithm that consists of $3k$ equations. For each set of three equations, it is solved a system for a variable while other two variables are updated explicitly. For applying explicit generalized-α method in combination with isogeometric discretization in space, at each time step we need to solve a linear system associated to the isogeometric mass matrix. The resolution of this linear systems could require a considerable computational effort, especially if we deal with splines of high degree. In this chapter, we combine the explicit fourth-order generalized-α method with the preconditioners presented in Chapter 3, which is very easy to implement but also extremely efficient and robust.

The structure of this chapter is as follows. In Section 4.1 we introduce the model problem and its spatial discretization. In Section 4.2 we recall the definition of the classical generalized-α method and its extension to the fourth-order accuracy. Finally, in Section 4.3 we present some numerical results assessing the accuracy of the generalized-α method and the performance of the preconditioner for both single patch and multipatch spatial domains.

4.1 Problem Statement

We start with a initial boundary-value hyperbolic problem that can describe a structural dynamics as

$$\begin{cases} \ddot{u}(\boldsymbol{x},t) - \Delta u(\boldsymbol{x},t) + C\left(\dot{u}(\boldsymbol{x},t)\right) &= f(\boldsymbol{x},t), & (\boldsymbol{x},t) \in \Omega \times (0,T], \\ u(\boldsymbol{x},t) &= u_D, & \boldsymbol{x} \in \partial\Omega, \\ u(\boldsymbol{x},0) &= u_0, & \boldsymbol{x} \in \Omega, \\ \dot{u}(\boldsymbol{x},0) &= v_0, & \boldsymbol{x} \in \Omega. \end{cases} \tag{4.1}$$

Let $\Omega = (0,1)^d \subset \mathbb{R}^d, d = 1,2,3$, an open bounded domain. The operator Δ denotes Laplacian and superscript dot shows derivative with respect to time as $\dot{u}(\boldsymbol{x},t) = \frac{\partial u(\boldsymbol{x},t)}{\partial t}$

and $\ddot{u}(\boldsymbol{x},t) = \frac{\partial^2 u(\boldsymbol{x},t)}{\partial t^2}$. $C\left(\dot{u}(\boldsymbol{x},t)\right)$ denotes a linear function of damping. The source f, the initial data u_0, v_0, and the Dirichlet boundary condition u_D are given and assumed regular enough so that the problem admits a weak solution.
To solve (4.1), we first obtain a semi-discretized problem by considering spatial dimensions. Then, we deploy our explicit generalized-α method to have a fully discretized system.

4.1.1 Spatial discretization

We adopt an isogeometric method for the spatial discretization. For this aim we consider a finite-dimensional spline space V_h on Ω as in 2.2 or 2.3, depending on if Ω is a single patch or multipatch domain. We multiply the hyperbolic equation (4.1) with a sufficiently regular test function $w \in V_h$, integrate over Ω, and apply the divergence theorem to obtain the the semi-discretised form of the continuous problem as: find $u_h(t) = u_h(\cdot,t) \in V_h$ for $t > 0$, such that

$$(\ddot{u}_h, w_h) + (\nabla u_h, \nabla w_h) = (f, w_h), \qquad \forall w_h \in V_h, \tag{4.2}$$

where $(\cdot,\cdot)$ is the L_2 scalar product. Besides, we approximate $u(x,t)$ for each fixed t by a function that belongs to V_h denoted by $u_h(x,t)$. We consider the variational formulation (4.2) with $u_{0,h} = u_h(\cdot,0)$ and $\dot{u}_{0,h} = \dot{u}_h(\cdot,0)$ being the L^2-projection of u_0 and v_0 in V_h, respectively.
Then, one can obtain the matrix form of the discrete problem (4.2) as:

$$M\ddot{U} + C\dot{U} + KU = F, \tag{4.3}$$

where M, C, and K are the mass, damping, and stiffness matrices, respectively. U denotes the vector of the unknowns, and F is the source vector. The initial conditions also read:

$$U(0) = U_0, \qquad V(0) = V_0, \tag{4.4}$$

where U_0 and V_0 are the given vectors of initial conditions $u_{0,h}$ and $\dot{u}_{0,h}$, respectively. In the next section, we present the numerical technique to deal with the time derivative $\ddot{U}$ and $\dot{U}$ in (4.3) with accuracy of order $2k$ in the temporal domain with $k \in \mathbb{N}$.

4.1.2 Time-discretization

To obtain a fully discretized description of the (4.2), we require to adopt an appropriate time integrator to deal with $\ddot{u}_h$. For this aim, one can consider the discretization of the temporal domain and then choose an appropriate algorithms including implicit or explicit families. In the next section, we propose our novel high-order explicit generalized-α method.

4.2 Explicit generalized-α method

We start introducing the method by taking into account a partitioning of the time interval $[0,T]$ with a grid size τ: $0 = t_0 < t_1 < \cdots < t_N = T$ and approximating $U(t_n), \dot{U}(t_n), \ddot{U}(t_n)$ using U_n, V_n, A_n, respectively. To solve (4.3) at time-step $n+1$,

the explicit generalized-α method with second-order of accuracy in time reads:

$$MA_{n+\alpha_m} + CV_n + KU_n = F_{n+\alpha_f} \tag{4.5a}$$
$$V_{n+1} = V_n + \tau A_n + \tau\gamma[\![A_n]\!] \tag{4.5b}$$
$$U_{n+1} = U_n + \tau V_n + \frac{\tau^2}{2}A_n + \tau^2\beta[\![A_n]\!], \tag{4.5c}$$

where we have set

$$\begin{aligned} F_{n+\alpha_f} &= F(t_{n+\alpha_f}) \\ A_{n+\alpha_m} &= A_n + \alpha_m[\![A_n]\!]. \end{aligned} \tag{4.6}$$

with

$$[\![A_n]\!] = A_{n+1} - A_n.$$

To retrieve the unknown A at the initial state, we solve

$$A_0 = M^{-1}(F_0 - KU_0). \tag{4.7}$$

Plugging (4.6) into (4.5) results in the method which consists of two steps. Firstly, we solve an explicit system to find $[\![A_n]\!]$. Then, apply the result to the (4.5b) and (4.5c) to update V_{n+1} and U_{n+1}, respectively. We continue this approach until we find the solutions at the final time step.
In the method introduced in (4.5), the order of accuracy in time is controlled by the truncation errors of $\mathcal{O}(\tau^3)$ applied to the system by the Taylor expansion used to derive the formulations (for more details, see [17]). To overcome this limitations, assuming sufficient regularity in the time dimension, we exploit a Taylor expansion with higher-order terms. For this aim, let $\mathcal{L}^a(\cdot)$ denotes the a-th order derivative in time operator. Therefore, for example, to derive a fourth-order explicit generalized-α method, we propose an approach based on solving

$$\begin{aligned} MA_n^{\alpha_1} + CV_n + KU_n &= F_{n+\alpha_{f1}} \\ M\mathcal{L}^3(A_n^{\alpha_2}) + C\mathcal{L}^2(A_n) + K\mathcal{L}^1(A_n) &= \mathcal{L}^3(F_{n+\alpha_{f2}}), \end{aligned} \tag{4.8}$$

with updating conditions

$$\begin{aligned} U_{n+1} &= U_n + \tau V_n + \frac{\tau^2}{2}A_n + \frac{\tau^3}{6}\mathcal{L}^1(A_n) + \frac{\tau^4}{24}\mathcal{L}^2(A_n) + \frac{\tau^5}{120}\mathcal{L}^3(A_n) + \beta_1\tau^2 P_n \\ V_{n+1} &= V_n + \tau A_n + \frac{\tau^2}{2}\mathcal{L}^1(A_n) + \frac{\tau^3}{6}\mathcal{L}^2(A_n) + \frac{\tau^4}{24}\mathcal{L}^3(A_n) + \gamma_1\tau P_n \\ \mathcal{L}^1(A_{n+1}) &= \mathcal{L}^1(A_n) + \tau\mathcal{L}^2(A_n) + \frac{\tau^2}{2}\mathcal{L}^3(A_n) + \tau^2\beta_2[\![\mathcal{L}^3(A_n)]\!] \\ \mathcal{L}^2(A_{n+1}) &= \mathcal{L}^2(A_n) + \tau\mathcal{L}^3(A_n) + \tau\gamma_2[\![\mathcal{L}^3(A_n)]\!], \end{aligned} \tag{4.9}$$

where

$$\begin{aligned} P_n &= A_{n+1} - A_n - \tau\mathcal{L}^1(A_n) - \frac{\tau^2}{2}\mathcal{L}^2(A_n) - \frac{\tau^3}{6}\mathcal{L}^3(A_n) \\ A_n^{\alpha_1} &= A_n + \tau\mathcal{L}^1(A_n) + \frac{\tau^2}{2}\mathcal{L}^2(A_n) + \frac{\tau^3}{6}\mathcal{L}^3(A_n) + \alpha_1 P_n \\ \mathcal{L}^3(A_n^{\alpha_2}) &= \mathcal{L}^3(A_n) + \alpha_2[\![\mathcal{L}^3(A_n)]\!]. \end{aligned} \tag{4.10}$$

Following the approach stated in (4.7), one can readily obtain the initial data of the unknowns using the given information on U_0 and V_0 as

$$\begin{aligned} A_0 &= M^{-1}(F_0 - KU_0) \\ \mathcal{L}^1(A_0) &= M^{-1}(\mathcal{L}^1(F_0) - KV_0) \\ \mathcal{L}^2(A_0) &= M^{-1}(\mathcal{L}^2(F_0) - KA_0) \\ \mathcal{L}^3(A_0) &= M^{-1}(\mathcal{L}^3(F_0) - K\mathcal{L}^1(A_0)). \end{aligned}$$

In the next section, we discuss the accuracy of the proposed method.

4.2.1 Order of accuracy in time

Herein, we report the conditions on the parameters γ_1 and γ_2 to guarantee the fourth-order accuracy of the scheme in the form of (4.8). For the generalization to $2k$th-order we refer to [21]. We have the following result.

Theorem 5. *Assuming that the solution is sufficiently smooth with respect to time, the method in* (4.8) *is fourth-order accurate in time given*

$$\gamma_1 = \frac{1}{2} - \alpha_{f1} + \alpha_1, \qquad \gamma_2 = \frac{1}{2} - \alpha_{f2} + \alpha_2. \tag{4.11}$$

Proof. For the proof we refer to [21]. □

Before closing this section, we should notice that a possible drawback of using explicit time integrators can be the cost inverting the mass matrix. To overcome this shortcoming we propose the use of the preconditioner for isogeometric mass matrix presented in Chapter 3.

4.3 Numerical results

In this section, we provide different numerical results to show the performance of our method. All the tests are performed with Matlab R2015a and GeoPDEs toolbox [70]. The linear systems are solved by PCG, with tolerance equal to 10^{-12} and with the null vector as initial guess. We focus only on the fourth-order in time method and we restrict our tests to splines of maximal regularity. In this context, for all the numerical

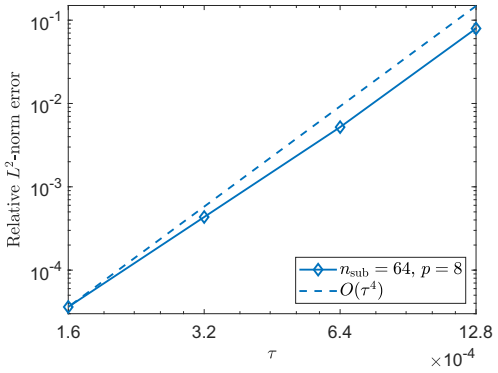

FIGURE 4.1: $L^2(\Omega)$ norm relative error at $T = 0.0205$ on $\Omega = [0, 1]$, with $n_{\text{sub}} = 64$ and $p = 8$.

tests we set:

$$\begin{aligned}
\alpha_{f1} &= 1 \\
\alpha_{f2} &= 0 \\
\alpha_1 &= \frac{2 - \rho(1+\rho)}{(1-\rho)^2} \\
\alpha_2 &= \frac{2 + \rho(1-\rho)}{(1+\rho)^2} \\
\beta_1 &= \frac{(1+\rho)^3}{(1-\rho)(2-\rho(1+\rho))} \\
\beta_2 &= \frac{-5 - 7\rho + \rho^2 + 3\rho^3}{(1+\rho)^2(2 - 23\rho + \rho^3)},
\end{aligned}$$

with $\rho = 0.8$ while γ_1 and γ_2 are chosen as in Theorem 5.

4.3.1 Convergence of the generalized-α method

For verifying the accuracy of the 4-th order explicit generalized-α method, we solve (4.1) on $\Omega = [0, 1]$, choosing the source term, Dirichlet boundary conditions and initial conditions such that the exact solution is

$$u(x, t) = \sin(x) \left[\cos(60\pi t) + \sin(60\pi t)\right].$$

Figure 4.1 confirms the 4-th order of convergence of our method with respect to τ.

4.3.2 Performance of the preconditioners

In order to analyze the behaviour of the proposed preconditioners, we solve (4.1) on a regular single patch domain (Figure 4.2a), a singular one (Figure 4.2b) and a multipatch domain (Figure 4.2c), obtained by gluing together 7 blade-shaped patches like the one represented in Figure 4.2a. For each of them, source term, Dirichlet boundary condition and initial conditions are chosen such that the exact solution is always

$$u(x_1, x_2, x_3, t) = \sin(x_1) \sin(x_2) \sin(x_3) \left[\cos(20\pi t) + \sin(20\pi t)\right].$$

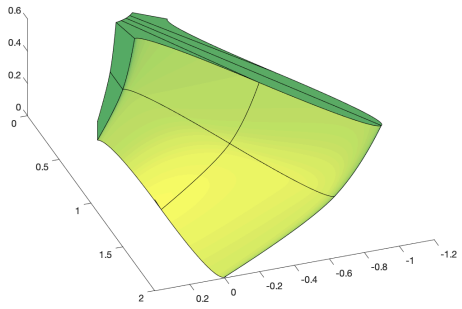

(A) Blade.

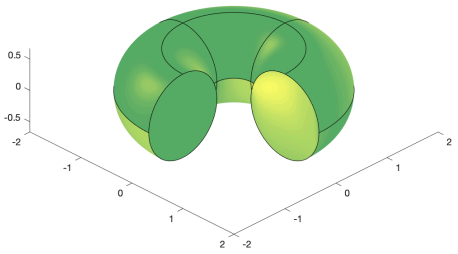

(B) Donut.

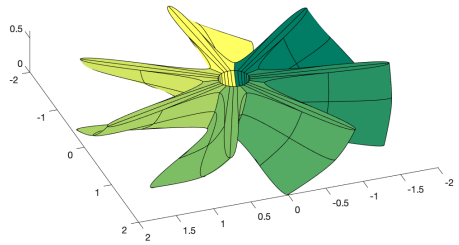

(C) Multipatch Fan.

FIGURE 4.2: Spatial domains.

n_{sub}	$p=1$	$p=2$	$p=3$	$p=4$
8	7.5	10.1	10.2	10.4
16	6.1	8.4	8.4	8.9
32	5.5	6.5	6.5	7.2
64	5.0	5.5	5.5	6.0

TABLE 4.1: Mean values, across all the time steps, of the iterations needed by PCG on the Blade, for $\tau = 10^{-5}$ and $T = 64 \cdot \tau$.

n_{sub}	$p=1$	$p=2$	$p=3$	$p=4$
8	6.0	8.0	9.0	10.0
16	5.0	7.0	8.0	8.0
32	5.0	6.0	7.0	8.0
64	5.3	6.5	7.0	7.8

TABLE 4.2: Mean values, across all the time steps, of the iterations needed by PCG on the Donut, for $\tau = 10^{-5}$ and $T = 64 \cdot \tau$.

We report the mean value, across all the time steps, of the number of iterations needed by PCG for reaching the given tolerance for the three different spatial domains. Tables 4.1 and 4.3 shows that the number of PCG iterations is always very low and decreases when the subdivisions are increased. This is true also for the singularly parametrized Donut domain (see Table 4.2), even though this case is beyond the robustness result presented in Section 3.1.

Furthermore, for assessing the good behaviour of the isogeometric discretization, for each spatial domain, we report the relative error in $L^2(\Omega)$ norm at the final instant $T = 6.4 \cdot 10^{-4}$ with $\tau = 10^{-5}$ for different mesh size and spline degree. In Figure 4.3, we can see that the rates of convergence are optimal with respect to the mesh size $h \approx n_{\text{sub}}^{-1}$, i.e. of order $O(h^{p+1})$, for $p = 1, 2, 3, 4$, as expected from standard a priori error estimate.

4.4 Conclusions

In this chapter we have combined an explicit high-order time integrator with an isogeometric discretization in space for the solution of an hyperbolic boundary-value problem. In order to recover computational efficiency, we have exploited the preconditioning technique presented in Chapter 3. Numerical tests shows that our method performs very well in terms of both accuracy and computational costs.

n_{sub}	$p=1$	$p=2$	$p=3$	$p=4$
8	22.5	32.0	37.7	41.9
16	21.0	27.8	30.8	35.6
32	19.0	25.5	27.9	29.9
64	17.0	22.5	26.0	27.5

TABLE 4.3: Mean values, across all the time steps, of the iterations needed by PCG on the Donut, for $\tau = 5 \cdot 10^{-5}$ and $T = 64 \cdot \tau$.

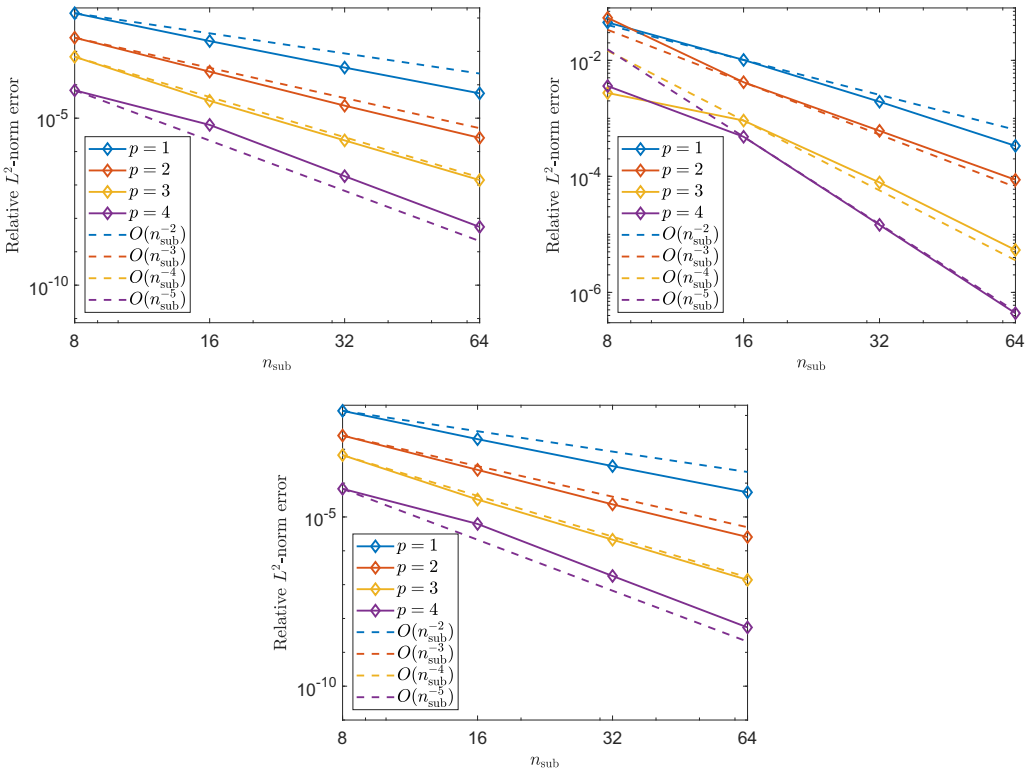

FIGURE 4.3: $L^2(\Omega)$ norm relative error at $T = 64 \cdot \tau$ with $\tau = 10^{-5}$ for Blade (top-left), Donut (top-right) and Fan (bottom).

Chapter 5

A projected super-penalty method for the isogeometric bilaplace problem

A distinguishing feature of splines is the high regularity achievable by construction, which allows the approximation of higher-order variational problems directly in their primal, for instance Kirchhoff plates [58, 50], Kirchhoff-Love shells [45, 60, 46, 43] and the Cahn-Hilliard equation [31]. For a detailed review of the method and its recent applications, the reader is referred to [41, 18, 42], whereas its mathematical foundations can be found in [5, 72].

Although smoothness is attained naturally within a patch, geometries of engineering relevance are in general described by multiple patches, where typically the underlying spline representations are non-conforming at the common interface. Clearly, in this scenario, a direct strong coupling between patches is not straightforward to achieve. Moreover, as in the scope of this chapter we are interested in the bilaplace problem, an efficient strategy to obtain C^1-coupling is needed since a global C^1-continuity is required to obtain a well-defined bilinear form for the problem at hand. In the literature, three methods are predominantly used to achieve the latter coupling in a weak sense and they are summarized in the following.

High-order mortar methods have been studied in [40, 36] in the context of Kirchhoff plates and Kirchhoff-Love shells, respectively, and have been extended to a general C^n-coupling in [23]. For a detailed review in the context of isogeometric analysis, we refer to the review article [35]. However, mortar methods leads to the formulation of a saddle point problem, where the associated Lagrange multipliers constitute additional unknowns to be solved for in the global system of equations.

Nitsche method has been analyzed in [64] for coupling isogeometric Kirchhoff plates in the scope of immersed methods and in [32] for imposing weakly kinematic boundary conditions for fourth-order PDEs. Although this family of method is less sensitive to the choice of parameters compared to classical penalty approaches, their formulation requires additional consistency terms which, in the Kirchhoff problem, involve the computation of derivatives of shape functions up to order three. This adds some extra steps of complexity in the implementation and increases the overall computational cost of the coupling strategy.

Finally, penalty methods are widely used in the engineering community due to their conceptual simplicity, see the seminal work [3]. Furthermore, they can be easily and efficiently incorporated into a numerical code, where we refer to [44, 1, 24, 34] for more insights and some applications in the context of isogeometric Kirchhoff-Love shells. Nonetheless, a major drawback of this approach resides in their lack of robustness with respect to the choice of penalty parameters. Typically, the choice of penalty coefficients is problem-dependent and is based on a time-consuming, heuristic process.

As noted in [34], on one hand, if the penalty factors are chosen too small the interface constraint is satisfied only loosely. On the other hand, if the coefficients are too high, the condition number of the resulting system matrix is negatively impacted and the convergence behaviour is spoiled by spurious locking phenomena.

Our contribution falls into this realm. Inspired by the *super-penalty* method studied in [4], our goal is to introduce a simple coupling procedure for the displacement and rotation fields, respectively, for non-conforming multi-patch Kirchhoff plates, which preserves the high-order optimal convergence rates achievable by B-splines while mitigating the detrimental effects related to locking. To alleviate the over-constraint of the solution space we perform an L^2-projection of the penalty terms onto a space of reduced degree defined on the slave side of the coupling interface where, motivated by the work in [12] for mortar methods, we select a $p/p-2$ pairing, where p denotes the B-splines degree. In particular, starting from the perturbed saddle point formulation of the bilaplace model problem, we show how the corresponding Lagrange multipliers can be eliminated from the system and, more importantly, how the perturbation gives us insights into the optimal choice for the penalty coefficients. Indeed, the proposed methodology is truly parameter-free, as the penalty factors are fully determined by the given physical constants, the geometry and its discretization, i.e. mesh size and spline degree. We remark that the proposed methodology is especially advantageous for moderate degrees $p = 2, 3$, where locking phenomena are particularly pronounced and the L^2-projection proves to be an effective and computationally efficient remedy. Then, we address the ill-conditioning issues stemming from our choice of super-penalty parameters. We adapt the block preconditioner based on an inexact Schur Complement Reduction (SCR) introduced in [48, 49] and we combine it with a preconditioner tailored to the isogeometric discretization of the bilaplace problem, where we exploit the tensor product structure of B-splines and an efficient algorithm for the solution of the arising Sylvester-like system; for a detailed derivation we refer to [62, 57, 51]. Finally, we show through several numerical benchmarks the optimal convergence properties of the presented methodology, where our approach does not suffer from locking also on very coarse meshes. This leads to a substantial improvement in the accuracy achievable per degree-of-freedom (dof).

The structure of this chapter is as follows. Section 5.1 describes in details the derivation of the proposed methodology. In Section 5.2 we provide an estimate of the a priori error and motivates our choice of penalty parameters. In Section 5.3 we discuss how to actually impose the continuity at the cross-points. Section 5.4 presents the ideas used in the construction of the preconditioner employed in this work. In Section 5.5 the method is validated on several numerical benchmarks and it is applied to the analysis of an idealized multi-patch design of an L-bracket. Finally, some conclusions are drawn in Section 5.6.

5.1 The projected super-penalty method

In this section, we introduce a method which alleviates locking phenomena arising when coupling non-conforming isogeometric patches. Inspired by the work presented in [12] in the context of isogeometric mortar methods, the proposed technique is based on the projection of the coupling terms at the interface, typically defined in terms of the degree p of the solution space, onto a reduced space of B-splines of degree $p^{\text{red}} = p - 2$ defined on the slave side of the interface.

5.1.1 The strong form of the Kirchhoff plate problem

Let us introduce the governing PDE, characterized by the bilaplace differential operator, that describes the bending-dominated problem of a Kirchhoff plate, following the notation in [60]. Let us define an open set $\Omega \subset \mathbb{R}^2$ with a sufficiently smooth boundary $\partial\Omega$, such that the normal vector $\boldsymbol{n}$ to the boundary is well-defined (almost) everywhere. Let us also introduce two admissible splittings of the boundary $\partial\Omega$ into $\partial\Omega = \overline{\Gamma_u \cup \Gamma_Q}$ and $\partial\Omega = \overline{\Gamma_\phi \cup \Gamma_M}$, such that $\Gamma_u \cap \Gamma_Q = \varnothing$ and $\Gamma_\phi \cap \Gamma_M = \varnothing$, respectively. Consequently, the strong form of the problem reads:

$$\begin{aligned} D\Delta^2 u &= g && \text{in} \quad \Omega \\ u &= u_\Gamma && \text{on} \quad \Gamma_u \\ -\nabla u \cdot \boldsymbol{n} &= \phi_\Gamma && \text{on} \quad \Gamma_\phi \\ \nu D\Delta u + (1-\nu) D\, \boldsymbol{n} \cdot (\nabla\nabla u)\boldsymbol{n} &= M_\Gamma && \text{on} \quad \Gamma_M \\ D(\nabla(\Delta u) + (1-\nu)\,\boldsymbol{\Psi}(u)\,) \cdot \boldsymbol{n} &= Q_\Gamma && \text{on} \quad \Gamma_Q\,, \end{aligned} \tag{5.1}$$

where u represents the deflection of the plate, D its bending stiffness, ν is the Poisson ratio, g is the load per unit area in the thickness direction, u_Γ, ϕ_Γ, M_Γ and Q_Γ are the prescribed deflection, rotation, bending moments and effective shear, respectively. The bending stiffness D is defined as:

$$D = \frac{Et^3}{12(1-\nu^2)}\,,$$

where E is the Young modulus and t denotes the thickness of the plate. For the sake of simplicity and without loss of generality, these are assumed to be a constant in Ω. Finally, the differential operator $\boldsymbol{\Psi}(\cdot)$ reads:

$$\boldsymbol{\Psi}(\cdot) = \left[\frac{\partial^3(\cdot)}{\partial x \partial^2 y}\,,\, \frac{\partial^3(\cdot)}{\partial^2 x \partial y}\right]^\top .$$

5.1.2 The multi-patch formulation of the perturbed saddle point Kirchhoff problem

Here, following the notation used in [12], we introduce a decomposition of Ω into N non-overlapping subdomains Ω^i such that:

$$\overline{\Omega} = \bigcup_{i=1}^{N} \overline{\Omega^i}\,, \quad \text{where} \quad \Omega^i \cap \Omega^j = \varnothing \quad \text{for} \quad i \neq j\,.$$

Now, let us define the interface $\gamma^{k,\ell}$ between two adjacent patches $\Omega^k, \Omega^\ell, 1 \leq k, \ell \leq N$ as the intersection of their corresponding boundaries:

$$\gamma^{k,\ell} = \partial\Omega^k \cup \partial\Omega^\ell\,.$$

Then, the skeleton Γ is defined as the union of all non-empty interfaces (which we suppose to be labelled with an index $\ell = 1, \ldots, L$) and reads:

$$\Gamma = \bigcup_{\ell=1}^{L} \gamma^\ell\,.$$

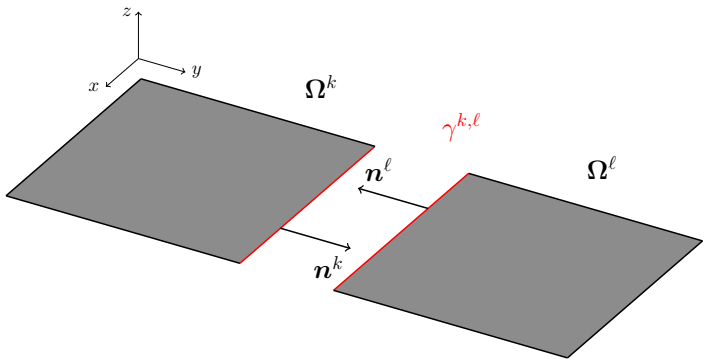

FIGURE 5.1: Example of two subdomains Ω^k, Ω^ℓ with their coupling interface $\gamma^{k,\ell}$, highlighted in red, and their corresponding normal vectors $\boldsymbol{n}^k, \boldsymbol{n}^\ell$. Note that we have separated the subdomains for visualization purposes. For a correct interpretation of the colours, the reader is referred to the web version of this manuscript.

Consequently, we can denote by u^k and $\boldsymbol{n}^k$ the value of the primary field and the outward normal on $\partial\Omega^k$, and u^ℓ and $\boldsymbol{n}^\ell$ the value of the primary field and outward normal on the neighbouring subdomain $\partial\Omega^\ell$, see Figure 5.1 for an example on two patches. Then, for each interface $\gamma^{k,\ell}$ we can write the following coupling conditions:

$$\begin{aligned} u^k - u^\ell &= 0 \quad \text{on} \quad \gamma^{k,\ell} \\ \nabla u^k \cdot \boldsymbol{n}^k + \nabla u^\ell \cdot \boldsymbol{n}^\ell &= 0 \quad \text{on} \quad \gamma^{k,\ell}, \end{aligned}$$

which can be rewritten using the standard jump and normal jump operators, respectively, as:

$$\begin{aligned} [\![u]\!] &= 0 \quad \text{on} \quad \gamma^{k,\ell} \\ [\![\nabla u]\!]_n &= 0 \quad \text{on} \quad \gamma^{k,\ell}. \end{aligned} \tag{5.2}$$

Further, given $1 \leq s, t \leq L$, $s \neq t$, we denote the cross-points by $c^{s,t} = \overline{\gamma}^s \cap \overline{\gamma}^t$ and we label them with an ordered index c^s, $s = 1, \dots, S$. For ease of notation and without loss of generality, in the following we assume the flexural rigidity D to be constant in Ω and the Poisson ratio ν to be zero. Further, we assume $\partial\Omega = \Gamma_u = \Gamma_\phi$, that is we restrict our analysis to the case of fully Dirichlet boundary conditions.

Now, let us introduce for each subdomain Ω^i the following space:

$$H^2_\star(\Omega^i) = \left\{ v^i \in H^2(\Omega^i) : v^i|_{\partial\Omega \cap \partial\Omega^i} = \left. \frac{\partial v^i}{\partial n} \right|_{\partial\Omega \cap \partial\Omega^i} = 0 \right\},$$

from which the following broken Sobolev space can be characterized as:

$$V = \left\{ v \in L^2(\Omega) : v|_{\Omega^i} \in H^2_\star(\Omega^i),\ i = 1, \dots, N,\ v \text{ is continuous in } c^s,\ s = 1, \dots, S \right\},$$

endowed with the broken norm $\|\cdot\|^2_V = \sum_{i=1}^N \|\cdot\|^2_{H^2(\Omega^i)}$. Then, let us also define the spaces:

$$\begin{aligned} H^{\frac{1}{2}}_\star(\Gamma) &= \{ [\![\nabla v]\!]_n : v \in V \} \\ H^{\frac{3}{2}}_\star(\Gamma) &= \{ [\![v]\!] : v \in V \}, \end{aligned}$$

equipped, respectively, with the norms

$$\|\cdot\|^2_{H^{1/2}_\star(\Gamma)} = \sum_{\ell=1}^{L} \|\cdot\|^2_{H^{1/2}(\gamma^\ell)}$$
$$\|\cdot\|^2_{H^{3/2}_\star(\Gamma)} = \sum_{\ell=1}^{L} \|\cdot\|^2_{H^{3/2}(\gamma^\ell)}.$$

Lastly, we need to introduce the following dual spaces:

$$Q_1 = \left[H^{\frac{3}{2}}_\star(\Gamma)\right]'$$
$$Q_2 = \left[H^{\frac{1}{2}}_\star(\Gamma)\right]'.$$

Let u be a smooth function and $v \in V$. Thanks to standard Green's identities, it holds

$$\begin{aligned}
&\int_\Omega \Delta^2 uv = \\
&\sum_{i=1}^{N} \int_{\Omega^i} \Delta u \Delta v + \sum_{\ell=1}^{L} \int_{\gamma^\ell} \left(\partial_n \Delta u [\![v]\!] - \Delta u \, [\![\nabla v]\!]_n\right) = \\
&\sum_{i=1}^{N} \int_{\Omega^i} \nabla(\nabla u) : \nabla(\nabla v) + \sum_{\ell=1}^{L} \int_{\gamma^\ell} \left(\partial_n \Delta u [\![v]\!] - \Delta u \, [\![\nabla v]\!]_n + \partial_{tt} u \, [\![\nabla v]\!]_n - \partial_{nt} u \, [\![\nabla v]\!]_t\right) = \\
&\sum_{i=1}^{N} \int_{\Omega^i} \nabla(\nabla u) : \nabla(\nabla v) + \sum_{\ell=1}^{L} \int_{\gamma^\ell} \left(\partial_n \Delta u [\![v]\!] - \Delta u \, [\![\nabla v]\!]_n + \partial_{tt} u \, [\![\nabla v]\!]_n + \partial_{ntt} u \, [\![v]\!]\right),
\end{aligned} \tag{5.3}$$

where ∂_n and ∂_t denotes the normal and the tangential derivative, respectively.
We are now ready to formulate (5.1) as a saddle point problem. Given $f \in V'$, find $(u, \lambda_1, \lambda_2) \in V \times Q_1 \times Q_2$ such that:

$$\begin{aligned}
\sum_{i=1}^{N} \int_{\Omega^i} \nabla(\nabla u) : \nabla(\nabla v) + \sum_{\ell=1}^{L} \left(\int_{\gamma^\ell} [\![v]\!]\lambda_1 + \int_{\gamma^\ell} [\![\nabla v]\!]_n \lambda_2\right) &= (f, v) \qquad \forall v \in V \\
\sum_{\ell=1}^{L} \int_{\gamma^\ell} [\![u]\!]\mu_1 = 0 \qquad &\forall \mu_1 \in Q_1 \\
\sum_{\ell=1}^{L} \int_{\gamma^\ell} [\![\nabla u]\!]_n \, \mu_2 = 0 \qquad &\forall \mu_2 \in Q_2 \,.
\end{aligned} \tag{5.4}$$

We also define three continuous bilinear forms $a : V \times V \to \mathbb{R}$, $b_1 : V \times Q_1 \to \mathbb{R}$ and $b_2 : V \times Q_2 \to \mathbb{R}$ as follows:

$$\begin{aligned} a(u,v) &= \sum_{i=1}^{N} \int_{\Omega^i} \nabla(\nabla u) : \nabla(\nabla v) && u, v \in V \\ b_1(v,\mu_1) &= \sum_{\ell=1}^{L} \int_{\gamma^\ell} [\![v]\!] \mu_1 && v \in V,\ \mu_1 \in Q_1 \\ b_2(v,\mu_2) &= \sum_{\ell=1}^{L} \int_{\gamma^\ell} [\![\nabla v]\!]_n \, \mu_2 && v \in V,\ \mu_2 \in Q_2\,. \end{aligned}$$

Further, we denote by $A : V \to V'$, $B_1 : V \to Q_1'$ and $B_2 : V \to Q_2'$, respectively, the linear continuous operators associated with a, b_1 and b_2, namely

$$\begin{aligned} \langle Au, v\rangle_{V'\times V} &= a(u,v) && \forall u, v \in V \\ \langle B_1 v, \mu_1\rangle_{Q_1'\times Q_1} &= \left\langle v, B_1^T \mu_1 \right\rangle_{V\times V'} = b_1(v,\mu_1) && \forall v \in V, \forall \mu_1 \in Q_1 \\ \langle B_2 v, \mu_2\rangle_{Q_2'\times Q_2} &= \left\langle v, B_2^T \mu_2 \right\rangle_{V\times V'} = b_2(v,\mu_2) && \forall v \in V, \forall \mu_2 \in Q_2. \end{aligned}$$

For $i = 1, 2$, we set $K_i = \ker B_i$, $H_i = \ker B_i^T$ and $K = K_1 \cap K_2$.

Theorem 6. *The following characterization holds:*

$$H_0^2(\Omega) = K.$$

Proof. If $v \in H_0^2(\Omega)$, then for all $\ell = 1, \ldots, L$ it follows

$$[\![u]\!] = [\![\nabla u]\!]_n = 0 \quad \text{on} \quad \gamma^\ell.$$

In particular, it holds

$$b_1(v,\mu_1) = b_2(v,\mu_2) = 0 \qquad \forall \mu_1 \in Q_1,\ \forall \mu_2 \in Q_2,$$

which corresponds to have $v \in K$.
On the other hand, let be $v \in K$, which means

$$b_1(v,\mu_1) = b_2(v,\mu_2) = 0 \qquad \forall \mu_1 \in Q_1,\ \forall \mu_2 \in Q_2. \tag{5.5}$$

We observe that for every $v \in V$, it holds $[\![v]\!] \in Q_1'$ and $[\![\nabla v]\!]_n \in Q_2'$. Then (5.5) implies

$$\begin{aligned} b_1(v, [\![v]\!]) &= \sum_{\ell=1}^{L} \|[\![v]\!]\|^2_{L^2(\gamma^\ell)} = 0 \\ b_2\left(v, [\![\nabla v]\!]_n\right) &= \sum_{\ell=1}^{L} \|[\![\nabla v]\!]_n\|^2_{L^2(\gamma^\ell)} = 0. \end{aligned}$$

Thus, for all $\ell = 1, \ldots, L$ it follows

$$[\![u]\!] = [\![\nabla u]\!]_n = 0 \quad \text{on} \quad \gamma^\ell,$$

then we get $v \in H_0^2(\Omega)$. □

Combining Theorem 6 with generalized Poincaré-Friedrichs inequality, it follows that there exists a constant $C_{\mathrm{P}} > 0$ such that

$$C_{\mathrm{P}}\|v_0\|_V^2 \leq a(v_0, v_0), \qquad \forall v_0 \in K.$$

Further, we are able to prove the coercivity of the bilinear form a in a subspace of V bigger than K.

Theorem 7. *There exists a constant $\alpha > 0$ such that*

$$\alpha\|v\|_V^2 \leq a(v, v), \qquad \forall v \in V_0,$$

where we have set

$$V_0 = \left\{ v \in V : \int_{\gamma^\ell} [\![\nabla v]\!]_n = \int_{\gamma^\ell} [\![v]\!] = 0,\ l = 1, \dots, L \right\}.$$

Proof. First of all, we recall that

$$a(v, v) = \sum_{i=1}^{N} \|\partial_{xx} v\|_{L^2(\Omega_i)}^2 + \|\partial_{yy} v\|_{L^2(\Omega_i)}^2 + 2\|\partial_{xy} v\|_{L^2(\Omega_i)}^2.$$

We proceed by contradiction. Suppose the thesis does not hold for any constant $\alpha > 0$. Then there exists a sequence $\{v_m\} \subset V_0$, with $\|v_m\|_V = 1$ for all $m \in \mathbb{N}$, such that

$$\frac{1}{m} > \sum_{i=1}^{N} \|\partial_{xx} v\|_{L^2(\Omega_i)}^2 + \|\partial_{yy} v\|_{L^2(\Omega_i)}^2 + 2\|\partial_{xy} v\|_{L^2(\Omega_i)}^2.$$

We observe that

$$\lim_{m\to\infty} \sum_{i=1}^{N} \|\partial_{xx} v_m\|_{L^2(\Omega_i)}^2 + \|\partial_{yy} v_m\|_{L^2(\Omega_i)}^2 + 2\|\partial_{xy} v_m\|_{L^2(\Omega_i)}^2 = 0. \tag{5.6}$$

Thanks to the compact embedding $H^2(\Omega_i) \hookrightarrow H^1(\Omega_i)$, there exists a subsequence, that with an abuse of notation we still denote by $\{v_m\}$, such that

$$v_m \to v \qquad \text{w.r.t.} \qquad \|\cdot\|_{\mathcal{H}^1(\Omega)} = \sum_{k=1}^{N} \|\cdot\|_{H^1(\Omega^i)}.$$

From (5.6), it follows that $\{v_m\}$ converges in V_0, w.r.t. $\|\cdot\|_V$, and $\nabla v_{|\Omega_i}$ is constant for all $i = 1, \dots, N$. To proceed, we consider two different cases:

1. If $\partial\Omega_i \cap \partial\Omega$ has positive measure, denoting by $\mathbf{n}$ and $\mathbf{t}$ respectively the normal and tangent versor to $\partial\Omega_i \cap \partial\Omega$, we have

   $$(\nabla v \cdot \mathbf{n})_{|\partial\Omega_i \cap \partial\Omega} = (\nabla v \cdot \mathbf{t})_{|\partial\Omega_i \cap \partial\Omega} = 0,$$

   which implies

   $$\nabla v_{|\partial\Omega_i \cap \partial\Omega} = 0. \tag{5.7}$$

   Combining (5.7) with the fact that $\nabla v_{|\Omega_i}$ is constant, it follows

   $$\nabla v|_{\Omega_i} = 0.$$

Further, recalling homogeneous Dirichlet boundary conditions for v, we obtain

$$v|_{\Omega_i} = 0.$$

2. Let Ω_i and Ω_j be such that $\gamma^\ell \subset \partial\Omega_i \cap \partial\Omega_j$, for some $l = 1, \dots, L$, and let us assume $v_{|\Omega_i} = 0$. From the continuity at cross-points, we have $v_{|\partial\gamma^\ell} = 0$, that implies

$$\int_{\gamma^\ell} \nabla v \cdot \mathbf{t} = 0. \tag{5.8}$$

Moreover, combining the definition of V_0 with $v_{|\Omega_i} = 0$, it holds

$$\int_{\gamma^\ell} \nabla v \cdot \mathbf{n} = \int_{\gamma^\ell} [\![\nabla v]\!]_n = 0. \tag{5.9}$$

Having ∇v constant on each patch, (5.8) and (5.9) become

$$\begin{aligned} \nabla v|_{\gamma^\ell} \cdot \int_{\gamma^\ell} \mathbf{n} &= 0 \\ \nabla v|_{\gamma^\ell} \cdot \int_{\gamma^\ell} \mathbf{t} &= 0. \end{aligned} \tag{5.10}$$

Recalling that γ^ℓ is not a closed path, we obtain that

$$\left\{ \int_{\gamma^\ell} \mathbf{n}, \int_{\gamma^\ell} \mathbf{t} \right\}$$

form an orthogonal basis of $\mathbb{R}^2$. As a consequence, from (5.10) it follows

$$\nabla v|_{\gamma^\ell} = 0,$$

which, combined with the fact that ∇v_{Ω_j} is constant, implies

$$\nabla v|_{\Omega_j} = 0,$$

Hence $v|_{\Omega_j}$ is constant and, having

$$\int_{\gamma^\ell} v = 0,$$

we have $v|_{\Omega_j} = 0$.

Starting from a patch Ω^i as in the first case, iterating the considerations in the second one for all the remaining patches, we obtain $v = 0$ on Ω, which is in contradiction to the fact

$$\lim_{n\to\infty} \|v_m\|_V = \|v\|_V = 1.$$

□

By construction it holds

$$\begin{aligned}\mathrm{Im}\,(B_1) &= Q_1'\\ \mathrm{Im}\,(B_2|_{K_1}) &= Q_2'.\end{aligned}$$

Finally, we are in the hypothesis of Appendix A Theorem 11, hence there exists a unique solution $(u, \lambda_1, \lambda_2)$ of (5.4).

5.1.3 Perturbed saddle point problem

Now, given $\varepsilon_1^{(\ell)}, \varepsilon_2^{(\ell)} > 0, \ell = 1, \dots, L$, we can introduce the singularly perturbed version of (5.4): given $f \in V'$, find $(u_\varepsilon, \lambda_{1,\varepsilon}, \lambda_{2,\varepsilon}) \in V \times L^2(\Gamma) \times L^2(\Gamma)$, such that

$$\begin{aligned}\sum_{i=1}^{N} \int_{\Omega^i} \nabla(\nabla u_\varepsilon) : \nabla(\nabla v) + \sum_{\ell=1}^{L} \left(\int_{\gamma^\ell} [\![v]\!] \lambda_{1,\varepsilon} + \int_{\gamma^\ell} [\![\nabla v]\!]_n \, \lambda_{2,\varepsilon} \right) &= (f, v) && \forall v \in V\\ \sum_{\ell=1}^{L} \left(\int_{\gamma^\ell} [\![u_\varepsilon]\!] \mu_1 - \varepsilon_1^{(\ell)} \int_{\gamma^\ell} \lambda_{1,\varepsilon} \mu_1 \right) &= 0 && \forall \mu_1 \in L^2(\Gamma)\\ \sum_{\ell=1}^{L} \left(\int_{\gamma^\ell} [\![\nabla u_\varepsilon]\!]_n \, \mu_2 - \varepsilon_2^{(\ell)} \int_{\gamma^\ell} \lambda_{2,\varepsilon} \mu_2 \right) &= 0 && \forall \mu_2 \in L^2(\Gamma)\,.\end{aligned} \tag{5.11}$$

Proposition 2. *For all $\varepsilon_1^{(\ell)}, \varepsilon_2^{(\ell)} > 0$, there exists a constant $\widetilde{\alpha} > 0$ such that*

$$\widetilde{\alpha} \|v\|_V^2 \le a(v, v) + \sum_{\ell=1}^{L} \left(\frac{1}{\varepsilon_1^{(\ell)}} \|[\![v]\!]\|_{L^2(\gamma^\ell)}^2 + \frac{1}{\varepsilon_2^{(\ell)}} \|[\![\partial_n v]\!]\|_{L^2(\gamma^\ell)}^2 \right), \qquad \forall v \in V.$$

Proof. We proceed by contradiction. Suppose the thesis does not hold for any constant $\widetilde{\alpha}$. Then there exists a sequence $\{v_m\} \subset V$, with $\|v_m\|_V = 1$ for all $m \in \mathbb{N}$, such that

$$\frac{1}{m} > a(v_m, v_m) + \sum_{\ell=1}^{L} \left(\frac{1}{\varepsilon_1^{(\ell)}} \|[\![v_m]\!]\|_{L^2(\gamma^\ell)}^2 + \frac{1}{\varepsilon_2^{(\ell)}} \|[\![\partial_n v]\!]\|_{L^2(\gamma^\ell)}^2 \right).$$

We observe that

$$\lim_{m\to\infty} a(v_m, v_m) = \lim_{m\to\infty} \sum_{i=1}^{N} \|\partial_{xx} v_m\|_{L^2(\Omega_i)}^2 + \|\partial_{yy} v_m\|_{L^2(\Omega_i)}^2 + 2\|\partial_{xy} v_m\|_{L^2(\Omega_i)}^2 = 0 \tag{5.12}$$

$$\lim_{m\to\infty} \sum_{\ell=1}^{L} \|[\![v_m]\!]\|_{L^2(\gamma^\ell)}^2 = 0 \tag{5.13}$$

$$\lim_{m\to\infty} \sum_{\ell=1}^{L} \|[\![\nabla v_m]\!]_n\|_{L^2(\gamma^\ell)}^2 = 0. \tag{5.14}$$

Thanks to the compact embedding $H^2(\Omega^i) \hookrightarrow H^1(\Omega^i)$, there exists a subsequence, that with an abuse of notation we still denote by $\{v_m\}$, such that

$$v_m \to v \qquad \text{w.r.t.} \qquad \|\cdot\|_{\mathcal{H}^1(\Omega)} = \sum_{k=1}^{N} \|\cdot\|_{H^1(\Omega^i)}.$$

From (5.12), it follows that $\{v_m\}$ converges in V and $\nabla v_{|\Omega^i}$ is constant. To proceed, we consider two different cases:

1. If $\partial\Omega^i \cap \partial\Omega$ has positive measure, homogeneous Dirichlet boundary conditions imply $\nabla v_{|\Omega^i} = 0$ and $v_{|\partial\Omega^i} = 0$.
2. Let be Ω^i and Ω_j such that $\gamma^\ell \subset \partial\Omega^i \cap \partial\Omega_j$, for some $\ell = 1, \dots, L$, and let us assume $v_{|\Omega^i} = 0$. From (5.13) and (5.14), it follows $v_{|\Omega_j} = 0$.

Starting from a patch Ω^i as in the first case, iterating the considerations in the second one for all the remaining patches, we obtain $v = 0$ on Ω, which is in contradiction to the fact

$$\lim_{m\to\infty} \|v_m\|_V = \|v\|_V = 1.$$

□

Combining Proposition 2 with

$$\begin{aligned} \|B_1 v\|_{L^2(\Gamma)} &= \sup_{w\in L^2(\Gamma)} \frac{(B_1 v, w)_{L^2(\Gamma)}}{\|w\|_{L^2(\Gamma)}} \geq \frac{\sum_{l=1}^{L} \int_{\gamma^\ell} [\![v]\!]^2}{\|[\![v]\!]\|_{L^2(\Gamma)}} = \|[\![v]\!]\|_{L^2(\Gamma)} \\ \|B_2 v\|_{L^2(\Gamma)} &= \sup_{w\in L^2(\Gamma)} \frac{(B_2 v, w)_{L^2(\Gamma)}}{\|w\|_{L^2(\Gamma)}} \geq \frac{\sum_{l=1}^{L} \int_{\gamma^\ell} [\![\nabla v]\!]_n^2}{\|[\![\nabla v]\!]_n\|_{L^2(\Gamma)}} = \|[\![\nabla v]\!]_n\|_{L^2(\Gamma)}, \end{aligned} \tag{5.15}$$

we obtain that for all $\varepsilon_0 > 0$, there exists a constant $\widetilde{\alpha} > 0$ such that, for all $0 < \varepsilon_1^{(\ell)}, \varepsilon_2^{(\ell)} \leq \varepsilon_0$,

$$\widetilde{\alpha}\|v\|_V^2 \leq a(v,v) + \sum_{\ell=1}^{L} \left(\frac{1}{\varepsilon_1^{(\ell)}} \|B_1 v\|^2_{L^2(\gamma^\ell)} + \frac{1}{\varepsilon_2^{(\ell)}} \|B_2 v\|^2_{L^2(\gamma^\ell)} \right).$$

From Appendix A Theorem 12, it follows that (5.11) has a unique solution $(u_\varepsilon, \lambda_{1,\varepsilon}, \lambda_{2,\varepsilon})$. The following estimation of the error introduced by the perturbations $\varepsilon_1^{(\ell)}$ and $\varepsilon_2^{(\ell)}$ on the solution of the original saddle point problem (5.4) holds.

Lemma 3. *If we assume $u \in H^5(\Omega)$, then there exists a constant $C > 0$ such that*

$$\begin{aligned} \|u - u_\varepsilon\|_V + \|\lambda_1 - \lambda_{1,\varepsilon}\|_{Q_1} + \|\lambda_2 - \lambda_{2,\varepsilon}\|_{Q_2} \\ \leq C \left(\overline{\varepsilon}_1 \|\lambda_1\|_{H_\star^{3/2}(\Gamma)} + \overline{\varepsilon}_2 \|\lambda_2\|_{H_\star^{1/2}(\Gamma)} \right), \end{aligned}$$

where we have defined:

$$\overline{\varepsilon}_1 = \max_{\ell=1,\dots,L} \varepsilon_1^{(\ell)} \qquad \text{and} \qquad \overline{\varepsilon}_2 = \max_{\ell=1,\dots,L} \varepsilon_2^{(\ell)}.$$

Proof. From (5.3) and (5.4), it follows

$$\lambda_1 = (\partial_n \Delta u + \partial_{ntt} u)\,|_\Gamma$$
$$\lambda_2 = (\partial_{tt} u - \Delta u)\,|_\Gamma$$

and, under the assumption $u \in H^5(\Omega)$, it follows

$$\lambda_1 \in W_1^+ = \{w \in L^2(\Gamma) : \|w\|_{Q_1'} = \|w\|_{H_\star^{3/2}(\Gamma)} < \infty\}$$
$$\lambda_2 \in W_2^+ = \{w \in L^2(\Gamma) : \|w\|_{Q_2'} = \|w\|_{H_\star^{1/2}(\Gamma)} < \infty\}.$$

Hence, the thesis follows from Appendix A Remark 12. □

5.1.4 The projected super-penalty formulation

For each patch Ω^i, we assume $p \geq 2$ and we indicate with $\overline{\mathcal{S}^p_{h_i}(\Omega^i)}$ the space trivially obtained extending by zero the elements of $\mathcal{S}^p_{h_i}(\Omega^i)$ over $\Omega \setminus \Omega^i$. Additionally, let us define:

$$V_{i,h} = \operatorname{span}\left\{ B_j^{(i)} \in \overline{\mathcal{S}^p_{h_i}(\Omega^i)} : B_j^{(i)}|_{\partial\Omega} = \partial_n B_j^{(i)}|_{\partial\Omega} = 0 \right\}.$$

This allows us to introduce the following finite dimensional subspace of V,

$$V_h = \left\{ v \in \bigcup_{i=1}^{N} V_{i,h} : v \text{ is continuous in } c^s,\ s = 1, \ldots, S \right\}.$$

Moreover, for each interface γ^ℓ, we denote by Ξ^ℓ the knot vector on γ^ℓ inherited from the slave side. Motivated by the choice of the $p/p-2$ stable pairing in [12], we construct the following isogeometric space $\mathcal{S}^{p-2}_{h,M}(\gamma^\ell)$ on the reduced knot vector $\Xi^\ell_\star$ obtained by removing from Ξ^ℓ the first and last two knots, for reducing the spline degree, and the first and last internal knots, for a further reduction of the dual space dimension:

$$\Xi^\ell = \{\xi_1, \xi_2, \ldots, \xi_{p+1}, \xi_{p+2}, \ldots, \xi_m, \xi_{m+1}, \ldots, \xi_{m+p}, \xi_{m+p+1}\}$$
$$\Xi^\ell_\star = \{\cancel{\xi_1}, \cancel{\xi_2}, \ldots, \xi_{p+1}, \cancel{\xi_{p+2}}, \ldots, \cancel{\xi_m}, \xi_{m+1}, \ldots, \cancel{\xi_{m+p}}, \cancel{\xi_{m+p+1}}\},$$

with

$$\xi_1 = \xi_2 = \ldots = \xi_{p+1} < \xi_{p+2} < \ldots < \xi_m < \xi_{m+1} = \ldots = \xi_{m+p} = \xi_{m+p+1}.$$

Similarly to before, we indicate with $\overline{\mathcal{S}^{p-2}_{h,M}(\gamma^\ell)}$ the space obtained extending by zero over $\Gamma \setminus \gamma^\ell$ the elements of $\mathcal{S}^{p-2}_{h,M}(\gamma^\ell)$. We can now define the discrete counterpart of the Lagrange multiplier spaces as:

$$Q_{1,h} = Q_{2,h} = \bigcup_{\ell=1}^{L} \overline{\mathcal{S}^{p-2}_{h,M}(\gamma^\ell)}.$$

Denoting by h_ℓ the mesh size on γ^ℓ, we can endow $Q_{1,h}$ and $Q_{2,h}$ with the following mesh-dependent norms

$$\|\cdot\|^2_{Q_{1,h}} = \sum_{\ell=1}^{L} \|\cdot\|^2_{Q_{1,h,\ell}} \qquad\qquad \|\cdot\|^2_{Q_{2,h}} = \sum_{\ell=1}^{L} \|\cdot\|^2_{Q_{2,h,\ell}},$$

where we have defined

$$\|\cdot\|^2_{Q_{1,h,\ell}} = h_\ell^{\frac{3}{2}} \|\cdot\|^2_{L^2(\gamma^\ell)} \qquad\qquad \|\cdot\|^2_{Q_{2,h,\ell}} = h_\ell^{\frac{1}{2}} \|\cdot\|^2_{L^2(\gamma^\ell)}.$$

Remark 4. *The inf-sup stabilities are proved on the reduced knot vector $\Xi^\ell_\star$. However, from a numerical standpoint, we retain the optimality of the method without removing the first and last internal knots and in all our examples we directly employ, as the projection spaces, $S_h^{p-2}(\gamma^\ell)$, defined on*

$$\Xi^\ell_{\star\star} = \{\cancel{\xi_1}, \cancel{\xi_2}, \dots, \xi_{p+1}, \xi_{p+2}, \dots, \xi_m, \xi_{m+1}, \dots, \cancel{\xi_{m+p}}, \cancel{\xi_{m+p+1}}\}.$$

Remark 5. *By construction, it holds $V_h \subset V$. Moreover, we have*

$$Q_{1,h} \subset L^2(\Gamma) \subset \left[H^{\frac{3}{2}}_\star(\Gamma)\right]' = Q_1,$$
$$Q_{2,h} \subset L^2(\Gamma) \subset \left[H^{\frac{1}{2}}_\star(\Gamma)\right]' = Q_2.$$

With these definitions at hand, the discretized version of (5.11) reads: find $(u_h, \lambda_{1,h}, \lambda_{2,h}) \in V_h \times Q_h \times Q_h$ such that:

$$\sum_{i=1}^{N} \int_{\Omega^i} \nabla(\nabla u_h) : \nabla(\nabla v_h) + \sum_{\ell=1}^{L} \left(\int_{\gamma^\ell} [\![v_h]\!] \lambda_{1,h} + \int_{\gamma^\ell} [\![\nabla v_h]\!]_n \lambda_{2,h} \right) = (f, v_h) \tag{5.16}$$

$$\sum_{\ell=1}^{L} \left(\int_{\gamma^\ell} [\![u_h]\!] \mu_{1,h} - \varepsilon_1^{(\ell)} \int_{\gamma^\ell} \lambda_{1,h}\mu_{1,h} \right) = 0 \tag{5.17}$$

$$\sum_{\ell=1}^{L} \left(\int_{\gamma^\ell} [\![\nabla u_h]\!]_n \mu_{2,h} - \varepsilon_2^{(\ell)} \int_{\gamma^\ell} \lambda_{2,h}\mu_{2,h} \right) = 0 \tag{5.18}$$

$\forall v_h \in V_h$, $\mu_{1,h} \in Q_{1,h}$ and $\mu_{2,h} \in Q_{2,h}$.
We can now formally eliminate the Lagrange multipliers and recast (5.16) into its primal form. Indeed, we can write:

$$\lambda_{1,h}|_{\gamma^\ell} = \frac{1}{\varepsilon_1^{(\ell)}} \Pi^\ell [\![u_h]\!]$$
$$\lambda_{2,h}|_{\gamma^\ell} = \frac{1}{\varepsilon_2^{(\ell)}} \Pi^\ell [\![\nabla u_h]\!]_n ,$$

where $\Pi^\ell : L^2(\gamma^\ell) \to \mathcal{S}_h^{p-2}(\gamma^\ell)$ denotes the L^2-projection, associated to the interface γ^ℓ, onto the reduced space $\mathcal{S}_{h,M}^{p-2}(\gamma^\ell)$. Finally, employing the previous results and the properties of the L^2-projection, the resulting discretized bilinear form, augmented by suitable penalty terms that weakly enforce the coupling conditions (5.2), reads: find

$u_h \in V_h$ such that:

$$\sum_{i=1}^{N} \int_{\Omega^i} \nabla(\nabla u_h) : \nabla(\nabla v_h) + \\ + \sum_{\ell=1}^{L} \left(\frac{1}{\varepsilon_1^{(\ell)}} \int_{\gamma^\ell} \Pi^\ell [\![u_h]\!] \Pi^\ell [\![v_h]\!] + \frac{1}{\varepsilon_2^{(\ell)}} \int_{\gamma^\ell} \Pi^\ell \left[\![\nabla u_h]\!\right]_n \Pi^\ell \left[\![\nabla v_h]\!\right]_n \right) = (f, v_h) \qquad \forall v_h \in V_h \,. \tag{5.19}$$

5.2 A priori error analysis

In section 5.1.3, we have already provided an estimate for the error introduced by perturbating the original saddle point problem (5.4). In order to state an estimation of the discretization error for the perturbed saddle point problem (5.11), we need to prove the coercivity of the bilinear form a in the discrete kernel

$$K_h = \{v_h \in V_h : \; b_1(v_h, \mu_1) = b_1(v_h, \mu_2) = 0, \; \forall \mu_1, \mu_2 \in Q_h\},$$

and the inf-sup stability condition for both the bilinear forms b_1 and b_2.

5.2.1 Coercivity in the discrete kernel

By observing that for all $h > 0$, $Q_{1,h}$ and $Q_{2,h}$ contain constant functions, it holds $K_h \subset V_0$, for all $h > 0$. Thus, Theorem 7 yields coercivity for the bilinear form a in the discrete kernel K_h, uniformly with respect to the mesh size h.

5.2.2 Discrete inf-sup stability

In this section, in order to apply the convergence results of [10] for singularly perturbed saddle point problems, we prove the inf-sup stability for the bilinear form b_1 between $Q_{1,h}$ and V_h and the inf-sup stability for b_2 between $Q_{2,h}$ and $V_h \cap K_1$.
From now on, C will denote a positive constant, independent of h, possibly different at each occurrence.

Theorem 8. *For h sufficiently small, there exists a constant $\beta_1 > 0$, independent of h, such that*

$$\inf_{\mu_h \in Q_{1,h}} \sup_{v_h \in V_h} \frac{b_1(v_h, \mu_h)}{\|v_h\|_V \|\mu_h\|_{Q_{1,h}}} \geq \beta_1.$$

Proof. The thesis follows by combining Appendix B Theorem 14 with arguments similar to the ones in the proof of [12, Theorem 13] and the ones in the proof of [74, Lemma 1.9]. □

Theorem 9. *For h sufficiently small, there exists a constant $\beta_2 > 0$, independent of h, such that*

$$\inf_{\mu_h \in Q_{2,h}} \sup_{v_h \in V_h \cap K_1} \frac{b_2(v_h, \mu_h)}{\|v_h\|_{V_h} \|\mu_h\|_{Q_{2,h}}} \geq \beta_2.$$

Proof. Fixed $\ell \in \{1, \ldots, L\}$, let us set $k = s(\ell)$. There are four possible cases:

- $\gamma^\ell = \{\mathbf{F}_k(0, \widehat{y}) : \widehat{y} \in [0, 1]\}$,

- $\gamma^\ell = \{\mathbf{F}_k(1,\widehat{y}) : \widehat{y} \in [0,1]\}$,
- $\gamma^\ell = \{\mathbf{F}_k(\widehat{x},0) : \widehat{x} \in [0,1]\}$,
- $\gamma^\ell = \{\mathbf{F}_k(\widehat{x},1) : \widehat{x} \in [0,1]\}$.

We focus only on the first case. Indeed, the other cases can be treated with a similar argument. On the physical interface γ^ℓ, the outward normal $\mathbf{n}_\ell$, w.r.t. the master side, can be expressed in parametric coordinates as

$$\mathbf{n}_\ell \circ \mathbf{F}_k(0,\widehat{y}) = \frac{1}{\|\partial_{\widehat{y}}\mathbf{F}_k(0,\widehat{y})\|}\begin{bmatrix}\partial_{\widehat{y}}\mathbf{F}_{k,2}(0,\widehat{y})\\ -\partial_{\widehat{y}}\mathbf{F}_{k,1}(0,\widehat{y})\end{bmatrix}$$

or

$$\mathbf{n}_\ell \circ \mathbf{F}_k(0,\widehat{y}) = \frac{1}{\|\partial_{\widehat{y}}\mathbf{F}_k(0,\widehat{y})\|}\begin{bmatrix}-\partial_{\widehat{y}}\mathbf{F}_{k,2}(0,\widehat{y})\\ \partial_{\widehat{y}}\mathbf{F}_{k,1}(0,\widehat{y})\end{bmatrix},$$

depending on the orientation of $\mathbf{F}_k$. As before, we focus only on the first case. It holds

$$\begin{aligned}
&J_{\mathbf{F}_k}^{-1}(\mathbf{n}_\ell \circ \mathbf{F}_k(0,\widehat{y})) = \\
&\frac{1}{\det(J_{\mathbf{F}_k})\|\partial_{\widehat{y}}\mathbf{F}_k(0,\widehat{y})\|}\begin{bmatrix}\partial_{\widehat{y}}\mathbf{F}_{k,2}(0,\widehat{y}) & -\partial_{\widehat{y}}\mathbf{F}_{k,1}(0,\widehat{y})\\ -\partial_{\widehat{x}}\mathbf{F}_{k,2}(0,\widehat{y}) & \partial_{\widehat{x}}\mathbf{F}_{k,1}(0,\widehat{y})\end{bmatrix}\begin{bmatrix}\partial_{\widehat{y}}\mathbf{F}_{k,2}(0,\widehat{y})\\ -\partial_{\widehat{y}}\mathbf{F}_{k,1}(0,\widehat{y})\end{bmatrix} = \\
&\frac{1}{\det(J_{\mathbf{F}_k})\|\partial_{\widehat{y}}\mathbf{F}_k(0,\widehat{y})\|}\begin{bmatrix}\partial_{\widehat{y}}\mathbf{F}_{k,2}(0,\widehat{y})^2 + \partial_{\widehat{y}}\mathbf{F}_{k,1}(0,\widehat{y})^2\\ -\partial_{\widehat{x}}\mathbf{F}_k(0,\widehat{y})\cdot\partial_{\widehat{y}}\mathbf{F}_k(0,\widehat{y})\end{bmatrix} = \\
&\frac{1}{\det(J_{\mathbf{F}_k})}\begin{bmatrix}\|\partial_{\widehat{y}}\mathbf{F}_k(0,\widehat{y})\|\\ -\frac{\partial_{\widehat{x}}\mathbf{F}_k(0,\widehat{y})\cdot\partial_{\widehat{y}}\mathbf{F}_k(0,\widehat{y})}{\|\partial_{\widehat{y}}\mathbf{F}_k(0,\widehat{y})\|}\end{bmatrix}.
\end{aligned}$$

For each $v_k = \widehat{v}_k \circ \mathbf{F}_k^{-1} \in V_{k,h}$, it holds

$$\begin{aligned}
\int_{\gamma^\ell} \partial_n v_k \mu &= \int_{\widehat{\gamma}} \nabla\widehat{v}_k(0,\widehat{y}) \cdot J_{\mathbf{F}_k}^{-1}(\mathbf{n}_\ell \circ \mathbf{F}_k(0,\widehat{y}))\widehat{\mu}\det(J_{\mathbf{F}^{(k)}})d\widehat{y}\\
&= \int_{\widehat{\gamma}} \left[\rho_\ell(\widehat{y})\partial_{\widehat{x}}\widehat{v}_k(0,\widehat{y}) + \sigma_\ell(\widehat{y})\partial_{\widehat{y}}\widehat{v}_k(0,\widehat{y})\right]\widehat{\mu}d\widehat{y},
\end{aligned} \tag{5.20}$$

where we have set

$$\begin{aligned}
\rho_\ell(\widehat{y}) &= \|\partial_{\widehat{y}}\mathbf{F}_k(0,\widehat{y})\|\\
\sigma_\ell(\widehat{y}) &= -\frac{\partial_{\widehat{x}}\mathbf{F}_k(0,\widehat{y})\cdot\partial_{\widehat{y}}\mathbf{F}_k(0,\widehat{y})}{\|\partial_{\widehat{y}}\mathbf{F}_k(0,\widehat{y})\|}.
\end{aligned}$$

If we restrict ourselves to $v_k \in Y$, with

$$Y_k = \left\{v_k = \widehat{v}_k \circ \mathbf{F}_k^{-1} \in V_{k,h} \cap K_1 : \partial_{\widehat{y}}\widehat{v}_k(0,\widehat{y}) = 0,\ \forall \widehat{y} \in [0,1]\right\},$$

equation (5.20) reduces to

$$\int_{\gamma^\ell} \partial_n v_k \mu = \int_{\widehat{\gamma}} \rho_\ell(\widehat{y})\partial_{\widehat{x}}\widehat{v}_k(0,\widehat{y})\widehat{\mu}d\widehat{y}.$$

We observe that ρ_ℓ is smooth except at the mesh line, where it is only C^{p-3}, it is bounded by above and below and it is h-independent. Moreover, it is straightforward to see that for each

$$\widehat{w} \in \mathcal{S}^p_{h_\ell}(\widehat{\gamma}) : \widehat{w}(0) = \widehat{w}'(0) = \widehat{w}(1) = \widehat{w}'(1) = 0,$$

there exists $v_k \in Y_k$ such that $\partial_{\widehat{x}} \widehat{v}_k(0, \cdot) = \widehat{w}$. Consequently, the thesis can be proven with an argument similar to the proof of Theorem 8. □

5.2.3 Error estimates

Thanks to Theorem 7, 8 and 9, we are in the hypothesis of Appendix A Theorem 13, hence there exists a constant $C > 0$, independent of h, such that

$$\begin{aligned}
&\|u_\varepsilon - u_h\|_V + \|\lambda_{1,\varepsilon} - \lambda_{1,h}\|_{Q_{1,h}} + \|\lambda_{2,\varepsilon} - \lambda_{2,h}\|_{Q_{2,h}} \\
&\leq C \Bigg(\inf_{v_h \in V_h} \|u_\varepsilon - v_h\|_V + \inf_{\mu_{1,h} \in Q_{1,h}} \left\{ \|\lambda_{1,\varepsilon} - \mu_{1,h}\|_{Q_{1,h}} + \sqrt{\overline{\varepsilon}_1} \|\lambda_{1,\varepsilon} - \mu_{1,h}\|_{L^2(\Gamma)} \right\} + \\
&\qquad \inf_{\mu_{2,h} \in Q_{2,h}} \left\{ \|\lambda_{2,\varepsilon} - \mu_{2,h}\|_{Q_{2,h}} + \sqrt{\overline{\varepsilon}_2} \|\lambda_{2,\varepsilon} - \mu_{2,h}\|_{L^2(\Gamma)} \right\} \Bigg). \qquad (5.21)
\end{aligned}$$

Theorem 10. *Let q be an integer such that $2 \leq q \leq p+1$. If $u \in H^5(\Omega) \cap H^q(\Omega)$, then there exists a constant $C > 0$, independent of h, such that*

$$\begin{aligned}
&\|u - u_h\|_V + \|\lambda_1 - \lambda_{1,h}\|_{Q_{1,h}} + \|\lambda_2 - \lambda_{2,h}\|_{Q_{2,h}} \\
&\qquad \leq C \Bigg[\sum_{i=1}^N h_i^{q-2} \|u\|_{H^q(\Omega^i)} + \sum_{\ell=1} h_\ell^{q-2} (h_\ell^{3/2} + \sqrt{\overline{\varepsilon}_1}) \|\lambda_{1,\varepsilon}\|_{H^{q-2}(\gamma^\ell)} + \\
&\qquad \sum_{\ell=1} h_\ell^{q-2} (h_\ell^{1/2} + \sqrt{\overline{\varepsilon}_2}) \|\lambda_{2,\varepsilon}\|_{H^{q-2}(\gamma^\ell)} + \overline{\varepsilon}_1 \|\lambda_1\|_{H^{3/2}_\star(\Gamma)} + \overline{\varepsilon}_2 \|\lambda_2\|_{H^{1/2}_\star(\Gamma)} \Bigg].
\end{aligned}$$

Proof. We start by observing that

$$\|u - u_h\|_V \leq \|u - u_\varepsilon\|_V + \|u_\varepsilon - u_h\|_V. \qquad (5.22)$$

For the estimation of $\|u_\varepsilon - u_h\|_V$ we can rely on (5.21). Firstly, it holds

$$\inf_{v_h \in V_h} \|u_\varepsilon - v_h\|_V = \|u - u_\varepsilon\|_V + \inf_{v_h \in V_h} \|u - v_h\|_V. \qquad (5.23)$$

Further, recalling the definitions of $Q_{1,h}$ and $Q_{2,h}$, we have

$$\begin{aligned}
\|\lambda_{1,\varepsilon} - \mu_{1,h}\|_{Q_{1,h}} + \sqrt{\overline{\varepsilon}_1} \|\lambda_{1,\varepsilon} - \mu_{1,h}\|_{L^2(\Gamma)} &= \sum_{\ell=1} (h_\ell^{3/2} + \sqrt{\overline{\varepsilon}_1}) \|\lambda_{1,\varepsilon} - \mu_{1,h}\|_{L^2(\gamma^\ell)}, \\
\|\lambda_{2,\varepsilon} - \mu_{2,h}\|_{Q_{2,h}} + \sqrt{\overline{\varepsilon}_2} \|\lambda_{2,\varepsilon} - \mu_{2,h}\|_{L^2(\Gamma)} &= \sum_{\ell=1} (h_\ell^{1/2} + \sqrt{\overline{\varepsilon}_2}) \|\lambda_{2,\varepsilon} - \mu_{2,h}\|_{L^2(\gamma^\ell)}.
\end{aligned} \qquad (5.24)$$

From standard approximation results for splines, see [5], we get

$$\begin{aligned}
\inf_{v_h \in V_h} \|u - v_h\|_V &\leq C \sum_{i=1}^{N} h_i^{q-2} \|u\|_{H^q(\Omega^i)}, \\
\inf_{\mu_{1,h} \in Q_{1,h}} \sum_{\ell=1} (h_\ell^{3/2} + \sqrt{\bar{\varepsilon}_1}) \|\lambda_{1,\varepsilon} - \mu_{1,h}\|_{L^2(\gamma^\ell)} &\leq C \sum_{\ell=1} h_\ell^{q-2} (h_\ell^{3/2} + \sqrt{\bar{\varepsilon}_1}) \|\lambda_{1,\varepsilon}\|_{H^{q-2}(\gamma^\ell)}, \\
\inf_{\mu_{2,h} \in Q_{2,h}} \sum_{\ell=1} (h_\ell^{1/2} + \bar{\varepsilon}_2) \|\lambda_{2,\varepsilon} - \mu_{2,h}\|_{L^2(\gamma^\ell)} &\leq C \sum_{\ell=1} h_\ell^{q-2} (h_\ell^{1/2} + \sqrt{\bar{\varepsilon}_2}) \|\lambda_{2,\varepsilon}\|_{H^{q-2}(\gamma^\ell)}.
\end{aligned} \tag{5.25}$$

Finally, combining Lemma 3 with (5.21), (5.22), (5.23), (5.24) and (5.25), we get the thesis. □

5.2.4 On the choice of penalty parameters

It is well-known that the penalized problem (5.19) is variationally consistent only in the limit $\varepsilon_1^{(\ell)} = \varepsilon_2^{(\ell)} \to 0$ $\ell = 1, \dots, L$. On the other hand, the well-posedness of this problem is robust with respect to the choice of the parameters $\varepsilon_1^{(\ell)}$ and $\varepsilon_2^{(\ell)}$. Therefore, the proposed methodology will not suffer from locking for any choice of penalty values. As a consequence, $\varepsilon_1^{(\ell)}$ and $\varepsilon_2^{(\ell)}$ can be chosen solely to guarantee the optimal accuracy of the method.

Remark 6. *A clear trade-off of this choice is the negative impact on the conditioning of the resulting system matrix. A possible remedy based on an ad-hoc preconditioner will be discussed in a later section. Another drawback consists in the loss of significant digits due to the (potentially big) difference in magnitude between the penalty contribution and the internal stiffness. For this reason (amongst other which will be pointed out in the rest of manuscript), we advise to use this method in combination with splines of degree $p = 2, 3$, as these round-off errors occur below a tolerance threshold of significance to most engineering applications.*

Inspired by the method proposed in [34] in the context of Kirchhoff-Love shells, we want to develop a fully parameter-free penalty method. To this end, we scale the deflection and rotation penalty parameters by the physical constants, the local mesh size and the geometry as:

$$\begin{aligned}
\frac{1}{\varepsilon_1^{(\ell)}} &= \text{meas}(\gamma^\ell)^{\theta-1} \frac{Et}{(h_\ell)^\theta (1-\nu^2)} \\
\frac{1}{\varepsilon_2^{(\ell)}} &= \text{meas}(\gamma^\ell)^{\theta-1} \frac{Et^3}{12(h_\ell)^\theta (1-\nu^2)},
\end{aligned} \tag{5.26}$$

where the exponent θ is chosen to ensure the optimal convergence of the method with respect to the degree p of the underlying discretization. Note that all of these parameters are known and depend only on the problem definition, meaning that no user-defined factor is required. We highlight that our choice is based on the fact that the perturbations introduced in (5.11) cannot be "big" compared to the accuracy with which we want to solve the original problem and the estimate provided in Theorem 10 guides the choice of θ. Moreover, as we want to recover optimal rates of convergence for the error, the exponent θ must be a function of the underlying splines degree p.
From the numerical experiments conducted thus far, as expected from Theorem 10, the scaling factor $\theta = p - 1$ in (5.26) is necessary to ensure optimal convergence of

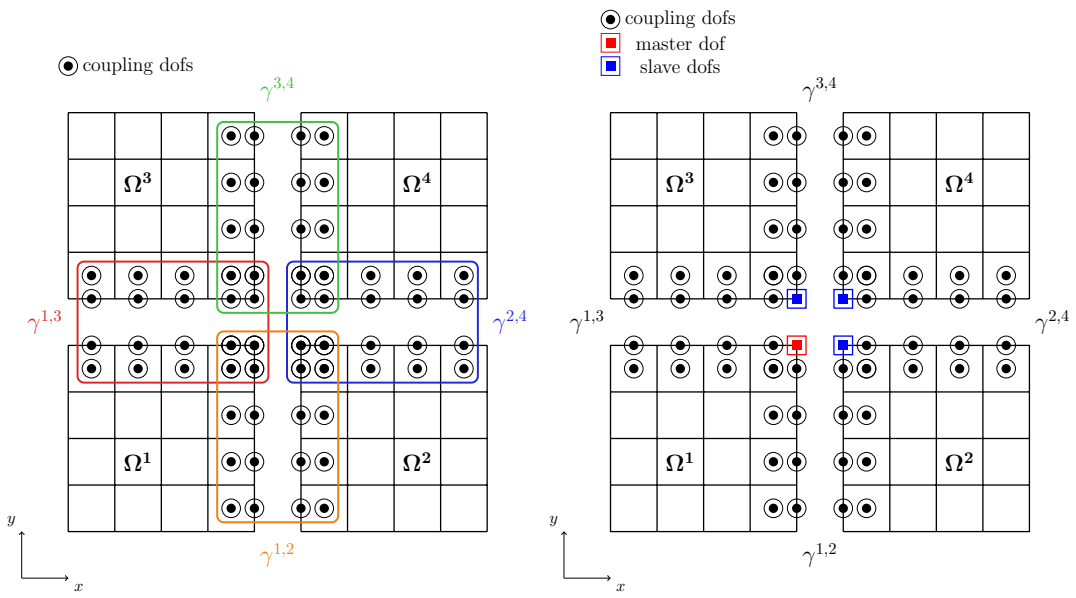

(A) B-splines involved in the computation of the coupling terms, where each coloured box contains the dofs associated to the corresponding coupling interface $\gamma^{k,\ell}$.

(B) Cross-point modification, where the black dots represent the untouched control points associated to basis functions that give non-zero contribution to the interface coupling. The squares are the control variables used to impose the C^0 constraint, where we choose a master node (the red one) and the rest are labelled as slave nodes (the blue ones) and are eliminated from the system, see Algorithm 2.

FIGURE 5.2: Example of the dofs involved in the computation of the coupling integrals and cross-point modification in a four patches setup.

the method in the H^2 norm, whereas for a scaling of $\theta = p$ we observed optimality in the H^2 and H^1 norms. Finally, a factor of $\theta = p + 1$ provides optimality in the H^2, H^1 and L^2 norms. If not stated otherwise, we will use $\theta = p + 1$ in all our numerical examples.

5.3 Cross-points modification

In the literature of mortar methods, it is well-known that the treatment of cross-points requires extra considerations, see [22] and references therein for a discussion in the context of mortar coupling of isogeometric multi-patches. Analogously, our method also inherits the need for a cross-points modification. Indeed, in order to retain optimality of the method, a linear constraint must be imposed to the control variables meeting at the cross-point to ensure C^0-continuity. An example with four patches is depicted in Figure 5.2, where in Figure 5.2a we depict the dofs associated to each coupling interface and in Figure 5.2b we visualize the imposition of the constraint. To explain the procedure, let us start from the following unconstrained system of equations:

$$\mathcal{A}\boldsymbol{u}_h = \boldsymbol{f}\,. \tag{5.27}$$

Now, the constraint can be incorporated easily into the standard linear system in a fully algebraic fashion, where a possible implementation is presented in Algorithm 2.

Algorithm 2 Algorithm for applying a C^0 constraint at a cross-point.

1: **procedure** APPLY_C^0_CONSTRAINT(vector of dofs at cross-points $\boldsymbol{u}_{\text{cp}}$)
2: Label one dof in $\boldsymbol{u}_{\text{cp}}$ as master
3: Label the remaining dofs in $\boldsymbol{u}_{\text{cp}}$ as slaves
4: Build the rectangular matrix $\mathcal{C}$ representing the linear master-slaves constraints (see (5.28))
5: Solve the reduced system $\widehat{\mathcal{A}}\widehat{\boldsymbol{u}}_h = \widehat{\boldsymbol{f}}$, where $\widehat{\mathcal{A}} = \mathcal{C}^\top \mathcal{A}\mathcal{C}$ and $\widehat{\boldsymbol{f}} = \mathcal{C}^\top \boldsymbol{f}$
6: Recover the solution $\boldsymbol{u}_h$ from $\boldsymbol{u}_h = \mathcal{C}\widehat{\boldsymbol{u}}_h$
7: **end procedure**

The construction of the rectangular matrix $\mathcal{C}$ is best explained with an example. Let us assume that the dofs at the cross-point are numbered as $\boldsymbol{u}_{\text{cp}} = [u_{\text{cp1}}\, u_{\text{cp2}}\, u_{\text{cp3}}\, u_{\text{cp4}}]$. Now, without loss of generality, we pick u_{cp1} as the master control point and the rest as slave nodes. Then, the constraint can be expressed via the matrix $\mathcal{C}$ as follows:

$$\boldsymbol{u}_h = \begin{bmatrix} u_1 \\ \vdots \\ u_{\text{cp1}} \\ \vdots \\ u_{\text{cp2}} \\ \vdots \\ u_{\text{cp3}} \\ \vdots \\ u_{\text{cp4}} \\ \vdots \\ u_{\text{ndof}} \end{bmatrix} = \begin{bmatrix} 1 & 0 & 0 & 0 & 0 \\ \vdots & & \ddots & & \\ 0 & 0\ldots & 1 & 0\ldots & 0 \\ \vdots & & \ddots & & \\ 0 & 0\ldots & 1 & 0\ldots & 0 \\ \vdots & & & \ddots & \\ 0 & 0\ldots & 1 & 0\ldots & 0 \\ \vdots & & & \ddots & \\ 0 & 0\ldots & 1 & 0\ldots & 0 \\ \vdots & & & & \ddots \\ 0 & 0 & 0 & 0 & 1 \end{bmatrix} \cdot \begin{bmatrix} u_1 \\ \vdots \\ u_{\text{cp1}} \\ \vdots \\ u_{\text{ndof}} \end{bmatrix} = \mathcal{C}\widehat{\boldsymbol{u}}_h\,, \tag{5.28}$$

where ndof denotes the total number of degrees-of-freedom in the system. This procedure allows to eliminate the unknowns associated to the slave nodes from the system.

5.4 A nested preconditioner based on the Schur Complement Reduction

In this section, following the notation introduced in [59] and building upon the work presented in [48, 49] in the context of elastodynamics and hemodynamics, we present an efficient way to mitigate the detrimental effects on the condition number stemming from our choice of super-penalty parameters. This preconditioner is based on the approximate solution of the block factorization of the system matrix known as Schur Complement Reduction (SCR). We remind the reader that before performing the algorithm described in the following, we apply a symmetric diagonal scaling to the system matrix.

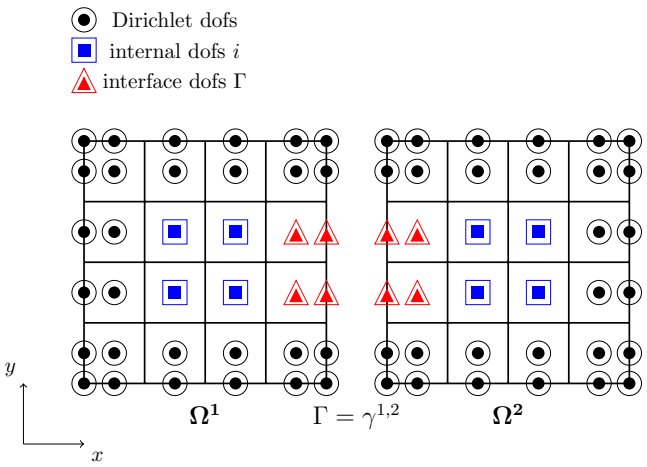

FIGURE 5.3: Example of reordering of the dofs in a two patches setup, discretized by B-splines of degree $p = 2$, associated to the block system matrix $\mathcal{A}$.

5.4.1 The Schur Complement Reduction

We begin by reordering the matrix $\mathcal{A} \in \mathbb{R}^{\text{ndof}\times\text{ndof}}$ stemming from (5.19) in blocks as follows:

$$\mathcal{A} = \begin{bmatrix} \mathbf{A}_{i,i} & \mathbf{B}_{i,\Gamma} \\ \mathbf{B}_{i,\Gamma}^\top & \mathbf{C}_{\Gamma,\Gamma} \end{bmatrix},$$

where the subscripts i and Γ refer to internal and interface dofs, respectively, where an example is depicted in Figure 5.3. Let us remark that $\mathbf{A}_{i,i}$ is a block-diagonal matrix where every block is the matrix associated to an homogeneous Dirichlet problem (fully clamped) on the corresponding patch Ω^i. Moreover, with a slight abuse of notation, we assume that, if needed, $\mathcal{A}$ has already been modified to account for the constraints related to the cross-points introduced in the previous section.

Now, we can perform the following block factorization of $\mathcal{A}$:

$$\mathcal{A} = \mathcal{L}\mathcal{D}\mathcal{U} = \begin{bmatrix} \mathbf{I} & \mathbf{0} \\ \mathbf{B}_{i,\Gamma}^\top \mathbf{A}_{i,i}^{-1} & \mathbf{I} \end{bmatrix} \begin{bmatrix} \mathbf{A}_{i,i} & \mathbf{0} \\ \mathbf{0} & \mathbf{S}_{\Gamma,\Gamma} \end{bmatrix} \begin{bmatrix} \mathbf{I} & \mathbf{A}_{i,i}^{-1}\mathbf{B}_{i,\Gamma} \\ \mathbf{0} & \mathbf{I} \end{bmatrix},$$

where we have introduced the Schur complement $\mathbf{S}_{\Gamma,\Gamma} := \mathbf{C}_{\Gamma,\Gamma} - \mathbf{B}_{i,\Gamma}^\top \mathbf{A}_{i,i}^{-1}\mathbf{B}_{i,\Gamma}$ and $\mathbf{I}$ denotes the identity matrix. Multiplying by $\mathcal{L}$ on both sides we get:

$$\begin{aligned} \begin{bmatrix} \mathbf{A}_{i,i} & \mathbf{B}_{i,\Gamma} \\ \mathbf{0} & \mathbf{S}_{\Gamma,\Gamma} \end{bmatrix} \begin{bmatrix} \mathbf{x}_i \\ \mathbf{x}_\Gamma \end{bmatrix} &= \begin{bmatrix} \mathbf{I} & \mathbf{0} \\ \mathbf{B}_{i,\Gamma}^\top \mathbf{A}_{i,i}^{-1} & \mathbf{I} \end{bmatrix}^{-1} \begin{bmatrix} \mathbf{r}_i \\ \mathbf{r}_\Gamma \end{bmatrix} \\ &= \begin{bmatrix} \mathbf{I} & \mathbf{0} \\ -\mathbf{B}_{i,\Gamma}^\top \mathbf{A}_{i,i}^{-1} & \mathbf{I} \end{bmatrix} \begin{bmatrix} \mathbf{r}_i \\ \mathbf{r}_\Gamma \end{bmatrix} \\ &= \begin{bmatrix} \mathbf{r}_i \\ \mathbf{r}_\Gamma - \mathbf{B}_{i,\Gamma}^\top \mathbf{A}_{i,i}^{-1}\mathbf{r}_i \end{bmatrix}. \end{aligned} \tag{5.29}$$

We highlight that, up to this point, this factorization is performed in exact algebra. Then, from (5.29), we can solve for $\mathbf{x}$ in a segregated fashion by exploiting Algorithm 3.

Algorithm 3 SCR algorithm

1: **procedure** SOLUTION OF $\mathcal{A}\mathbf{x} = \mathbf{r}$ BASED ON SCR
2: Solve for an intermediate solution $\hat{\mathbf{x}}_i$

$$\mathbf{A}_{i,i}\hat{\mathbf{x}}_i = \mathbf{r}_i \tag{5.30}$$

3: Update the interface residual $\mathbf{r}_\Gamma = \mathbf{r}_\Gamma - \mathbf{B}_{i,\Gamma}^\top \hat{\mathbf{x}}_i$
4: Solve for the interface solution $\mathbf{x}_\Gamma$ from the Schur equation

$$\mathbf{S}_{\Gamma,\Gamma}\mathbf{x}_\Gamma = \mathbf{r}_\Gamma \tag{5.31}$$

5: Update the internal residual $\mathbf{r}_i = \mathbf{r}_i - \mathbf{B}_{i,\Gamma}\mathbf{x}_\Gamma$
6: Solve for the internal solution $\mathbf{x}_i$ from

$$\mathbf{A}_{i,i}\mathbf{x}_i = \mathbf{r}_i \tag{5.32}$$

7: **end procedure**

Clearly, the Schur complement $\mathbf{S}_{\Gamma,\Gamma}$ is in practice expensive and often infeasible to compute explicitly. A way around this issue is given in Algorithm 4, where we summarize a matrix-free procedure to apply the Schur complement to a vector.

Algorithm 4 Algorithm for applying the Schur complement to a vector

1: **procedure** APPLICATION OF $\mathbf{S}_{\Gamma,\Gamma}$ TO A VECTOR $\mathbf{x}_\Gamma$
2: Compute the matrix-vector multiplication $\hat{\mathbf{x}}_\Gamma = \mathbf{C}_{\Gamma,\Gamma}\mathbf{x}_\Gamma$
3: Compute the matrix-vector multiplication $\overline{\mathbf{x}}_\Gamma = \mathbf{B}_{i,\Gamma}\mathbf{x}_\Gamma$
4: Solve for an intermediate solution $\tilde{\mathbf{x}}_\Gamma$ from

$$\mathbf{A}_{i,i}\tilde{\mathbf{x}}_\Gamma = \overline{\mathbf{x}}_\Gamma \tag{5.33}$$

5: Compute the matrix-vector multiplication $\overline{\mathbf{x}}_\Gamma = \mathbf{B}_{i,\Gamma}^\top \tilde{\mathbf{x}}_\Gamma$
6: Return $\hat{\mathbf{x}}_\Gamma - \overline{\mathbf{x}}_\Gamma$
7: **end procedure**

Remark 7. *As noted in [48], the cost of the preconditioner is often dominated by the solution of the Schur system* (5.31)*. To reduce the computational burden of this step, we use as preconditioner a coarse approximation of the Schur complement obtained by applying only a few iterations of GMRES to* $\mathbf{A}_{i,i}$ *for assembling* $\tilde{\mathbf{S}}_{\Gamma,\Gamma} = \mathbf{C}_{\Gamma,\Gamma} - \mathbf{B}_{i,\Gamma}^\top \tilde{\mathbf{A}}_{i,i}^{-1}\mathbf{B}_{i,\Gamma}$*, where for efficiency we leverage again the FD algorithm. Although this choice works reasonably well for our numerical examples, we remark that more research is needed to find a robust (both in* h *and* p*) and scalable preconditioner for the Schur complement and, more in general, for fourth-order PDEs.*

5.4.2 Nested block preconditioner strategy based on SCR

The main idea presented in [48] is to combine the robustness of the SCR factorization with the ease of application of a block preconditioners (such as SIMPLE or variants thereof [59]). Indeed, we can build a preconditioner $\mathcal{P}_{\text{SCR}}$ based on an approximate factorization of (5.29), where equations (5.30), (5.31) and (5.32) are solved within a prescribed tolerance. Given that $\mathcal{P}_{\text{SCR}}$ changes its algebraic definition at every iteration, following [48], we employ a flexible GMRES algorithm (FGMRES) as the iterative method for the most outer solve $\mathcal{A}\mathbf{x} = \mathbf{r}$. At each iteration of FGMRES, we

can apply the preconditioner $\mathcal{P}_{\text{SCR}}$ via Algorithm 3, where this entails the solution of the blocks $\mathbf{A}_{i,i}$ and $\mathbf{S}_{\Gamma,\Gamma}$. This part of the algorithm is denoted as intermediate solver. Last, since we do not assemble the Schur complement explicitly, but we apply its action on a vector through Algorithm 4, we perform a final solve for $\mathbf{A}_{i,i}$ in (5.33), denoted as inner solver. The final performance of the preconditioner is therefore determined by the prescribed tolerances for the outer, intermediate and inner layers, respectively, where the objective is finding a good balance between the computational cost and the robustness of the method. In the following, we denote the aforementioned tolerances by η_o, η_t and η_n for the outer, intermediate and inner layers, respectively.

A preconditioner based on the Fast Diagonalization (FD) algorithm

Since each outer iteration of the nested preconditioner is based on the solution of three systems involving the block $\mathbf{A}_{i,i}$, an efficient and robust preconditioner for this block is required. In this work, we extend the isogeometric preconditioner studied in [62, 57], based on the Fast Diagonalization algorithm, to the Kirchhoff plate problem. In the following, we focus our derivation on the single-patch case. The extension to the multi-patch case is straightforward by construction, since the block $\mathbf{A}_{i,i}$ is formed by disjoint sub-blocks associated to each patch Ω^i.

Now, exploiting the tensor product structure of the B-spline basis at the patch level, let us introduce the preconditioner $\mathcal{P}_{\text{FD}}$ in Kronecker form as:

$$\mathcal{P}_{\text{FD}} = M_1 \otimes K_2 + K_1 \otimes M_2 \,, \tag{5.34}$$

where M_k and K_k with $k = 1, 2$ refer to the one-dimensional, parametric mass and hessian matrices associated to the k-th parametric dimension, respectively. They can be expanded as follows:

$$\begin{aligned} [M_k]_{i,j} &= \int_0^1 b_{i,p}(\eta_k)\, b_{j,p}(\eta_k)\ \mathrm{d}\eta_k \\ [K_k]_{i,j} &= \int_0^1 b''_{i,p}(\eta_k)\, b''_{j,p}(\eta_k)\ \mathrm{d}\eta_k \,, \end{aligned}$$

where b indicates the univariate B-spline basis functions introduced in Chapter 2. Then, analogously to [56], we partially include the geometry and physical coefficients inside the preconditioner. In particular, let us denote by $\mathfrak{C}$ the following function:

$$\mathfrak{C}(\boldsymbol{\eta}) = D \left(\left|\left| J_{\mathbf{F}}^{-1} \right|\right|_2 \right)^4 |\det\ (J_{\mathbf{F}})| \,,$$

where we recall that $J_{\mathbf{F}}$ represents the jacobian of the B-spline parametrization $\mathbf{F}$ and D is the flexural stiffness of the plate. Now, as explained in [56, Appendix A.3], we perform a separation of variables on $\mathfrak{C}$ such that we can write:

$$\mathfrak{C}(\boldsymbol{\eta}) \approx \widetilde{\mathfrak{C}}(\boldsymbol{\eta}) = \begin{bmatrix} \omega_1(\eta_1)\tau_2(\eta_2) & 0 \\ 0 & \tau_1(\eta_1)\omega_2(\eta_2) \end{bmatrix} ,$$

where this matrix is evaluated at each quadrature point. With this, we can modify the preconditioner given in (5.34) to partially account for the geometry and coefficients information as follows:

$$\mathcal{P}_{\text{FD}}^{\mathbf{F}} = \widetilde{M}_1 \otimes \widetilde{K}_2 + \widetilde{K}_1 \otimes \widetilde{M}_2 \,, \tag{5.35}$$

where

$$\left[\widetilde{M}_k\right]_{i,j} = \int_0^1 \omega_k(\eta_k) b_{i,p}(\eta_k)\, b_{j,p}(\eta_k)\, \mathrm{d}\eta_k$$
$$\left[\widetilde{K}_k\right]_{i,j} = \int_0^1 \tau_k(\eta_k) b''_{i,p}(\eta_k)\, b''_{j,p}(\eta_k)\, \mathrm{d}\eta_k\,.$$

Finally, each iteration of the iterative solver requires the solution of the following system:

$$\mathcal{P}^{\mathbf{F}}_{\mathrm{FD}} s = r\,, \tag{5.36}$$

where r denotes the current residual. Due to the tensor structure of the preconditioner, we can rewrite (5.36) as a Sylvester matrix equation [66]:

$$\widetilde{M}_2 S \widetilde{K}_1 + \widetilde{K}_2 S \widetilde{M}_1 = R\,,$$

where $s = \mathrm{vec}(S)$ and $r = \mathrm{vec}(R)$.

Remark 8. *Let us recall that for any matrix $Z \in \mathbb{R}^{r\times c}$ the operator* $\mathrm{vec}(Z)$ *gives as output the vector $z \in \mathbb{R}^{rc}$ formed by stacking the columns of Z.*

Let us now consider the generalized eigendecomposition of the matrix pencils $(\widetilde{K}_1, \widetilde{M}_1)$ and $(\widetilde{K}_2, \widetilde{M}_2)$, respectively, as:

$$\begin{aligned}\widetilde{K}_1 U_1 &= \widetilde{M}_1 U_1 D_1\\ \widetilde{K}_2 U_2 &= \widetilde{M}_2 U_2 D_2\,.\end{aligned} \tag{5.37}$$

Here, D_1 and D_2 are diagonal matrices containing the eigenvalues of $\widetilde{M}_1^{-1}\widetilde{K}_1$ and $\widetilde{M}_2^{-1}\widetilde{K}_2$, respectively. Further, U_1 and U_2 are defined as:

$$\begin{aligned}U_1^\top \widetilde{M}_1 U_1 &= \mathbf{I}\\ U_2^\top \widetilde{M}_2 U_2 &= \mathbf{I}\,.\end{aligned}$$

With these definitions at hand, we can rewrite (5.35) in Kronecker form as:

$$(U_1 \otimes U_2)^{-\top} (D_1 \otimes \mathbf{I} + \mathbf{I} \otimes D_2) (U_1 \otimes U_2)^{-1} s = r\,,$$

where the preconditioner can be efficiently applied via Algorithm 5.

Algorithm 5 FD method for applying $\mathcal{P}^{\mathbf{F}}_{\mathrm{FD}}$

1: **procedure** UPDATE OF THE ITERATION RESIDUAL VIA THE FD METHOD
2: Compute the generalized eigendecomposition in (5.37)
3: Compute the intermediate result $\tilde{r} = (U_1 \otimes U_2)^\top r$
4: Compute the intermediate residual $\tilde{s} = (D_1 \otimes \mathbf{I} + \mathbf{I} \otimes D_2)^{-1} \tilde{r}$
5: Return $s = (U_1 \otimes U_2)\, \tilde{s}$
6: **end procedure**

Remark 9. *We remark that the application of the nested preconditioner $\mathcal{P}_{SCR}$ combined with $\mathcal{P}^{\mathbf{F}}_{FD}$ can be implemented in a fully matrix-free framework. Furthermore, although not investigated in this work, the patch-wise block structure of $\mathbf{A}_{i,i}$ could be further exploited for parallelization.*

For the sake of conciseness, we do not provide here further details of the FD algorithm, but we refer to [62, 57] for a thorough theoretical and numerical investigation of the method in the scope of isogeometric analysis.

5.5 Numerical Examples

In this section we assess the performance of the proposed coupling method with several numerical examples defined on multi-patch geometries. All the numerical experiments presented in the following have been implemented in the open-source and free Octave/Matlab package *GeoPDEs* [70], a software designed for the solution of partial differential equations in the context of isogeometric analysis.

5.5.1 A four patches example with non-matching curved interfaces

In this example we consider the computational domain $\Omega = [0,2] \times [0,2]$ depicted in Figure 5.4, split into four subdomains Ω^i. We remark that all meshes are non-conforming at every coupling interface, as the irrational factor $\sqrt{2}/100$ has been used to shift the interface knots. The body source and boundary data are computed such that the exact solution is smooth and it reads:

$$u^{\text{ex}} = \sin(\pi x)\cos(\pi x)\,.$$

This setup is used to test the robustness of our method in the case of severe non-matching discretizations and with respect to the problem parameters. To this end, we present the convergence results for all combinations of Young's moduli $E = [10^4, 10^8]\,[Pa]$ and thickness of the plate $t = [0.05, 0.01, 0.005]\,[m]$, where we set the Poisson's ratio $\nu = 0\,[-]$. We compare our method to a classical penalty approach, where we set $\frac{1}{\varepsilon_1^{(\ell)}} = \frac{1}{\varepsilon_2^{(\ell)}} = 10^4 E, \ell = 1, \dots, L$, and to a choice of penalty parameters scaled with respect to the physical parameters as proposed in [34]. In particular, they read:

$$\begin{aligned}\frac{1}{\varepsilon_1^{(\ell)}} &= \delta \frac{Et}{h_\ell(1-\nu^2)} \\ \frac{1}{\varepsilon_2^{(\ell)}} &= \delta \frac{Et^3}{12h_\ell(1-\nu^2)}\,,\end{aligned}$$

where the user-defined parameter $\delta = 10^3$ is chosen. From the results in Figure 5.5, we observe that the projection strategy shows robustness with respect to the input parameters and allows for an easy treatment of locking phenomena, where optimal convergence rates are attained also for very coarse meshes.

In Figure 5.6 the convergence behaviour of the error measured in the H^2 norm with and without the imposition of the C^0 constraint at the cross-point is plotted. We observe that the loss of accuracy hinders the convergence for $p = 3, 4$, whereas the expected optimal rates of convergence are recovered in all cases when the linear constraint is imposed to the system. This is further highlighted in Figure 5.7, where the element-wise H^2 error is depicted for a discretization of degree $p = 4$, without and with the constraint, respectively. On one hand, we remark how the error is concentrated and much higher in the elements around the cross-point, spoiling the optimal convergence, when the constraint is not imposed. On the other hand, with the linear constraint, we recover optimal convergence properties of the method.

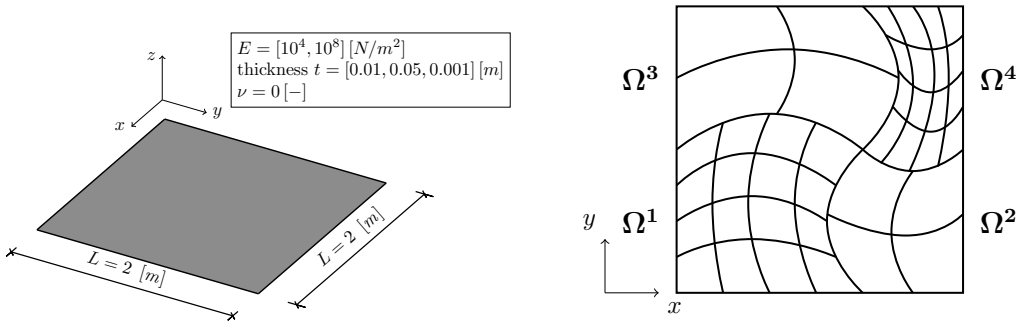

(A) Geometry setup and physical parameters. (B) Initial discretization.

FIGURE 5.4: Problem setup and initial multi-patch non-conforming discretization for the curved four patches example.

Finally, for this example we also analyze the performance of the nested preconditioner. In Table 5.1 we report the iterations needed by the external solver and in brackets the average number of intermediate iterations, for several degrees of the discretization $p = 2, 3$, and we compare it with a classical diagonally preconditioned conjugate gradient (PCG), a PCG where an incomplete LU (ILU) is used as preconditioner and a GMRES preconditioned with ILU. All the results refer to a global tolerance η_o of 10^{-10} and, for the nested SCR-FGMRES strategy, the intermediate and inner tolerances η_t and η_n are set to 10^{-6}. Further, the Schur complement is preconditioned by an approximation $\tilde{\mathbf{S}}_{\Gamma,\Gamma}$ obtained with a maximum of 6 iterations of GMRES. For the sake of completeness, we perform the same test with the choice of penalty parameters studied in [34]. The results are summarized in Table 5.2, where we observe no substantial difference regarding the iterations needed to solve the system compared to the case where our choice of parameters is employed. This suggests that the proposed preconditioner is robust with respect to the penalty factors and it is also suitable to precondition systems stemming from other penalty approaches.

	256 el.	1024 el.	4096 el.	16384 el.
Diagonally scaled PCG	792	953	–	–
PCG with ILU	111	980	–	–
GMRES with ILU	63	174	402	–
Nested SCR-FGMRES	3 (21.6/3.3/20.3)	3 (36/6/30.3)	4 (51/17.5/40.7)	6 (66.5/51/51.3)

(A) $p = 2$.

	256 el.	1024 el.	4096 el.	16384 el.
Diagonally scaled PCG	921	–	–	–
PCG with ILU	53	221	–	–
GMRES with ILU	35	73	–	–
Nested SCR-FGMRES	3 (26.6/4/24)	3 (41.6/9/35)	4 (58/25.5/45.7)	6 (76.3/68.3/55.3)

(B) $p = 3$.

TABLE 5.1: Number of iterations needed by different iterative methods, $p = 2, 3$, as a function of the elements (el.). For the nested SCR-FGMRES, the numbers in brackets indicate the average number of intermediate iterations needed to solve equations (5.30), (5.31) and (5.32) in Algorithm 3, respectively. Iterations marked with – did not reached convergence within the prescribed 1000 maximum number of iterations.

In Table 5.3 we study the influence of the intermediate and inner tolerances on the number of outer iterations required by the FGMRES solver, on a fixed mesh of 4096 elements, for B-splines of degree $p = 2, 3$. We note that as the chosen tolerances

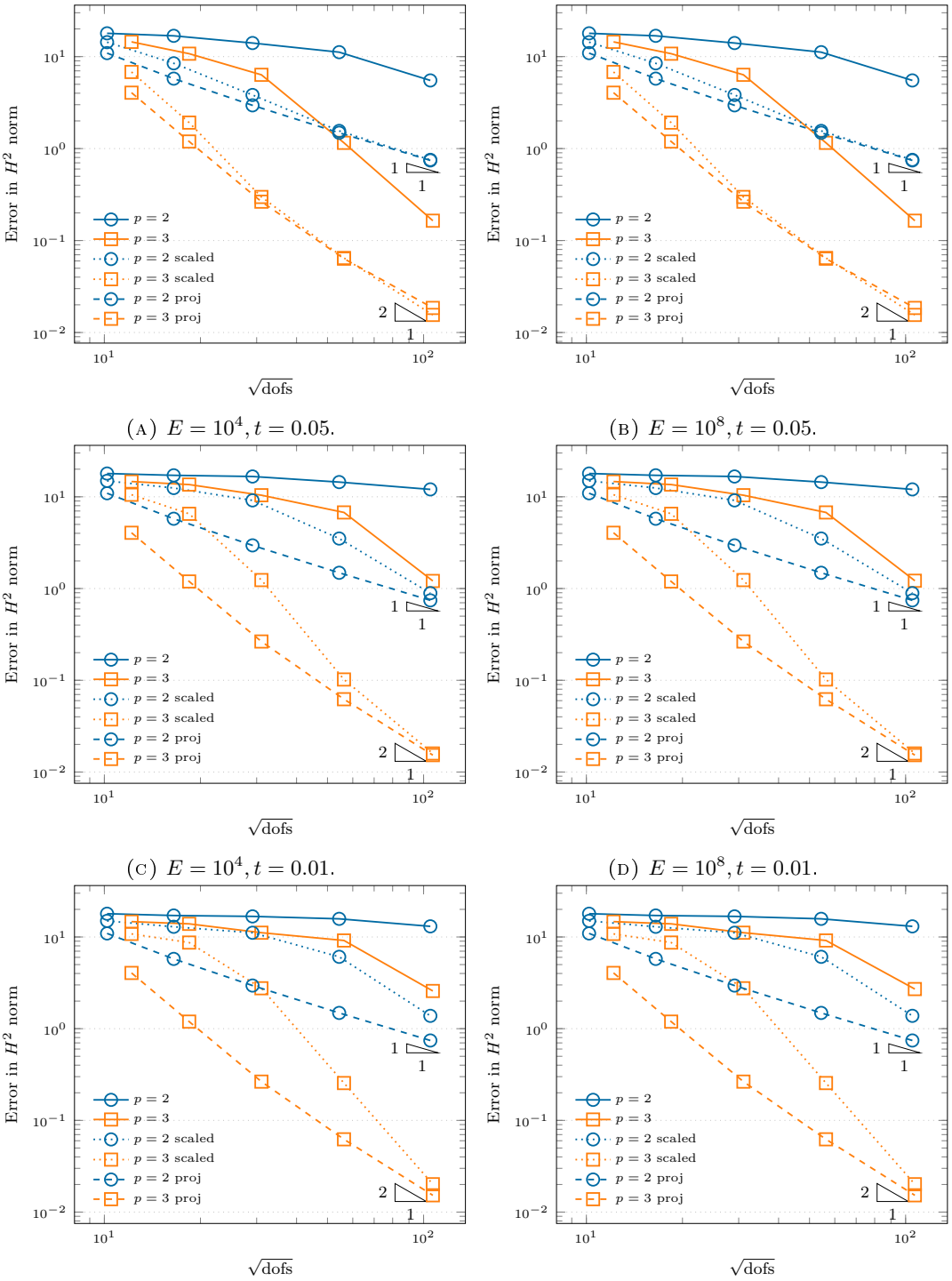

(A) $E = 10^4, t = 0.05$. (B) $E = 10^8, t = 0.05$.

(C) $E = 10^4, t = 0.01$. (D) $E = 10^8, t = 0.01$.

(E) $E = 10^4, t = 0.005$. (F) $E = 10^8, t = 0.005$.

FIGURE 5.5: Convergence study of the error measured in the H^2 norm in the non-matching case for four patches with curved interface example for different Young moduli and values of the thickness, B-splines of degree $p = 2, 3$. Comparison of a classic penalty method, the scaled version with respect to the problem parameters proposed in [34] (*scaled*) and our projection approach (*proj*).

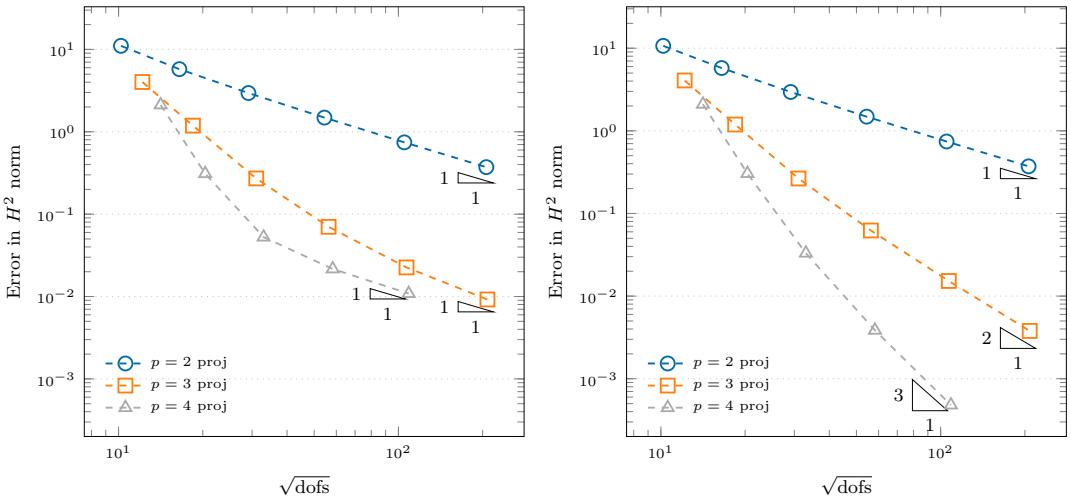

(A) Without C^0 constraint. (B) With C^0 constraint.

FIGURE 5.6: Convergence study of the error in the H^2 norm in the non-matching case for the curved four patches example. Influence of imposing a C^0 constraint at the cross point.

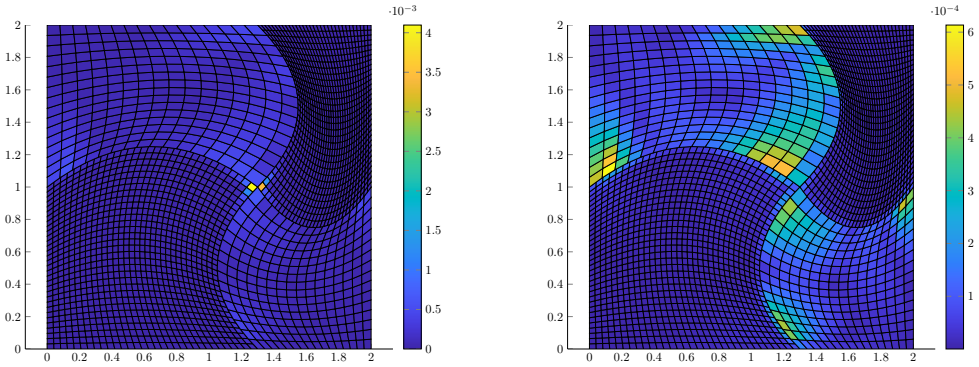

(A) Without C^0 constraint. (B) With C^0 constraint.

FIGURE 5.7: Element-wise plot of the error in the H^2 norm in the non-matching case for the curved four patches example, B-splines of degree $p = 4$. Influence of imposing a C^0 constraint at the cross point, notice the difference of one order of magnitude used in the two colorbars.

	256 el.	1024 el.	4096 el.	16384 el.
Diagonally scaled PCG	992	–	–	–
PCG with ILU	175	–	–	–
GMRES with ILU	79	209	478	–
Nested SCR-FGMRES	3 (22.3/4/21.6)	3 (32/7.3/28.3)	4 (44.5/20.2/34.7)	5 (63.2/55/50.2)

(A) $p = 2$.

	256 el.	1024 el.	4096 el.	16384 el.
Diagonally scaled PCG	778	–	–	–
PCG with ILU	697	–	–	–
GMRES with ILU	90	209	–	–
Nested SCR-FGMRES	3 (28.6/5.3/27.3)	3 (39.3/13/34.6)	5 (55.8/29.4/41)	6 (74/73.3/48.3)

(B) $p = 3$.

TABLE 5.2: Number of iterations needed by different iterative methods, $p = 2, 3$, as a function of the elements (el.) for the parameters proposed in [34]. For the nested SCR-FGMRES, the numbers in brackets indicate the average number of intermediate iterations needed to solve euqations (5.30), (5.31) and (5.32) in algorithm 3, respectively. Iterations marked with – did not reached convergence within the prescribed 1000 maximum number of iterations.

become smaller and smaller, we recover the algebraically exact SCR method, where in the limit the algorithm converges in one iteration. We also remark that finding an optimal choice for these parameters is, to the best of the authors' knowledge, still an open question in the community.

	$\eta_t = \eta_n = 10^{-4}$	$\eta_t = \eta_n = 10^{-5}$	$\eta_t = \eta_n = 10^{-6}$	$\eta_t = \eta_n = 10^{-8}$	$\eta_t = \eta_n = 10^{-10}$
$p = 2$	11	5	4	3	2
$p = 3$	13	7	4	3	2

TABLE 5.3: Influence of the intermediate and inner tolerances η_t and η_n (where we always set $\eta_t = \eta_n$) on the number of outer iterations needed by the FGMRES solver, $p = 2, 3$, on a fixed mesh with 4096 elements.

5.5.2 A nine patches geometry

In this example we consider the computational domain $\Omega = [0, 3] \times [0, 3]$ depicted in Figure 5.8, divided into nine subdomains Ω^i. Similarly to the previous example, all meshes are non-conforming at every coupling interface, where again an irrational factor of $\sqrt{2}/100$ has been used to shift the interface knots. The body source and boundary data are derived from the following analytical exact solution:

$$u^{\text{ex}} = \sin(\pi x) \cos(\pi x) .$$

Further, we set the Young's modulus to $E = 10^6\,[Pa]$, the thickness of the plate to $t = 0.01\,[m]$ and the Poisson's ratio to $\nu = 0\,[-]$. The convergence results of the error measured in the L^2, H^1 and H^2 are presented in Figure 5.9, for splines of degree $p = 2, 3$. In this example we test the robustness of the method with respect to:

- floating patches;
- the presence of multiple cross-points where a constraint must be applied.

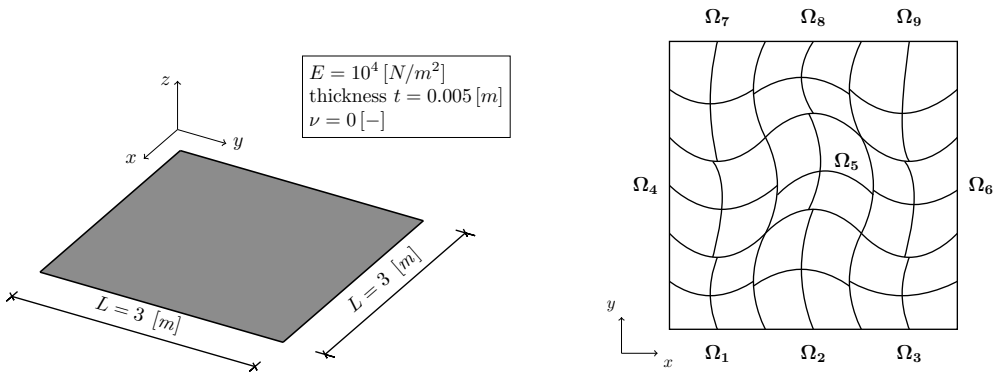

(A) Geometry setup and physical parameters. (B) Initial discretization.

FIGURE 5.8: Problem setup and initial multi-patch non-conforming discretization for the nine patches example.

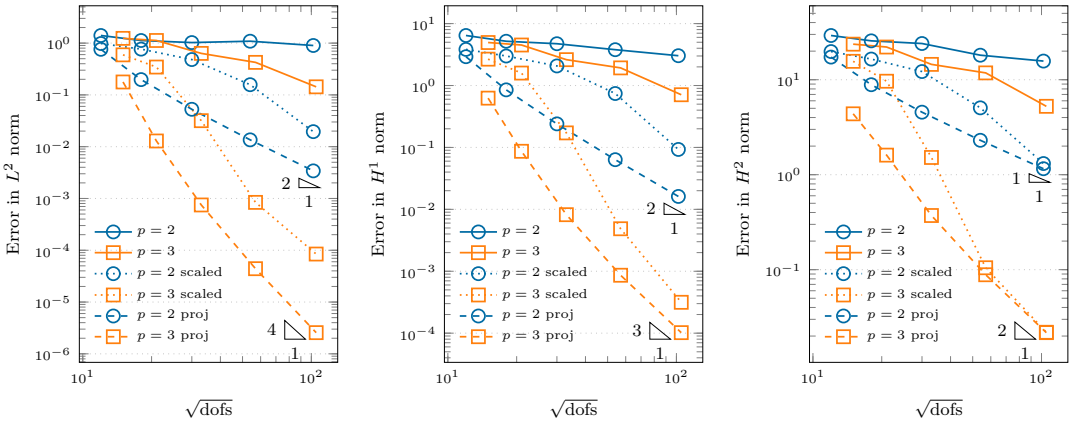

(A) Error L^2. (B) Error H^1. (C) Error H^2.

FIGURE 5.9: Convergence study of the error measured in the L^2, H^1 and H^2 norms in the non-matching case for nine patches example for different B-splines of degree $p = 2, 3$. Comparison of a classic penalty method, the scaled version with respect to the problem parameters proposed in [34] (*scaled*) and our projection approach (*proj*).

We observe again the expected asymptotic convergence rates of the error for all norms, where we remark that the method behaves optimally also for very coarse meshes, where locking phenomena are avoided. Indeed, on one hand, we notice again that a classical "vanilla" choice of the penalty parameters yield a severe overconstraint of the solution space, resulting in a loss of accuracy of several order of magnitudes compared to the projection method. On the other hand, the scaling studied in [34] leads to better results especially in the energy norm. However, for coarse meshes, we note that the method still suffers from locking, thus hindering the accuracy achievable by B-splines.

5.5.3 A three patches example with a geometrically non-conforming interface

In this example we consider the computational domain $\Omega = [0, 2] \times [0, 2]$, split into three subdomains Ω^i, see Figure 5.10a. The initial non-conforming discretization used in the following is depicted in Figure 5.10b, where the interface knots are again shifted by a factor of $\sqrt{2}/100$ to induce the non-conformity. The peculiarity of this example is

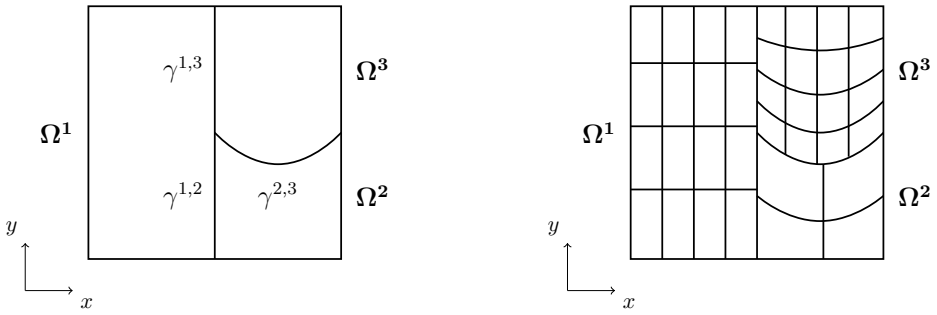

(A) Initial subdomains and corresponding interfaces.

(B) Non-conforming discretization.

FIGURE 5.10: Initial configuration and non-conforming discretization for the three patches example.

the presence of a geometrically non-conforming interface between the patches, which is further used to assess the robustness of our method.

Remark 10. *Similarly to [12], we define an interface as geometrically conforming if the pull-back with respect to both slave and master domains is an entire edge of each parametric domain* $\widehat{\Omega}^i$.

Similarly to the previous examples, the exact solution reads:

$$u^{\text{ex}} = \sin(\pi x)\cos(\pi x)\,,$$

from which the applied body load and imposed boundary conditions are derived. Regarding the problem parameters, we set the Young's modulus to $E = 10^6\,[Pa]$, the thickness of the plate to $t = 0.01\,[m]$ and the Poisson's ratio to $\nu = 0\,[-]$.

The convergence results of the error measured in the L^2, H^1 and H^2 are presented in Figure 5.11, for splines of degree $p = 2, 3$. Analogously to our previous results, our method attains optimal rates of convergence, even in the presence of a geometrically non-conforming interface. Moreover, this numerical experiment confirms again that our method is insensitive to locking, starting from very coarse discretizations, where a substantial gain in accuracy per degree-of-freedom is observed.

5.5.4 A flat L-bracket

The last example we present is meant to show the applicability of the method to more complex multi-patch geometries. Analogously to the example studied in [8], we modeled a flat L-bracket with 28 patches, coupled along 34 interfaces, as depicted in Figure 5.12. We applying a constant line load of $100\,[N/m]$ in the negative z-direction on the upper right edge and we impose clamped boundary conditions on the entire boundary of the upper left and lower left holes, respectively. Further, we set the Young's modulus to $E = 200 \cdot 10^9\,[Pa]$, the thickness of the plate to $t = 0.01\,[m]$ and the Poisson's ratio to $\nu = 0\,[-]$. The solution field obtained with B-splines of degree $p = 2, 3$ is depicted in Figure 5.13, where we remark the smoothness of the obtained solution, especially across the coupling interfaces. In Figure 5.14 we also plot the bending stress tensor $\mathbf{m}$, where its components are defined as:

$$m_{ij} = D\left(\nu\delta_{ij}u_{kk} + (1-\nu)u_{ij}\right)\,,$$

and where δ_{ij} denotes the standard Kronecker delta. We obtain again a smooth stress field, where no visible spurious oscillations are introduced by the proposed

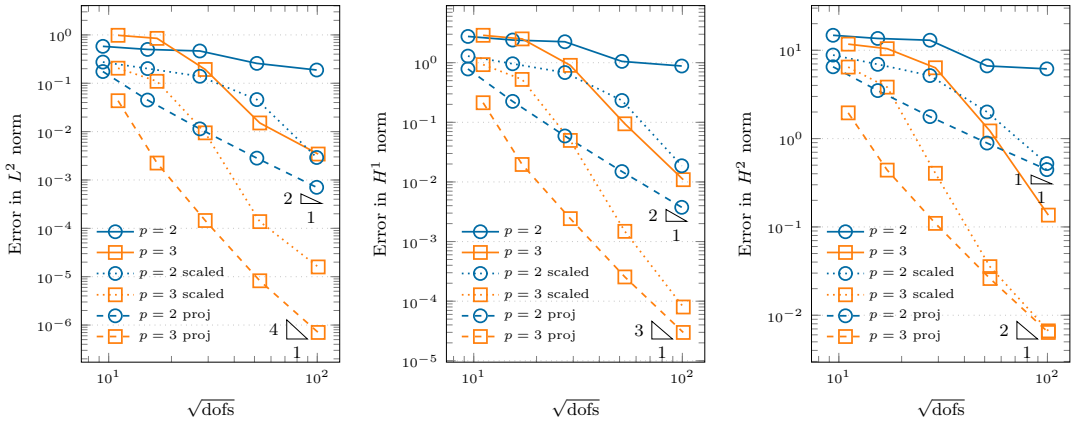

(A) Error L^2. (B) Error H^1. (C) Error H^2.

FIGURE 5.11: Convergence study of the error measured in the L^2, H^1 and H^2 norms in the non-matching case for the three patches example, B-splines of degree $p = 2, 3$. Comparison of a classic penalty method, the scaled version with respect to the problem parameters proposed in [34] (*scaled*) and our projection approach (*proj*).

coupling strategy. Finally, in Figure 5.15, we plot the convergence results of the stress component m_{11}, evaluated at point A marked in Figure 5.12a, as a function of the number of dofs on a series of uniformly refined meshes. We note that for the classical penalty approach, and only for this example, we have tuned the penalty parameters to converge towards the reference value, where we have set $\frac{1}{\varepsilon_1^{(\ell)}} = 10^4 E$, $\frac{1}{\varepsilon_2^{(\ell)}} = E, \ell = 1, \dots, L$. This example highlights once again the gain in accuracy achieved on coarse meshes by the proposed method, also for point-wise quantities of interest.

5.6 Conclusions

In this chapter we have introduced a simple methodology for the C^1-coupling of isogeometric patches based on the L^2-projection of suitable super-penalty terms in the context of bilaplace equation. Exploiting standard results for saddle point problems, we have proved that the mortar formulation and its singular perturbation, which is at the base of our penalty method, are well-posed. Further we have provided a criterion for choosing the penalty parameters, in function of the mesh size and the spline degree, in order to get optimal order convergence in the H^2 norm. The method does not suffer from locking phenomena, even in the case of severe non-matching discretization, where optimal rates of convergence of the error measured in the L^2, H^1 and H^2 norms have been attained also on very coarse meshes and a substantial gain in accuracy per degree-of-freedom has been observed compared to a classical penalty approach and to the scaled choice of parameters presented in [34] in the scope of Kirchhoff-Love shells. The method turns out to be particularly effective for moderate spline degrees $p = 2, 3$. Our choice of parameters is completely determined by the problem definition and is based upon the underlying perturbed saddle point formulation associated to the plate, from which the two Lagrange multipliers are eliminated and the magnitude of the corresponding perturbations gives us insights on how to appropriately select the penalty factors. Then, to mitigate the detrimental effects of this choice on the condition number of the system matrix, we have combined the nested block preconditioner introduced in [48] with a preconditioner based on the Fast Diagonalization algorithm tailored for isogeometric bilaplace equation, inspired by the strategy in [62].

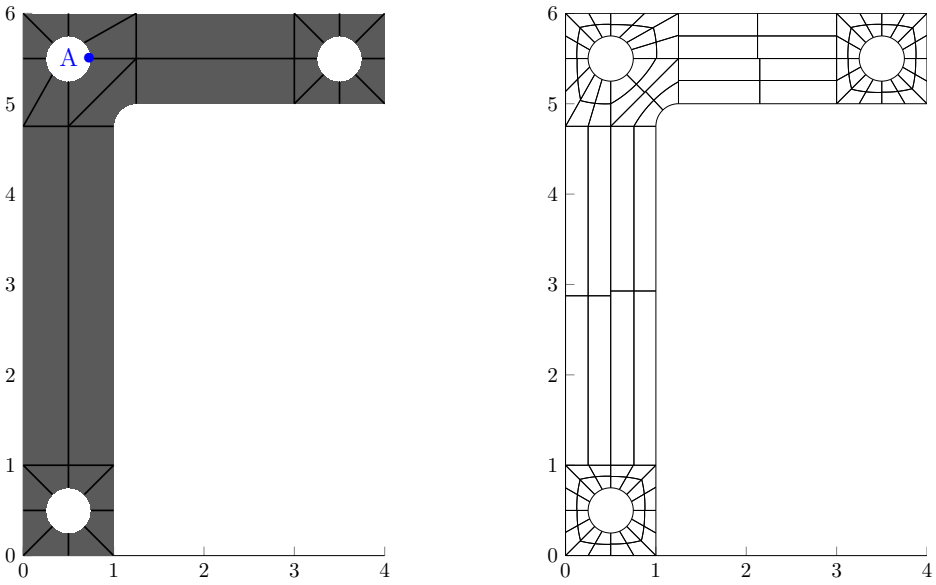

(A) Multi-patch design. (B) Non-conforming mesh.

FIGURE 5.12: Geometry setup and non-conforming discretization for the flat L-bracket example.

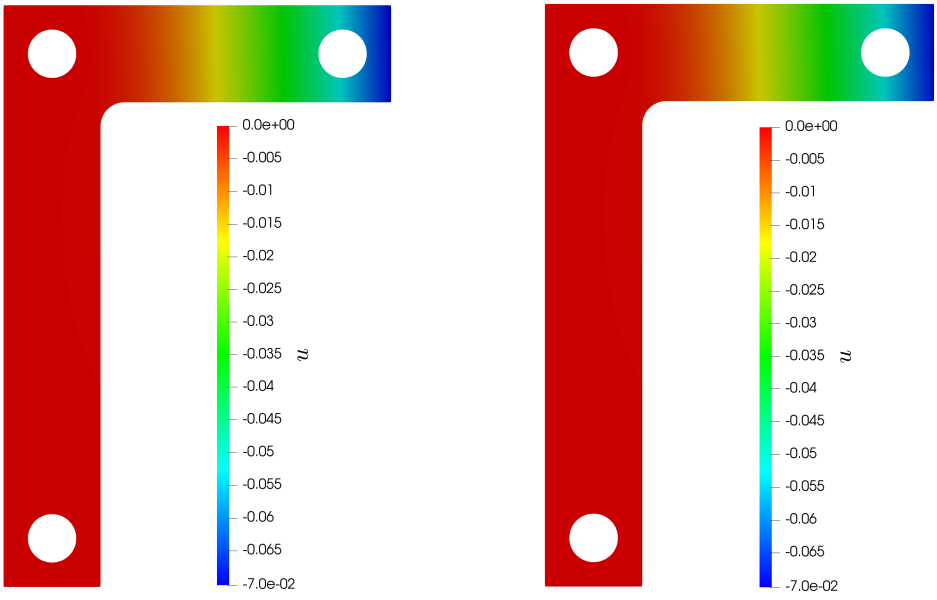

(A) $p = 2$. (B) $p = 3$.

FIGURE 5.13: Solution contour for the flat L-bracket example, B-splines of degree $p = 2, 3$.

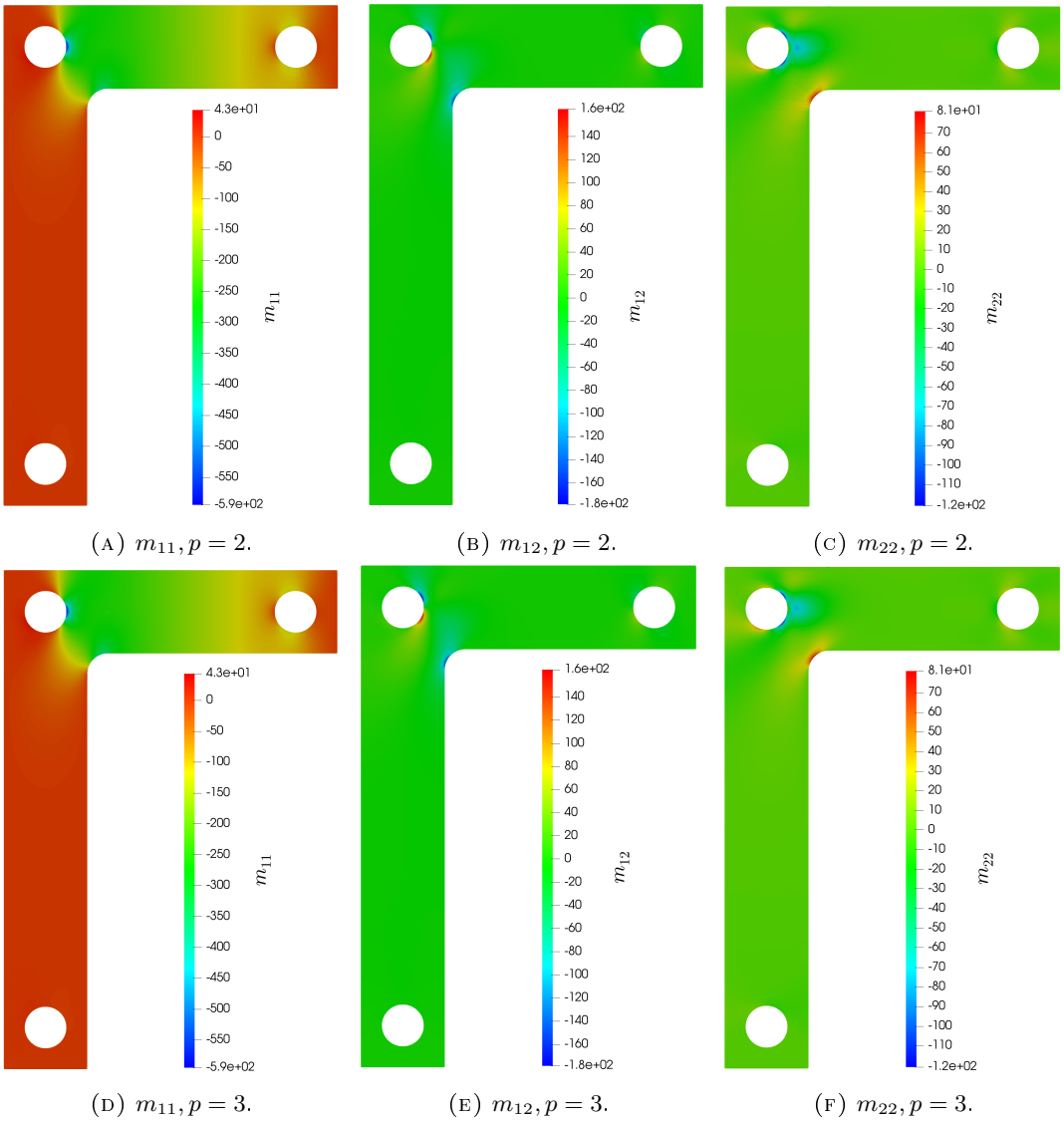

(A) $m_{11}, p = 2$. (B) $m_{12}, p = 2$. (C) $m_{22}, p = 2$.

(D) $m_{11}, p = 3$. (E) $m_{12}, p = 3$. (F) $m_{22}, p = 3$.

FIGURE 5.14: Components of the bending stress tensor $\mathbf{m}$ for the flat L-bracket example, B-splines of degree $p = 2, 3$.

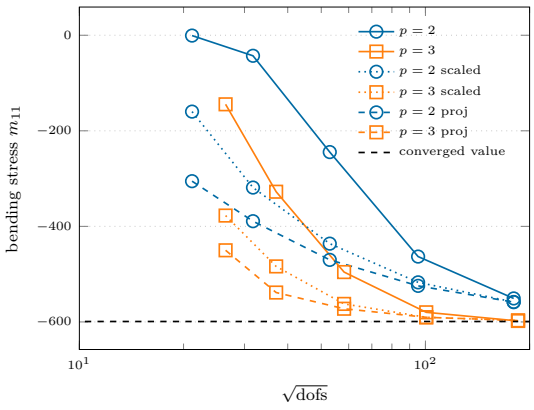

FIGURE 5.15: Convergence study of the stress component m_{11}, evaluated at point A in Figure 5.10a, for the flat L-bracket example for different B-splines of degree $p = 2, 3$. Comparison of a classic penalty method, the scaled version with respect to the problem parameters proposed in [34] (*scaled*) and our projection approach (*proj*).

To conclude, we have demonstrated numerically the applicability and robustness of the proposed projected super-penalty approach for the bilaplace equation discretized by non-conforming isogeometric patches, where the method does not show any locking also on very coarse meshes.

Appendix A

Analysis of doubly constrained saddle point problems

In what follows, we recall some useful results obtained generalizing the ones from [10] to saddle point problems with two constraints.

Assumption 5. *Let V, Q_1, Q_2 be three Hilbert spaces. Let be $a : V \times V \to \mathbb{R}$, $b_1 : V \times Q_1 \to \mathbb{R}$ and $b_2 : V \times Q_2 \to \mathbb{R}$ three continuous bilinear forms. We denote by A, B_1 and B_2, respectively, the linear continuous operators associated with them. We also set, for $i = 1, 2$,*

$$K_i = \ker B_i, \qquad K = K_1 \cap K_2, \qquad H_i = \ker B_i^T.$$

Let us consider the following *generalized saddle-point problem*: given $f \in V'$, $g_1 \in Q_1'$ and $g_2 \in Q_2'$, find $(u, \lambda_1, \lambda_2) \in V \times Q_1 \times Q_2$ such that

$$\begin{aligned} a(u,v) + b_1(v,\lambda_1) + b_2(v,\lambda_2) &= \langle f, v\rangle && \forall v \in V \\ b_1(u,\mu_1) &= \langle g_1, \mu_1\rangle && \forall \mu_1 \in Q_1 \\ b_2(u,\mu_2) &= \langle g_2, \mu_2\rangle && \forall \mu_2 \in Q_2. \end{aligned} \tag{A.1}$$

Theorem 11. *Together with Assumption 5, assume that $\mathrm{Im}B_{1|K_2} = Q_1'$, $\mathrm{Im}B_2 = Q_2'$ and that the bilinear form a is coercive on K, that is*

$$\exists \alpha_0 > 0 : \ \alpha_0 \|v_0\|_V^2 \le a(v_0, v_0) \qquad \forall v_0 \in K. \tag{A.2}$$

Then, for every $(f, g_1, g_2) \in V' \times Q_1' \times Q_2'$, problem (A.1) has a unique solution.

Proof. Let us first prove the *existence* of a solution. From the surjectivity of B_2 and Corollary [10, p. 4.1.1], we have that there exists a lifting operator L_{B_2} such that $B_2(L_{B_2} g) = g$ for every $g \in Q_2'$. Setting $u_g := L_{B_2} g$, we therefore have $B_2 u_g = g$. We now consider the new unknown $u_0 := u - u_g$ and, in order to have $B_2 u = g$, we require $u_0 \in K_2$. For every $v_0 \in K_2$, we obviously have $b_2(v_0, q) = 0$ for every $q \in Q_2$, so that the first two equations of (A.1) now imply

$$\begin{aligned} a(u_0,v_0) + b_1(v_0,\lambda_1) &= \langle f, v_0\rangle - a(u_g, v_0) && \forall v_0 \in K_2 \\ b_1(u_0,\mu_1) &= \langle g_1, \mu_1\rangle && \forall \mu_1 \in Q_1, \end{aligned} \tag{A.3}$$

and [10, Theorem 4.2.1] ensures that we have a unique $(u_0, \lambda_1) \in K_2 \times Q_1$ satisfying (A.3). Remark now that the functional

$$v \to \ell(v) := \langle f, v\rangle - a(u_g + u_0, v) - b_1(v, \lambda_1),$$

thanks to (A.3), vanishes identically for every $v \in K_2$. Hence, $\ell \in K_2^0$ (the polar space of K_2), which due to [10, Theorem 4.1.4], coincides with $\mathrm{Im}B_2^T$. Hence, ℓ is in the image of B_2^T, and there exists a $\lambda_2 \in Q_2$ such that $B_2^T\lambda_2 = \ell$. This means that

$$\left\langle B_2^T\lambda_2, v\right\rangle = \langle \ell, v\rangle = \langle f, v\rangle - a(u_g + u_0, v) - b_1(v, \lambda_1)$$

for every $v \in V$, and since $u = u_g + u_0$, the first two equations are satisfied. On the other hand, $B_2u = B_2u_g + B_2u_0 = g$ and the third equation is also satisfied.
We now prove *uniqueness*. By linearity, assume that $f = 0$, $g_1 = 0$ and $g_2 = 0$: then, $u \in K$. testing the first equation on $v = u$ we get $a(u, u) = 0$ and then $u = 0$ from (A.2). Using $u = 0$ and $f = 0$ in the first equation of (A.1), we have then

$$b_1(v, \lambda_1) + b_2(v, \lambda_2) = 0 \qquad \forall v \in V. \tag{A.4}$$

In particular, for all $v_2 \in K_2$ we have $b_1(v_2, \lambda_1) = \langle B_1v_2, \lambda_1\rangle = 0$ and from Corollary [10, p. 4.1.1], we have $\lambda_1 = 0$ and (A.4) reduces to $b_2(v, \lambda_2) = 0$, for all $v \in V$. Finally, Corollary [10, p. 4.1.1] implies $\lambda_2 = 0$. □

Assume that, for $i = 1, 2$, we are given a Hilbert space W_i continuously embedded in Q_i and dense in Q_i. We now consider, for every $\varepsilon_1, \varepsilon_2 > 0$, problems of the form: find $(u_\varepsilon, \lambda_{1,\varepsilon}, \lambda_{2,\varepsilon}) \in V \times W_1 \times W_2$ such that

$$a(u_\varepsilon, v) + b_1(v, \lambda_{1,\varepsilon}) + b_2(v, \lambda_{2,\varepsilon}) = \langle f, v\rangle \qquad \forall v \in V \tag{A.5a}$$

$$b_1(u_\varepsilon, \mu_1) - \varepsilon_1(\lambda_{1,\varepsilon}, \mu_1)_{W_1} = \langle g_1, \mu_1\rangle_{Q_1' \times Q_1} + \langle h_1, \mu_1\rangle_{W_1' \times W_1} \quad \forall \mu_1 \in W_1 \tag{A.5b}$$

$$b_2(u_\varepsilon, \mu_2) - \varepsilon_2(\lambda_{2,\varepsilon}, \mu_2)_{W_2} = \langle g_2, \mu_2\rangle_{Q_2' \times Q_2} + \langle h_2, \mu_2\rangle_{W_2' \times W_2} \quad \forall \mu_2 \in W_2. \tag{A.5c}$$

Assumption 6. *Let us assume that for every $\chi_* > 0$ there exists an $\alpha_* > 0$ such that:*

$$\forall \chi > \chi_* \; \exists \tilde{\alpha} > \alpha_* \; : \; \tilde{\alpha}\|u\|_V^2 \le a(u, u) + \chi\|B_iv\|_{W_i'}^2 \; \forall v \in V. \tag{A.6}$$

Theorem 12. *Together with Assumption 5, assume that, for $i = 1, 2$, $\mathrm{Im}B_i$ is closed in Q_i and that $a(\cdot, \cdot)$ is positive semi-definite and verifies Assumption 6. Then, for every $0 < \varepsilon_1, \varepsilon_2 \le 1/2$, for every $f \in V'$, for every $g_1 \in \mathrm{Im}B_1|_{K_2}$, $g_2 \in \mathrm{Im}B_2$ and for every $h_i \in W_i'$, for $i = 1, 2$, the problem* (A.5) *has a unique solution which, moreover, satisfies*

$$\|u_\varepsilon\|_V + \|\overline{\lambda}_{1,\varepsilon}\|_{Q_1} + \|\overline{\lambda}_{2,\varepsilon}\|_{Q_2} + \varepsilon_1^{1/2}\|\lambda_{1,\varepsilon}\|_{W_1} + \varepsilon_2^{1/2}\|\lambda_{2,\varepsilon}\|_{W_2} \le C\left(\|f\|_{V'} + \|g_1\|_{Q_1'} + \|g_2\|_{Q_2'} + \frac{1}{\varepsilon_1^{1/2}}\|h_1\|_{W_1'} + \frac{1}{\varepsilon_2^{1/2}}\|h_2\|_{W_2'}\right), \tag{A.7}$$

where, for $i = 1, 2$, $\overline{\lambda}_{i,\varepsilon}$ is the component of $\lambda_{i,\varepsilon}$ in $H_i^\perp$.

Proof. Since we do not yet have the existence of the solution, we apply a regularization argument. We first substitute a with a_δ given by

$$a_\delta(u, v) = a(u, v) + \delta(u, v)_V,$$

with $\delta > 0$. Then, we prove a-priori bounds independent of δ and we have the solution in the limit for $\delta \to 0^+$. For brevity, we do not re-write problem (A.5) with a_δ in

place of a, and we do not indicate the dependence of the solution of the regularised problem on δ. Taking the first equation (A.5a) with $v = u_\varepsilon$, and subtracting the second equation (A.5b) for $\mu_1 = \lambda_{1,\varepsilon}$ and the third equation (A.5c) for $\mu_2 = \lambda_{2,\varepsilon}$, we get

$$\begin{aligned}&\delta\|u_\varepsilon\|_V^2 + a(u_\varepsilon, u_\varepsilon) + \varepsilon_1(\lambda_{1,\varepsilon}, \lambda_{1,\varepsilon})_{W_1} + \varepsilon_2(\lambda_{2,\varepsilon}, \lambda_{2,\varepsilon})_{W_2}\\ &= \langle f, u_\varepsilon\rangle + \langle g_1, \lambda_{1,\varepsilon}\rangle_{Q_1'\times Q_1} + \langle h_1, \lambda_{1,\varepsilon}\rangle_{W_1'\times W_1} + \langle g_2, \lambda_{2,\varepsilon}\rangle_{Q_2'\times Q_2} + \langle h_2, \lambda_{2,\varepsilon}\rangle_{W_2'\times W_2}\,.\end{aligned} \tag{A.8}$$

From Corollary [10, p. 4.1.1] and the first equation (A.5a), we have

$$\beta_1\|\overline{\lambda}_{1,\varepsilon}\|_{Q_1} + \beta_2\|\overline{\lambda}_{2,\varepsilon}\|_{Q_2} \le C\left(\|u_\varepsilon\|_V + \|f\|_{V'}\right), \tag{A.9}$$

and since we assumed $g_i \in \mathrm{Im}B_i$ for $i = 1, 2$, we have

$$\langle g_1, \lambda_{1,\varepsilon}\rangle + \langle g_2, \lambda_{2,\varepsilon}\rangle = \left\langle g_1, \overline{\lambda}_{1,\varepsilon}\right\rangle + \left\langle g_2, \overline{\lambda}_{2,\varepsilon}\right\rangle \le C\left(\|g_1\|_{Q_1'} + \|g_2\|_{Q_2'}\right)\left(\|u_\varepsilon\|_V + \|f\|_{V'}\right). \tag{A.10}$$

On the other hand, we also have

$$\langle f, u_\varepsilon\rangle \le \|f\|_{V'}\|u_\varepsilon\|_V. \tag{A.11}$$

and, for $i = 1, 2$,

$$\langle h_i, \lambda_{i,\varepsilon}\rangle \le \frac{1}{\varepsilon_i^{1/2}}\|h_i\|_{W_i'}\varepsilon_i^{1/2}\|\lambda_{i,\varepsilon}\|_{W_i} \le \frac{1}{2\varepsilon_i}\|h_i\|_{W_i'}^2 + \frac{\varepsilon_i}{2}\|\lambda_{i,\varepsilon}\|_{W_i}. \tag{A.12}$$

Inserting (A.10) and (A.11) and (A.12) in (A.8) and dropping the term with δ (which is positive), we then easily have

$$\begin{aligned}&a(u_\varepsilon, u_\varepsilon) + \varepsilon_1\|\lambda_{1,\varepsilon}\|_{W_1}^2 + \varepsilon_2\|\lambda_{2,\varepsilon}\|_{W_2}^2\\ &\qquad\le C\Bigg[\left(\|g_1\|_{Q_1'} + \|g_2\|_{Q_2'}\right)\left(\|u_\varepsilon\|_V + \|f\|_{V'}\right) + \|f\|_{V'}\|u_\varepsilon\|_V +\\ &\qquad\qquad \|g_1\|_{Q_1'}^2 + \|g_2\|_{Q_2'}^2 + \frac{1}{\varepsilon_1}\|h_1\|_{W_1'}^2 + \frac{1}{\varepsilon_2}\|h_2\|_{W_2'}^2\Bigg]\\ &\qquad\le C\Bigg[\|u_\varepsilon\|_V\left(\|f\|_{V'} + \|g_1\|_{Q_1'} + \|g_2\|_{Q_2'}\right) + \|f\|_{V'}^2 +\\ &\qquad\qquad \|g_1\|_{Q_1'}^2 + \|g_2\|_{Q_2'}^2 + \frac{1}{\varepsilon_1}\|h_1\|_{Q_1'}^2 + \frac{1}{\varepsilon_2}\|h_2\|_{Q_2'}^2\Bigg].\end{aligned} \tag{A.13}$$

On the other hand, from the second equation (A.5b) we have that $\varepsilon_1 R_{W_1}\lambda_{1,\varepsilon}$ (where R_{W_1} is the Ritz operator in W_1) is equal to $B_1u_\varepsilon - g_1 - h_1$. Hence,

$$\varepsilon_1\|\lambda_{1,\varepsilon}\|_{W_1}^2 = \varepsilon_1\|R_{W_1}\lambda_{1,\varepsilon}\|_{W_1'}^2 = \frac{1}{\varepsilon_1}\|B_1u_\varepsilon - g_1 - h_1\|_{W_1'}^2. \tag{A.14}$$

Hence, using $(a+b)^2 \leq 2a^2 + 2b^2$, the assumption $\varepsilon_1 \leq 1/2$, (A.14) and $\|w\|_{W_1'} \leq C\|w\|_{Q_1'}$, we have

$$\begin{aligned}\|B_1 u_\varepsilon\|_{W_1'}^2 &\leq 2\|B_1 u_\varepsilon - g_1 - h_1\|_{W_1'}^2 + 2\|g_1 + h_1\|_{W_1'}^2 \\ &\leq \frac{1}{\varepsilon_1}\|B_1 u_\varepsilon - g_1 - h_1\|_{W_1'}^2 + 4\|g_1\|_{W_1'}^2 + 4\|h_1\|_{W_1'}^2 \\ &\leq \varepsilon_1\|\lambda_{1,\varepsilon}\|_{W_1}^2 + 4\|g_1\|_{W_1'}^2 + 4\|h_1\|_{W_1'}^2.\end{aligned} \tag{A.15}$$

Similarly, we also have

$$\|B_2 u_\varepsilon\|_{W_2'}^2 \leq \varepsilon_2\|\lambda_{2,\varepsilon}\|_{W_1}^2 + 4\|g_2\|_{W_2'}^2 + 4\|h_2\|_{W_2'}^2. \tag{A.16}$$

Combining (A.15), (A.16) and (A.13), we obtain

$$\begin{aligned}a(u_\varepsilon, u_\varepsilon) + \|B_1 u_\varepsilon\|_{W_1'} + \|B_2 u_\varepsilon\|_{W_2'} + \varepsilon_1\|\lambda_{1,\varepsilon}\|_{W_1}^2 + \varepsilon_2\|\lambda_{2,\varepsilon}\|_{W_2}^2 \\ \leq C\Bigg[\|u_\varepsilon\|_V\left(\|f\|_{V'} + \|g_1\|_{Q_1'} + \|g_2\|_{Q_2'}\right) + \|f\|_{V'}^2 + \\ \|g_1\|_{Q_1'}^2 + \|g_2\|_{Q_2'}^2 + \frac{1}{\varepsilon_1}\|h_1\|_{W_1'}^2 + \frac{1}{\varepsilon_2}\|h_2\|_{W_2'}^2\Bigg].\end{aligned} \tag{A.17}$$

Finally, using (A.9) together with (A.6) and (A.17) gives

$$\begin{aligned}&\|u_\varepsilon\|_V^2 + \|\overline{\lambda}_{1,\varepsilon}\|_{Q_1}^2 + \|\overline{\lambda}_{2,\varepsilon}\|_{Q_2}^2 + \varepsilon_1\|\lambda_{1,\varepsilon}\|_{W_1}^2 + \varepsilon_2\|\lambda_{2,\varepsilon}\|_{W_2}^2 \\ &\qquad \leq C\left(\|u_\varepsilon\|_V^2 + \|f\|_{V'}^2 + \varepsilon_1\|\lambda_{1,\varepsilon}\|_{W_1}^2 + \varepsilon_2\|\lambda_{2,\varepsilon}\|_{W_2}^2\right) \\ &\quad \leq C\left(a(u_\varepsilon, u_\varepsilon) + \|B_1 u_\varepsilon\|_{W_1'} + \|B_2 u_\varepsilon\|_{W_2'} + \|f\|_{V'}^2 + \varepsilon_1\|\lambda_{1,\varepsilon}\|_{W_1}^2 + \varepsilon_2\|\lambda_{2,\varepsilon}\|_{W_2}^2\right) \\ &\qquad \leq C\Bigg[\|u_\varepsilon\|_V\left(\|f\|_{V'} + \|g_1\|_{Q_1'} + \|g_2\|_{Q_2'}\right) + \|f\|_{V'}^2 + \\ &\qquad\qquad \|g_1\|_{Q_1'}^2 + \|g_2\|_{Q_2'}^2 + \frac{1}{\varepsilon_1}\|h_1\|_{W_1'}^2 + \frac{1}{\varepsilon_2}\|h_2\|_{W_2'}^2\Bigg],\end{aligned}$$

which easily yields the (A.7). Hence, the operator $M : (u_\varepsilon, \lambda_{1,\varepsilon}, \lambda_{2,\varepsilon}) \mapsto (f, g_1, g_2)$ is bounding. Then, M is injective and $M^T \equiv M$ is surjective. This ensures existence and uniqueness for the solution of (A.5). □

Remark 11. *Under the assumption* $\mathrm{Im}B_i = Q_i'$*, it holds* $H_i^0 = Q_i'$*, which implies* $H_i = \{0\}$ *and* $H_i^\perp = Q_i$*. Hence,* (A.7) *reduces to*

$$\begin{aligned}\|u_\varepsilon\|_v + \|\lambda_{1,\varepsilon}\|_{Q_1} + \|\lambda_{2,\varepsilon}\|_{Q_2} + \varepsilon_1^{1/2}\|\lambda_{1,\varepsilon}\|_{W_1} + \varepsilon_2^{1/2}\|\lambda_{2,\varepsilon}\|_{W_2} \\ \leq C\left(\|f\|_{V'} + \|g_1\|_{Q_1'} + \|g_2\|_{Q_2'} + \frac{1}{\varepsilon_1^{1/2}}\|h_1\|_{W_1'} + \frac{1}{\varepsilon_2^{1/2}}\|h_2\|_{W_2'}\right).\end{aligned} \tag{A.18}$$

For the sake of simplicity, from now on, we will restrict our analysis to the case $\mathrm{Im}B_i = Q_i'$.

Proposition 3. *With the same assumptions of Theorem 12, and assuming moreover that* $h_i = 0$ *for* $i = 1, 2$*, let* $(u_\varepsilon, \lambda_{1,\varepsilon}, \lambda_{2,\varepsilon}) \in V \times W_1 \times W_2$ *be the solution of problem*

(A.5) *and* $(u, \lambda_1, \lambda_2) \in V \times Q_1 \times Q_2$ *be the solution of problem* (A.1). *We then have*

$$\begin{aligned}&\|u - u_\varepsilon\|_V + \|\lambda_1 - \lambda_{1,\varepsilon}\|_{Q_1} + \|\lambda_2 - \lambda_{2,\varepsilon}\|_{Q_2} \\ &\leq C \left[\inf_{w_1 \in W_1} (\|\lambda_1 - w_1\|_{Q_1} + \sqrt{\varepsilon_1}\|w_1\|_{W_1}) + \inf_{w_2 \in W_2} (\|\lambda_2 - w_2\|_{Q_2} + \sqrt{\varepsilon_2}\|w_2\|_{W_2}) \right].\end{aligned} \tag{A.19}$$

Proof. Subtracting (A.5) from (A.1) with $\mu_1 \in W_1$ and $\mu_2 \in W_2$, one has

$$\begin{aligned} a(u - u_\varepsilon, v) + b_1(v, \lambda_1 - \lambda_{1,\varepsilon}) + b_2(v, \lambda_2 - \lambda_{2,\varepsilon}) &= 0 && \forall v \in V \\ b_1(u - u_\varepsilon, \mu_1) &= \varepsilon_1(\lambda_{1,\varepsilon}, \mu_1)_{W_1} && \forall \mu_1 \in W_1 \\ b_2(u - u_\varepsilon, \mu_2) &= \varepsilon_2(\lambda_{2,\varepsilon}, \mu_2)_{W_2} && \forall \mu_2 \in W_2. \end{aligned} \tag{A.20}$$

Let be $\lambda_{1,w} \in W_1$ and $\lambda_{2,w} \in W_2$. We rewrite (A.20) as

$$\begin{aligned} a(u - u_\varepsilon, v) + b_1(v, \lambda_{1,w} - \lambda_{1,\varepsilon}) + b_2(v, \lambda_{2,w} - \lambda_{2,\varepsilon}) &= \\ b_1(v, \lambda_{1,w} - \lambda_1) + b_2(v, \lambda_{2,w} - \lambda_2) && \forall v \in V \\ b_1(u - u_\varepsilon, \mu_1) + \varepsilon_1(\lambda_{1,w} - \lambda_{1,\varepsilon}, \mu_1)_{W_1} &= \varepsilon_1(\lambda_{1,\varepsilon}, \mu_1)_{W_1} && \forall \mu_1 \in W_1 \\ b_2(u - u_\varepsilon, \mu_2) + \varepsilon_2(\lambda_{2,w} - \lambda_{2,\varepsilon}, \mu_2)_{W_2} &= \varepsilon_2(\lambda_{2,\varepsilon}, \mu_2)_{W_2} && \forall \mu_2 \in W_2. \end{aligned} \tag{A.21}$$

Applying Theorem 12 with $\langle h_1, \mu_1 \rangle = \varepsilon_1(\lambda_{1,w}, \mu_1)_{W_1}$ and $\langle h_2, \mu_2 \rangle = \varepsilon_2(\lambda_{2,w}, \mu_2)_{W_2}$, and using estimate (A.18), we get

$$\begin{aligned}&\|u - u_\varepsilon\|_V^2 + \|\lambda_{1,w} - \lambda_{1,\varepsilon}\|_{Q_1}^2 + \|\lambda_{2,w} - \lambda_{2,\varepsilon}\|_{Q_2}^2 \\ &\qquad \leq C \left(\|\lambda_{1,w} - \lambda_1\|_{Q_1}^2 + \varepsilon_1 \|\lambda_{1,w}\|_{W_1}^2 + \|\lambda_{2,w} - \lambda_2\|_{Q_2}^2 + \varepsilon_2 \|\lambda_{2,w}\|_{W_2}^2 \right).\end{aligned} \tag{A.22}$$

From the triangle inequality and the arbitrariness of $\lambda_{1,w}$ and $\lambda_{2,w}$, one deduces (A.19). □

Remark 12. *Having defined*

$$W_i^+ = \left\{ w \in W_i : \|w\|_{Q_i'} < \infty \right\},$$

for every $\lambda_i^+ \in W_i^+$, *we have*

$$(\lambda_i^+, \mu_i)_{W_i} \leq \|\lambda_i^+\|_{Q_i'} \|\mu_i\|_{Q_i} \qquad \forall \mu_i \in W_i.$$

Taking now $\lambda_{i,w} \in W_i^+$, *we can go back to* (A.21), *considering this time that the right-hand side of the second and third equations (that are* $\varepsilon_1(\lambda_{1,w}, \mu_1)_{W_1}$ *and* $\varepsilon_2(\lambda_{2,w}, \mu_2)_{W_2}$*) corresponds to the choice* $h_1 = h_2 = 0$, $\langle g_1, \mu_1 \rangle = \varepsilon_1(\lambda_{1,w}, \mu_1)_{W_1}$ *and* $\langle g_2, \mu_2 \rangle = \varepsilon_2(\lambda_{2,w}, \mu_1)_{W_2}$ *when using Theorem 12. In particular, thanks to* (A.18), *we now have*

$$\begin{aligned}&\|u - u_\varepsilon\|_V + \|\lambda_1 - \lambda_{1,\varepsilon}\|_{Q_1} + \|\lambda_2 - \lambda_{2,\varepsilon}\|_{Q_2} \\ &\qquad \leq C \Bigg(\inf_{\lambda_{1,w} \in W_1^+} \left\{ \|\lambda_1 - \lambda_{1,w}\|_{Q_1} + \varepsilon_1 \|\lambda_{1,w}\|_{W_1^+} \right\} + \\ &\qquad\qquad \inf_{\lambda_{2,w} \in W_2^+} \left\{ \|\lambda_2 - \lambda_{2,w}\|_{Q_2} + \varepsilon_2 \|\lambda_{2,w}\|_{W_2^+} \right\} \Bigg).\end{aligned}$$

Finally, we observe that, whenever $\lambda_i \in W_i^+$, *we would have*

$$\|u - u_\varepsilon\|_V + \|\lambda_1 - \lambda_{1,\varepsilon}\|_{Q_1} + \|\lambda_2 - \lambda_{2,\varepsilon}\|_{Q_2} \leq C\left(\varepsilon_1\|\lambda_1\|_{W_1^+} + \varepsilon_2\|\lambda_2\|_{W_2^+}\right). \quad \text{(A.23)}$$

Let us consider the discretized version of the problem (A.5): given $f \in V'$, $g_1 \in Q_1'$ and $g_2 \in Q_2'$, find $(u_h, \lambda_{1,h}, \lambda_{2,h}) \in V_h \times Q_{1,h} \times Q_{2,h}$ such that

$$\begin{aligned} a(u_h, v_h) + b_1(v_h, \lambda_{1,h}) + b_2(v_h, \lambda_{2,h}) &= \langle f, v_h\rangle && \forall v_h \in V_h \\ b_1(u_\varepsilon, \mu_{1,h}) - \varepsilon_1(\lambda_{1,h}, \mu_{1,h})_{W_1} &= \langle g_1, \mu_{1,h}\rangle_{Q_1'\times Q_1} && \forall \mu_{1,h} \in Q_{1,h} \\ b_2(u_h, \mu_{2,h}) - \varepsilon_2(\lambda_{2,h}, \mu_{2,h})_{W_2} &= \langle g_2, \mu_{2,h}\rangle_{Q_2'\times Q_2} && \forall \mu_{2,h} \in Q_{2,h}. \end{aligned} \quad \text{(A.24)}$$

Assumption 7. *Together with Assumption 5, we assume that we are given three finite dimensional spaces* $V_h \subset V$, $Q_{1,h} \subset Q_1$ *and* $Q_{2,h} \subset Q_2$. *Let us define* A_h *and* $B_{i,h}$, *respectively, the restrictions* $A_{|V_h}$ *and* $B_{i|V_h}$. *Together with the kernels* K_i *and* H_i, *we consider then the discrete kernels*

$$K_{i,h} = \ker B_{i,h}, \qquad K_h = K_{1,h} \cap K_{2,h}, \qquad H_{i,h} = \ker B_{i,h}^T.$$

Assumption 8. *Let us assume that there exist two constants* $\beta_1, \beta_2 > 0$ *such that*

$$\inf_{\mu_h \in Q_{1,h}} \sup_{v_h \in K_{2,h}} \frac{b_1(v_h, \mu_h)}{\|v_h\|_V \|\mu_h\|_{Q_1}} \geq \beta_1$$

and

$$\inf_{\mu_h \in Q_{2,h}} \sup_{v_h \in V_h} \frac{b_2(v_h, \mu_h)}{\|v_h\|_V \|\mu_h\|_{Q_2}} \geq \beta_2.$$

Theorem 13. *Together with Assumption 6, 7 and 8, assume that, for* $i = 1, 2$, $Q_{i,h} \subset W_i$. *For every* $0 \leq \varepsilon_1, \varepsilon_2 \leq 1/2$, *let* $(u_\varepsilon, \lambda_{1,\varepsilon}, \lambda_{2,\varepsilon})$ *and* $(u_h, \lambda_{1,h}, \lambda_{2,h})$ *be the solutions of* (A.5) *and* (A.24) *respectively. Then, we have*

$$\begin{aligned} \|u_\varepsilon - u_h\|_V^2 + \|\lambda_{1,\varepsilon} - \lambda_{1,h}\|_{Q_1}^2 + \varepsilon_1\|\lambda_{1,\varepsilon} - \lambda_{1,h}\|_{W_1}^2 + \|\lambda_{2,\varepsilon} - \lambda_{2,h}\|_{Q_2}^2 + \varepsilon_2\|\lambda_{2,\varepsilon} - \lambda_{2,h}\|_{W_2}^2 \\ \leq C\Big(\inf_{v_h \in V_h} \|u - v_h\|_V^2 + \inf_{\mu_{1,h} \in Q_{1,h}} \left\{\|\lambda_{1,\varepsilon} - \mu_{1,h}\|_{Q_1}^2 + \varepsilon_1\|\lambda_{1,\varepsilon} - \mu_{1,h}\|_{W_1}^2\right\} + \\ \inf_{\mu_{2,h} \in Q_{2,h}} \left\{\|\lambda_{2,\varepsilon} - \mu_{2,h}\|_{Q_2}^2 + \varepsilon_2\|\lambda_{2,\varepsilon} - \mu_{2,h}\|_{W_2}^2\right\} \Big). \end{aligned}$$

Proof. For the proof we refer to [10, Theorem 5.5.4 and Remark 5.5.5]. □

Appendix B

Discrete inf-sup stability on the parametric domain

In this section, we report some useful results about the discrete inf-sup stability between spline spaces built on parametric domains, see [7]. Starting from a generic open knot vector, defined on $\widehat{\gamma} = [0, 1]$,

$$\Xi^p = \{\xi_1, \dots, \xi_{n+p+1}\},$$

with

$$0 = \xi_1 = \xi_2 = \ldots = \xi_{p+1} < \xi_{p+2} < \ldots < \xi_n < \xi_{n+1} = \ldots = \xi_{n+p} = \xi_{n+p+1} = 1,$$

we consider three reduced knot vectors:

$$\begin{aligned}
\Xi^{p-1} &= \{\cancel{\xi_1}, \xi_2, \dots, \xi_{p+1}, \xi_{p+2}, \dots, \xi_n, \xi_{n+1}, \dots, \xi_{n+p}, \cancel{\xi_{n+p+1}}\} \\
\Xi_M^{p-1} &= \{\cancel{\xi_1}, \xi_2, \dots, \xi_{p+1}, \cancel{\xi_{p+2}}, \dots, \cancel{\xi_n}, \xi_{n+1}, \dots, \xi_{n+p}, \cancel{\xi_{n+p+1}}\} \\
\Xi_M^{p-2} &= \{\cancel{\xi_1}, \cancel{\xi_2}, \dots, \xi_{p+1}, \cancel{\xi_{p+2}}, \dots, \cancel{\xi_n}, \xi_{n+1}, \dots, \cancel{\xi_{n+p}}, \cancel{\xi_{n+p+1}}\}.
\end{aligned}$$

We also introduce six different isogeometric spaces:

$$\begin{aligned}
S_{h,00}^p &= \left\{w \in S_h^p(\Xi^p) : w(0) = w(1) = w'(0) = w'(1) = 0\right\} \\
S_{h,0}^{p-1} &= \left\{w \in S_h^{p-1}\left(\Xi^{p-1}\right) : w(0) = w(1) = 0\right\} \\
S_{h,0,\mathrm{zmv}}^{p-1} &= \left\{w \in S_{h,0}^{p-1} : \int_{\widehat{\gamma}} w = 0\right\} \\
S_{h,M}^{p-1} &= \left\{w \in S_h^{p-1}\left(\Xi_M^{p-1}\right)\right\} \\
S_{h,M,\mathrm{zmv}}^{p-1} &= \left\{w \in S_{h,M}^{p-1} : \int_{\widehat{\gamma}} w = 0\right\} \\
S_{h,M}^{p-2} &= \left\{w \in S_h^{p-1}\left(\Xi_M^{p-2}\right)\right\}.
\end{aligned}$$

Assumption 9. *Let us assume $n \geq 3p - 1$.*

Proposition 4. *The derivative operators $D : S_{h,00}^p \to S_{h,0,\mathrm{zmv}}^{p-1}$ and $D : S_{h,\mathrm{M},\mathrm{zmv}}^{p-1} \to S_{h,\mathrm{M}}^{p-2}$ are bijections.*

Proof. Let us focus on the operator $D : S^p_{h,00} \to S^{p-1}_{h,0,\text{zmv}}$. For [65, Theorem 5.9] the derivative of a spline of degree p is a spline of degree $p-1$. Now, if $v \in S^p_{h,00}$ it holds

$$\int_{\widehat{\gamma}} Dv = v(1) - v(0) = 0,$$

then $Dv \in S^{p-1}_{h,0,\text{zmv}}$. To show the injectivity let $v, w \in S^p_{h,00}$ be such that $Dv = DW$. Then we have $v = w + c$, with $c \in \mathbb{R}$. But $v(0) = w(0) = 0$ and so $v = w$. The surjectivity is shown by constructing an element of the preimage space. Given $w \in S^{p-1}_{h,0,\text{zmv}}$ we define

$$v(x) = \int_0^x w(s)ds.$$

From [65, Theorem 5.16] it follows that v is a spline of degree p. We also have $v(0) = v(1) = 0$, $v'(0) = w(0) = w(1) = v'(1) = 0$. Thus $v \in S^p_{h,00}$.

Similarly, for $D : S^{p-1}_{h,\text{M,zmv}} \to S^{p-2}_{h,\text{M}}$, if $v \in S^{p-1}_{h,\text{M,zmv}}$, from [65, Theorem 5.9] it follows that $Dv \in S^{p-2}_{h,\text{M}}$. For the injectivity, if $v, w \in S^{p-1}_{h,\text{M,zmv}}$ are such that $Dv = Dw \in S^{p-2}_{h,\text{M}}$, then $v = w + c$, with $c \in \mathbb{R}$. From the hypothesis follows that

$$0 = \int_0^1 v = \int_0^1 w + c = c + \int_0^1 w,$$

but we have

$$\int_0^1 w = 0$$

so $c = 0$. For the surjectivity, if $w \in S^{p-2}_{h,\text{M}}$, we can define

$$v(x) = \int_0^x w(s)ds - \int_0^1 w(s)ds.$$

From [65, Theorem 5.16] it follows that $v \in S^{p-1}_{h,\text{M}}$ and from

$$\int_0^1 v(x)dx = \int_0^1 w(s)ds - \int_0^1 w(s)ds = 0$$

we obtain $v \in S^{p-1}_{h,\text{M,zmv}}$. □

Proposition 5. *There exists a constant $C > 0$ such that*

$$\|w\|_{L^2(\widehat{\gamma})} \leq C\|Dw\|_{[H^1(\widehat{\gamma})]'}, \qquad \forall w \in H^1_0(\widehat{\gamma}).$$

Proof. For all $w \in L^2(\widehat{\gamma})$, there exists a function $\overline{w} \in H^1_{\text{zmv}}(\widehat{\gamma})$, with

$$H^1_{\text{zmv}}(\widehat{\gamma}) = \left\{ \overline{w} \in H^1(\widehat{\gamma}) : \int_{\widehat{\gamma}} \overline{w} = 0 \right\},$$

such that $D\overline{w} = w$. For all $v \in H_0^1(\widehat{\gamma})$ it holds

$$\begin{aligned}\|v\|_{L^2(\widehat{\gamma})} &= \sup_{w \in L^2(\widehat{\gamma})} \frac{\int_{\widehat{\gamma}} vw}{\|w\|_{L^2(\widehat{\gamma})}} = \sup_{\overline{w} \in H^1_{\mathrm{zmv}}(\widehat{\gamma})} \frac{\int_{\widehat{\gamma}} vD\overline{w}}{|\overline{w}|_{H^1(\widehat{\gamma})}} \\ &\leq C \sup_{\overline{w} \in H^1_{\mathrm{zmv}}(\widehat{\gamma})} \frac{\int_{\widehat{\gamma}} \overline{w} Dv}{\|\overline{w}\|_{H^1(\widehat{\gamma})}} \leq C \|Dv\|_{[H^1(\widehat{\gamma})]'},\end{aligned}$$

where C is the Poincaré constant. □

Proposition 6. *Let be $2 \leq p \leq 9$. For a uniform knot vector defined on $\widehat{\gamma}$, there exists a constant $C > 0$, independent of h, such that*

$$\inf_{w \in S^{p-1}_{h,0}} \sup_{\mu \in S^{p-1}_{h,\mathrm{M}}} \frac{\int_{\widehat{\gamma}} w\mu}{\|w\|_{L^2(\widehat{\gamma})} \|\mu\|_{L^2(\widehat{\gamma})}} \geq C. \tag{B.1}$$

Proof. If we prove that, for all $w \in S^{p-1}_{h,0}$, there exists $\mu \in S^{p-1}_{h,\mathrm{M}}$ such that

$$\|\mu\|_{L^2(\widehat{\gamma})} \leq C_1 \|w\|_{L^2(\widehat{\gamma})} \tag{B.2}$$

$$\|w\|^2_{L^2(\widehat{\gamma})} \leq C_2 \int_{\widehat{\gamma}} w\mu, \tag{B.3}$$

then the thesis holds with $C = \frac{1}{C_1 C_2}$.
First of all, we observe that

$$\dim\left(S^{p-1}_{h,0}\right) = \dim\left(S^{p-1}_{h,\mathrm{M}}\right) = n - 2 = m.$$

Let $(\widehat{B}_i)_{i=1}^m$ and $(\widetilde{B}_i)_{i=1}^m$ be the B-spline basis functions of $S^{p-1}_{h,0}$ and $S^{p-1}_{h,\mathrm{M}}$, respectively. We denote by $\widehat{I}_i$ and $\widetilde{I}_i$ the supports of $\widehat{B}_i$ and $\widetilde{B}_i$, respectively, and by $|\widehat{I}_i|$ and $|\widetilde{I}_i|$ their respective lengths. Having $w \in S^{p-1}_{h,0}$, we can express it as

$$w = \sum_{i=1}^m w_i \widehat{B}_i$$

and we can define $\mu \in S^{p-1}_{h,\mathrm{M}}$ as

$$\mu = \sum_{i=1}^m w_i \widetilde{B}_i.$$

Let be $I \subset (0,1)$ a knot span. The restriction of μ on I can be expressed as

$$\mu_{|I} = \sum_{i:\, I \subset \widetilde{I}_i} w_i \widetilde{B}_i,$$

then we have

$$\|\mu\|^2_{L^2(\widehat{\gamma})} \leq \int_I \left(\sum_{i:\, I \subset \widetilde{I}_i} w_i \widetilde{B}_i \right)^2 \leq \int_I \left(\sum_{i:\, I \subset \widetilde{I}_i} w_i^2 \cdot \sum_{i:\, I \subset \widetilde{I}_i} \widetilde{B}_i^2 \right).$$

Since every function in B-spline basis $(\widetilde{B}_i)_{i=1}^m$ satisfies $0 \leq \widetilde{B}_i \leq 1$, we obtain

$$\|\mu\|^2_{L^2(\widehat{\gamma})} \leq |I| \sum_{i:\, I \subset \widetilde{I}_i} w_i^2.$$

From [65, Theorem 4.41], there exists a constant $C > 0$, independent of h, such that

$$\|\mu\|^2_{L^2(\widehat{\gamma})} \leq |I| \sum_{i:\, I \subset \widetilde{I}_i} w_i^2 \leq C|I| \sum_{i:\, I \subset \widetilde{I}_i} |\widehat{I}_i|^{-1} \|w\|^2_{L^2(\widehat{I}_i)} \leq C \sum_{i:\, I \subset \widetilde{I}_i} \|w\|^2_{L^2(\widehat{I}_i)}.$$

Finally, summing over all knot span I, we get (B.2).

In order to prove (B.3), we note that, for all $p+1 \leq i \leq n-p$, it holds $\widehat{B}_i = \widetilde{B}_i$, then

$$\int_{\widehat{\gamma}} w\mu = \int_0^{\xi_{2p+1}} w\mu + \|w\|^2_{L^2(\xi_{2p+1}, \xi_{n-1})} + \int_{\xi_{n-1}}^1 w\mu. \tag{B.4}$$

We focus on the first term of (B.4). We want to prove that there exists a constant $C_2 > 0$, independent of h, such that

$$\inf_{\substack{w \in S^{p-1}_{h,0}, \\ w \neq 0}} \frac{\int_0^{\xi_{2p+1}} w\mu}{\|w\|^2_{L^2(0,\xi_{2p+1})}} \geq C_2. \tag{B.5}$$

The restrictions of w and μ on $[0, \xi_{2p+2}]$ can be expressed as

$$\begin{aligned} w(\zeta)_{|[0,\xi_{2p+1}]} &= \sum_{i=1}^{2p} w_i \widehat{B}_i(\zeta)_{|[0,\xi_{2p+1}]} = \sum_{i=1}^{2p} w_i \widehat{B}^*_i \left(\frac{\zeta}{h}\right)_{|[0,\xi_{2p+1}]} \\ \mu_{|[0,\xi_{2p+1}]} &= \sum_{i=1}^{2p} w_i \widetilde{B}_i(\zeta)_{|[0,\xi_{2p+1}]} = \sum_{i=1}^{2p} w_i \widetilde{B}^*_i \left(\frac{\zeta}{h}\right)_{|[0,\xi_{2p+1}]}, \end{aligned}$$

where $(\widehat{B}^*_i)_{i=1}^m$ and $(\widetilde{B}^*_i)_{i=1}^m$ are, respectively, the B-spline basis analogous to $(\widehat{B}_i)_{i=1}^m$ and $(\widetilde{B}_i)_{i=1}^m$, but built on

$$\begin{aligned} \Xi^{p-1}_* &= \{\cancel{\xi^*_1}, \xi^*_2, \ldots, \xi^*_{p+1}, \xi^*_{p+2}, \ldots, \xi^*_n, \xi^*_{n+1}, \ldots, \xi^*_{n+p}, \cancel{\xi^*_{n+p+1}}\} \\ \Xi^{p-1}_{M,*} &= \left\{\cancel{\xi^*_1}, \xi^*_2, \ldots, \xi^*_{p+1}, \cancel{\xi^*_{p+2}}, \ldots, \cancel{\xi^*_n}, \xi^*_{n+1}, \ldots, \xi^*_{n+p}, \cancel{\xi^*_{n+p+1}}\right\}, \end{aligned}$$

with

$$0 = \xi^*_1 = \xi^*_2 = \ldots = \xi^*_{p+1} < \xi^*_{p+2} < \ldots < \xi^*_n < \xi^*_{n+1} = \ldots = \xi^*_{n+p} = \xi^*_{n+p+1},$$

$p=2$	$p=3$	$p=4$	$p=5$	$p=6$	$p=7$	$p=8$	$p=9$
0.5763	0.5889	0.6152	0.6268	0.6044	0.5321	0.3984	0.1819

TABLE B.1: Numerically computed value of C_3.

where each knot span in Ξ_*^{p-1} has size equal to 1. With a change of variables, we obtain

$$\begin{aligned}\inf_{\substack{w\in S_{h,0}^{p-1},\\ w\neq 0}} \frac{\int_0^{\xi_{2p+1}} w\mu}{\|w\|^2_{L^2(0,\xi_{2p+1})}} &= \inf_{\mathbf{w}\in\mathbb{R}^p\setminus\{0\}} \frac{\int_0^{\xi_{2p+1}} \left(\sum_{i=1}^{2p} \mathbf{w}_i \widehat{B}_i(\zeta)\cdot\sum_{i=1}^{2p} \mathbf{w}_i \widetilde{B}_i(\zeta)\right) d\zeta}{\int_0^{\xi_{2p+1}} \left(\sum_{i=1}^{2p} \mathbf{w}_i \widehat{B}_i(\zeta)\right)^2 d\zeta} \\ &= \inf_{\mathbf{w}\in\mathbb{R}^p\setminus\{0\}} \frac{\int_0^{\xi^*_{2p+1}} \left(\sum_{i=1}^{2p} \mathbf{w}_i \widehat{B}^*_i(z)\cdot\sum_{i=1}^{2p} \mathbf{w}_i \widetilde{B}^*_i(z)\right) dz}{\int_0^{\xi^*_{2p+1}} \left(\sum_{i=1}^{2p} \mathbf{w}_i \widehat{B}^*_i(z)\right)^2 dz} = C_3.\end{aligned} \tag{B.6}$$

We stress the fact that C_3 is independent of h. To conclude, we only need to show that it is positive. This step can be done numerically. In Table B.1 we report the value of C_3 for $p=2,\dots,9$. Thanks to the symmetry of B-spline basis, with a similar argument, we can also prove that

$$\inf_{\substack{w\in S_{h,0}^{p-1},\\ w\neq 0}} \frac{\int_{\xi_{n-1}}^{1} w\mu}{\|w\|^2_{L^2(\xi_{n-1},1)}} = C_3. \tag{B.7}$$

Combining (B.4), (B.6) and (B.7) we get (B.3). □

Remark 13. *The restriction to $p\leq 9$ in the assumptions of Proposition 6 is due to the fact that for $p\geq 10$ the constant C_2 appearing in* (B.5) *becomes negative. Nevertheless, numerical tests show that the quantity in* (B.1) *is positive and independent of h even for greater values of p.*

Definition 1. *The operator $\widehat{\mathcal{M}}_h^* : L^2(\widehat{\gamma}) \to S_{h,\mathrm{M}}^{p-1}$ given by*

$$\int_{\widehat{\gamma}} \widehat{\mathcal{M}}_h^* w\psi = \int_{\widehat{\gamma}} \varphi\psi, \qquad\qquad \forall \psi \in S_{h,0}^{p-1},$$

is well defined. This follows from the fact that $\dim(S_{h,0}^{p-1}) = \dim(S_{h,\mathrm{M}}^{p-1})$ and from Proposition 6.

Lemma 4. *The operator $\widehat{\mathcal{M}}_h^* : S_{h,0}^{p-1} \to S_{h,\mathrm{M}}^{p-1}$ is bijective.*

Proof. Let us assume that there exists $\varphi \in S_{h,0}^{p-1}$ such that $\widehat{\mathcal{M}}_h^*\varphi = 0$. For all $S_{h,0}^{p-1}$ it holds

$$\int_{\widehat{\gamma}} \varphi\psi = \int_{\widehat{\gamma}} \left(\varphi - \widehat{\mathcal{M}}_h^*\varphi\right)\psi = 0,$$

then $\varphi = 0$ on $\widehat{\gamma}$. By the fact that $\dim(S_{h,0}^{p-1}) = \dim(S_{h,M}^{p-1})$, surjectivity follows. □

Proposition 7. *There exists a constant $C > 0$, independent of h, such that, for any $\varphi \in S_{h,0}^{p-1}$, it holds*

$$\sup_{\lambda \in S_M^{p-1}} \frac{\int_{\widehat{\gamma}} \varphi\lambda}{\|\lambda\|_{H^1(\widehat{\gamma})}} \geq C\|\varphi\|_{[H^1(\widehat{\gamma})]'}.$$

Proof. First of all, we are interested in showing that $\widehat{\mathcal{M}}_h^*$ is L^2-stable. Thanks to Proposition [10, Proposition 3.4.3], we can interchange the spaces in Proposition 6 and we obtain

$$\sup_{w \in S_{h,0}^{p-1}} \frac{\int_{\widehat{\gamma}} w\mu}{\|w\|_{L^2(\widehat{\gamma})}} \geq C\|\mu\|_{L^2(\widehat{\gamma})} \qquad \forall \mu \in S_{h,M}^{p-1}.$$

In particular, for each $\lambda \in L^2(\widehat{\gamma})$ it holds $\widehat{\mathcal{M}}_h^*\lambda \in S_{h,M}^{p-1}$, thus

$$\|\widehat{\mathcal{M}}_h^*\lambda\|_{L^2(\widehat{\gamma})} \leq C \sup_{w \in S_{h,0}^{p-1}} \frac{\int_{\widehat{\gamma}} w\widehat{\mathcal{M}}_h^*\lambda}{\|w\|_{L^2(\widehat{\gamma})}} = C \sup_{w \in S_{h,0}^{p-1}} \frac{\int_{\widehat{\gamma}} w\lambda}{\|w\|_{L^2(\widehat{\gamma})}} \leq C\|\lambda\|_{L^2(\widehat{\gamma})}.$$

We check that $\widehat{\mathcal{M}}_h^*$ is also H^1-stable. Let be $\lambda \in H^1(\widehat{\gamma})$ and let λ_h be its best approximation in $S_{h,M}^{p-1}$. Using the inverse inequality for splines, we get

$$\begin{aligned}
\|\widehat{\mathcal{M}}_h^*\lambda\|_{H^1(\widehat{\gamma})} &\leq \|\widehat{\mathcal{M}}_h^*\lambda - \lambda_h\|_{H^1(\widehat{\gamma})} + \|\lambda_h\|_{H^1(\widehat{\gamma})} \\
&= \|\widehat{\mathcal{M}}_h^*(\lambda - \lambda_h)\|_{H^1(\widehat{\gamma})} + \|\lambda_h\|_{H^1(\widehat{\gamma})} \\
&\leq Ch^{-1}\|\widehat{\mathcal{M}}_h^*(\lambda - \lambda_h)\|_{L^2(\widehat{\gamma})} + \|\lambda_h\|_{H^1(\widehat{\gamma})},
\end{aligned}$$

but thanks to the L^2-stability we have

$$\begin{aligned}
\|\widehat{\mathcal{M}}_h^*\lambda\|_{H^1(\widehat{\gamma})} &\leq Ch^{-1}\|\lambda - \lambda_h\|_{L^2(\widehat{\gamma})} + \|\lambda_h\|_{H^1(\widehat{\gamma})} \\
&\leq C\|\lambda\|_{H^1(\widehat{\gamma})} + C'\|\lambda\|_{H^1(\widehat{\gamma})} \leq C\|\lambda\|_{H^1(\widehat{\gamma})}.
\end{aligned}$$

For any $\varphi \in [H^1(\widehat{\gamma})]'$ it holds

$$\sup_{\mu \in H^1(\widehat{\gamma})} \frac{\int_{\widehat{\gamma}} \mu\varphi}{\|\mu\|_{H^1(\widehat{\gamma})}} = C\|\varphi\|_{[H^1(\widehat{\gamma})]'}, \tag{B.8}$$

and, in particular, it holds for any $\varphi \in S_{h,0}^{p-1}$. Now, from Lemma 4, for each $\psi \in S_{h,M}^{p-1}$ there exists $\mu \in S_{h,0}^{p-1}$ such that $\psi = \widehat{\mathcal{M}}_h^*\mu$, that is

$$\int_{\widehat{\gamma}} \psi\varphi = \int_{\widehat{\gamma}} \mu\varphi \qquad \forall \varphi \in S_{h,0}^{p-1}$$

and $\|\psi\|_{H^1(\widehat{\gamma})} \leq C\|\mu\|_{H^1(\widehat{\gamma})}$. Hence, for all $\varphi \in S_{h,0}^{p-1}$ there exists $\psi = \widehat{\mathcal{M}}_h^*\mu \in S_{h,M}^{p-1}$ such that

$$\frac{\int_{\widehat{\gamma}} \psi\varphi}{\|\psi\|_{H^1(\widehat{\gamma})}} \geq C\frac{\int_{\widehat{\gamma}} \mu\varphi}{\|\mu\|_{H^1(\widehat{\gamma})}},$$

taking the supremum over $\mu \in H^1(\widehat{\gamma})$ and using (B.8) yields the thesis. □

Proposition 8. *There exists a constant $C > 0$, independent of h, such that, for any $\lambda \in S^{p-1}_{h,M,\mathrm{zmv}}$, it holds*

$$\sup_{\varphi \in S^{p-1}_{h,0,\mathrm{zmv}}} \frac{\int_{\widehat{\gamma}} \varphi\lambda}{\|\varphi\|_{[H^1(\widehat{\gamma})]'}} \geq C\|\lambda\|_{H^1(\widehat{\gamma})}.$$

Proof. From Proposition 7 we have that for all $\varphi \in S^{p-1}_{h,0}$ there exists $\lambda \in S^{p-1}_{h,M}$ such that

$$\int_{\widehat{\gamma}} \varphi\lambda \geq C\|\varphi\|_{[H^1(\widehat{\gamma})]'}\|\lambda\|_{H^1(\widehat{\gamma})},$$

and in particular it holds for all $\varphi \in S^{p-1}_{h,0,\mathrm{zmv}}$. Now we can choose

$$\lambda^* = \lambda - \int_{\widehat{\gamma}} \lambda.$$

In this way, we obtain

$$\int_{\widehat{\gamma}} \varphi\lambda^* = \int_{\widehat{\gamma}} \varphi\lambda \geq C\|\varphi\|_{[H^1(\widehat{\gamma})]'}\|\lambda\|_{H^1(\widehat{\gamma})}.$$

It is straightforward to see that $\|\lambda^*\|_{H^1(\widehat{\gamma})} \leq \|\lambda\|_{H^1(\widehat{\gamma})}$, then for all $\varphi \in S^{p-1}_{h,0,\mathrm{zmv}}$ it holds

$$\sup_{\lambda^* \in S^{p-1}_{h,M,\mathrm{zmv}}} \frac{\int_{\widehat{\gamma}} \varphi\lambda^*}{\|\lambda^*\|_{H^1(\widehat{\gamma})}} \geq C\|\varphi\|_{[H^1(\widehat{\gamma})]'}.$$

Thanks to [10, Proposition 3.4.3], we can interchange the spaces and we obtain the thesis. □

Theorem 14. *There exists a constant $C > 0$, independent of h, such that*

$$\inf_{\mu \in S^{p-2}_{h,M}} \sup_{w \in S^{p}_{h,00}} \frac{\int_{\widehat{\gamma}} w\mu}{\|w\|_{L^2(\widehat{\gamma})}\|\mu\|_{L^2(\widehat{\gamma})}} \geq C.$$

Proof. Let $\mu \in S^{p-2}_{h,M}$, then there exists $\lambda \in S^{p-1}_{h,M,\mathrm{zmv}}$ such that $\lambda' = \mu$. integrating by parts, we get

$$\sup_{w \in S^{p}_{h,00}} \frac{\int_{\widehat{\gamma}} w\mu}{\|w\|_{L^2(\widehat{\gamma})}} = \sup_{w \in S^{p}_{h,00}} \frac{\int_{\widehat{\gamma}} w\lambda'}{\|w\|_{L^2(\widehat{\gamma})}} = \sup_{w \in S^{p}_{h,00}} \frac{\int_{\widehat{\gamma}} w'\lambda}{\|w\|_{L^2(\widehat{\gamma})}}.$$

From Proposition 5 we have that for all

$$\|w\|_{L^2(\widehat{\gamma})} \leq C\|w'\|_{[H^1(\widehat{\gamma})]'} \qquad \forall w \in H^1_0(\widehat{\gamma}).$$

Then, setting $\varphi = w'$ we obtain

$$\sup_{w \in S^{p}_{h,00}} \frac{\int_{\widehat{\gamma}} w'\lambda}{\|w\|_{L^2(\widehat{\gamma})}} \geq C \sup_{w \in S^{p}_{h,00}} \frac{\int_{\widehat{\gamma}} w'\lambda}{\|w'\|_{[H^1(\widehat{\gamma})]'}} = C \sup_{\varphi \in S^{p-1}_{h,0,\mathrm{zmv}}} \frac{\int_{\widehat{\gamma}} \varphi\lambda}{\|\varphi\|_{[H^1(\widehat{\gamma})]'}}$$

and applying Proposition 8 we get the result

$$\sup_{\varphi \in S^{p-1}_{h,0,\mathrm{zmv}}} \frac{\int_{\widehat{\gamma}} \varphi \lambda}{\|\varphi\|_{[H^1(\widehat{\gamma})]'}} \geq C\|\lambda\|_{H^1(\widehat{\gamma})} \geq C|\lambda|_{H^1(\widehat{\gamma})} = C\|\mu\|_{L^2(\widehat{\gamma})}.$$

□

Bibliography

[1] A. Apostolatos, M. Breitenberger, R. Wüchner, and K. Bletzinger. "Domain Decomposition Methods and Kirchhoff-Love Shell Multipatch Coupling in Isogeometric Analysis". In: *Isogeometric Analysis and Applications 2014*. Ed. by Bert Jüttler and Bernd Simeon. Cham: Springer International Publishing, 2015, pp. 73–101. ISBN: 978-3-319-23315-4.

[2] F. Auricchio, L. Beirão da Veiga, T. J. R. Hughes, A. Reali, and G. Sangalli. "Isogeometric collocation for elastostatics and explicit dynamics". In: *Comput. Methods Appl. Mech. Engrg.* 249-252 (2012), pp. 2–14. ISSN: 0045-7825.

[3] I. Babuška. "The Finite Element Method with Penalty". In: *Mathematics of Computation* 27.122 (1973), pp. 221–228. ISSN: 00255718, 10886842.

[4] I. Babuška and M. Zlamal. "Nonconforming Elements in the Finite Element Method with Penalty". In: *SIAM Journal on Numerical Analysis* 10.5 (1973), pp. 863–875. ISSN: 00361429.

[5] Y. Bazilevs, L. Beirao Da Veiga, J. A. Cotrell, T. J. R. Hughes, and G. Sangalli. "Isogeometric Analysis: approximation, stability and error estimates for h-refined meshes". In: *Mathematical Models and Methods in Applied Sciences* 16.07 (2006), pp. 1031–1090.

[6] P. Behnoudfar, V. M. Calo, G. Loli, A. Reali, and G. Sangalli. "Explicit high-order generalized-α methods for isogeometric analysis of structural dynamics". In: *In preparation* (2020).

[7] A. Benvenuti, G. Loli, G. Sangalli, and T. Takacs. "Isogeometric Analysis for weak C^1-continuous Mortar Method". In: *In preparation* (2020).

[8] J. Benzaken, A. J. Herrema, M. C. Hsu, and J. A. Evans. "A rapid and efficient isogeometric design space exploration framework with application to structural mechanics". In: *Computer Methods in Applied Mechanics and Engineering* 316 (2017). Special Issue on Isogeometric Analysis: Progress and Challenges, pp. 1215 –1256. ISSN: 0045-7825.

[9] A. Bünger, S. Dolgov, and M. Stoll. "A Low-Rank Tensor Method for PDE-Constrained Optimization with Isogeometric Analysis". In: *SIAM Journal on Scientific Computing* 42.1 (2020), A140–A161.

[10] D. Boffi, F. Brezzi, and M. Fortin. *Mixed Finite Element Methods and Applications*. Springer Series in Computational Mathematics. Springer Berlin Heidelberg, 2013. ISBN: 9783642365195.

[11] A. Bressan and E. Sande. "Approximation in FEM, DG and IGA: a theoretical comparison". In: *Numerische Mathematik* 143.4 (2019), pp. 923–942.

[12] E. Brivadis, A. Buffa, B. Wohlmuth, and L. Wunderlich. "Isogeometric mortar methods". In: *Computer Methods in Applied Mechanics and Engineering* 284 (2015). Isogeometric Analysis Special Issue, pp. 292 –319. ISSN: 0045-7825.

[13] A. Buffa, L. Coradello, and G. Loli. *A projected super-penalty method for the C^1-coupling of multi-patch isogeometric Kirchhoff plates*. 2020. arXiv: 2007.14343.

[14] A. Buffa, L. Coradello, and G. Loli. "Isogeometric penalty method for the Bilaplace equation". In: *In preparation* (2020).

[15] F. Calabrò, G. Loli, G. Sangalli, and M. Tani. "Quadrature Rules in the Isogeometric Galerkin Method: State of the Art and an Introduction to Weighted Quadrature". In: *Advanced Methods for Geometric Modeling and Numerical Simulation*. Ed. by Carlotta Giannelli and Hendrik Speleers. Cham: Springer International Publishing, 2019, pp. 43–55.

[16] J. Chan and J. A. Evans. "Multi-patch discontinuous Galerkin isogeometric analysis for wave propagation: Explicit time-stepping and efficient mass matrix inversion". In: *Comput. Methods Appl. Mech. Engrg.* 333 (2018), pp. 22–54. ISSN: 0045-7825.

[17] J. Chung and G. M. Hulbert. "A time integration algorithm for structural dynamics with improved numerical dissipation: the generalized-α method". In: *Journal of Applied Mechanics* 60.2 (1993), pp. 371–375.

[18] J. A. Cottrell, T. J. R. Hughes, and Y. Bazilevs. *Isogeometric Analysis*. en. Chichester, UK: John Wiley & Sons, Ltd, 2009. ISBN: 978-0-470-74908-1 978-0-470-74873-2.

[19] C. De Boor. *A practical guide to splines, Revised Edition*. Vol. 27. Applied Mathematical Sciences. Springer-Verlag, New York, 2001.

[20] C. De Boor. "Splines as linear combinations of B-splines a Survey". In: *Approximation Theory, II*. New York: Academic Press, 1976, pp. 1–47.

[21] Q. Deng, P. Behnoudfar, and V. M. Calo. "High-order generalized-α methods for hyperbolic problems". In: (2019). arXiv: 1906.06081.

[22] M. Dittmann, S. Schuß, B. Wohlmuth, and C. Hesch. "Crosspoint modification for multi-patch isogeometric analysis". In: *Computer Methods in Applied Mechanics and Engineering* 360 (2020), p. 112768. ISSN: 0045-7825.

[23] M. Dittmann, S. Schuß, B. Wohlmuth, and C. Hesch. "Weak C^n coupling for multipatch isogeometric analysis in solid mechanics". In: *International Journal for Numerical Methods in Engineering* 118.11 (2019), pp. 678–699.

[24] T.X. Duong, F. Roohbakhshan, and R.A. Sauer. "A new rotation-free isogeometric thin shell formulation and a corresponding continuity constraint for patch boundaries". In: *Computer Methods in Applied Mechanics and Engineering* 316 (2017). Special Issue on Isogeometric Analysis: Progress and Challenges, pp. 43 –83. ISSN: 0045-7825.

[25] T. Elguedj, Y. Bazilevs, V. M. Calo, and T. J. R. Hughes. "B and F projection methods for nearly incompressible linear and non-linear elasticity and plasticity using higher-order NURBS elements". In: *Comput. Methods Appl. Mech. Engrg.* 197.33-40 (2008), pp. 2732–2762.

[26] H. C. Elman, D. J. Silvester, and A. J. Wathen. *Finite elements and fast iterative solvers: with applications in incompressible fluid dynamics*. Oxford University Press, USA, 2014.

[27] J. A. Evans, Y. Bazilevs, I. Babuška, and T. J. R. Hughes. "n-Widths, sup–infs, and optimality ratios for the k-version of the isogeometric finite element method". In: *Comput. Methods Appl. Mech. Engrg.* 198.21-26 (2009), pp. 1726–1741.

[28] J. A. Evans, R. R. Hiemstra, T. J. R. Hughes, and A. Reali. "Explicit higher-order accurate isogeometric collocation methods for structural dynamics". In: *Comput. Methods Appl. Mech. Engrg.* 338 (2018), pp. 208–240. ISSN: 0045-7825.

[29] K. P. S. Gahalaut, S. K. Tomar, and C. Douglas. "Condition number estimates for matrices arising in NURBS based isogeometric discretizations of elliptic partial differential equations". In: (2014). arXiv: 1406.6808.

[30] L. Gao and V. M. Calo. "Fast isogeometric solvers for explicit dynamics". In: *Comput. Methods Appl. Mech. Engrg.* 274 (2014), pp. 19–41. ISSN: 0045-7825.

[31] H. Gómez, V. M. Calo, Y. Bazilevs, and T. J. R. Hughes. "Isogeometric analysis of the Cahn-Hilliard phase-field model". In: *Computer Methods in Applied Mechanics and Engineering* 197.49 (2008), pp. 4333 –4352. ISSN: 0045-7825.

[32] I. Harari and E. Grosu. "A unified approach for embedded boundary conditions for fourth-order elliptic problems". In: *International Journal for Numerical Methods in Engineering* 104.7 (2015), pp. 655–675.

[33] S. Hartmann, D. Benson, and A. Nagy. "Isogeometric Analysis with LS-DYNA". In: *Journal of Physics: Conference Series* 734 (2016), p. 032125.

[34] A. J. Herrema, E. L. Johnson, D. Proserpio, M. C. H. Wu, J. Kiendl, and M. Hsu. "Penalty coupling of non-matching isogeometric Kirchhoff-Love shell patches with application to composite wind turbine blades". In: *Computer Methods in Applied Mechanics and Engineering* 346 (2019), pp. 810 –840. ISSN: 0045-7825.

[35] C. Hesch, U. Khristenko, R. Krause, A. Popp, A. Seitz, W. Wall, and B. Wohlmuth. *Frontiers in Mortar Methods for Isogeometric Analysis*. 2020. arXiv: 2006.06677 [cs.CE].

[36] T. Hirschler, R. Bouclier, D. Dureisseix, A. Duval, T. Elguedj, and J. Morlier. "A dual domain decomposition algorithm for the analysis of non-conforming isogeometric Kirchhoff-Love shells". In: *Computer Methods in Applied Mechanics and Engineering* 357 (2019), p. 112578. ISSN: 0045-7825.

[37] C. Hofreither. "A black-box low-rank approximation algorithm for fast matrix assembly in isogeometric analysis". In: *Comput. Methods Appl. Mech. Engrg.* 333 (2018), pp. 311–330.

[38] C. Hofreither and S. Takacs. "Robust multigrid for isogeometric analysis based on stable splittings of spline spaces". In: *SIAM J. Numer. Anal.* 55.4 (2017), pp. 2004–2024.

[39] C. Hofreither and W. Zulehner. "Mass smoothers in geometric multigrid for isogeometric analysis". In: *International Conference on Curves and Surfaces*. Springer, Cham, 2014, pp. 272–279.

[40] T. Horger, A. Reali, B. Wohlmuth, and L. Wunderlich. "A hybrid isogeometric approach on multi-patches with applications to Kirchhoff plates and eigenvalue problems". In: *Computer Methods in Applied Mechanics and Engineering* 348 (2019), pp. 396 –408. ISSN: 0045-7825.

[41] T. J. R. Hughes, J. A. Cottrell, and Y. Bazilevs. "Isogeometric Analysis: CAD, Finite Elements, NURBS, Exact Geometry and Mesh Refinement". In: *Computer Methods in Applied Mechanics and Engineering* 194.39–41 (2005), pp. 4135–4195. ISSN: 0045-7825.

[42] "Isogeometric analysis: Progress and challenges". In: *Computer Methods in Applied Mechanics and Engineering* 316 (2017). Special Issue on Isogeometric Analysis: Progress and Challenges, pp. 1 –1270. ISSN: 0045-7825.

[43] J. Kiendl, M. Ambati, L. De Lorenzis, H. Gomez, and A. Reali. "Phase-field description of brittle fracture in plates and shells". In: *Computer Methods in Applied Mechanics and Engineering* 312 (2016). Phase Field Approaches to Fracture, pp. 374 –394. ISSN: 0045-7825.

[44] J. Kiendl, Y. Bazilevs, M. C. Hsu, R. Wüchner, and K. U. Bletzinger. "The bending strip method for isogeometric analysis of Kirchhoff-Love shell structures comprised of multiple patches". In: *Computer Methods in Applied Mechanics and Engineering* 199.37 (2010), pp. 2403 –2416. ISSN: 0045-7825.

[45] J. Kiendl, K. U. Bletzinger, J. Linhard, and R. Wüchner. "Isogeometric shell analysis with Kirchhoff-Love elements". In: *Computer Methods in Applied Mechanics and Engineering* 198.49 (2009), pp. 3902 –3914. ISSN: 0045-7825.

[46] J. Kiendl, M. Hsu, M. C. H. Wu, and A. Reali. "Isogeometric Kirchhoff-Love shell formulations for general hyperelastic materials". In: *Computer Methods in Applied Mechanics and Engineering* 291 (2015), pp. 280 –303. ISSN: 0045-7825.

[47] T. G. Kolda and B. W. Bader. "Tensor decompositions and applications". In: *SIAM Rev.* 51.3 (2009), pp. 455–500.

[48] J. Liu and A. L. Marsden. "A robust and efficient iterative method for hyperelastodynamics with nested block preconditioning". In: *Journal of Computational Physics* 383 (2019), pp. 72 –93. ISSN: 0021-9991.

[49] J. Liu, W. Yang, M. Dong, and A. L. Marsden. "The nested block preconditioning technique for the incompressible Navier-Stokes equations with emphasis on hemodynamic simulations". In: *Computer Methods in Applied Mechanics and Engineering* 367 (2020), p. 113122. ISSN: 0045-7825.

[50] N. Liu and A. E. Jeffers. "A geometrically exact isogeometric Kirchhoff plate: Feature-preserving automatic meshing and C1 rational triangular Bézier spline discretizations". In: *International Journal for Numerical Methods in Engineering* 115.3 (2018), pp. 395–409.

[51] G. Loli, M. Montardini, G. Sangalli, and M. Tani. "An efficient solver for space–time isogeometric Galerkin methods for parabolic problems". In: *Computers & Mathematics with Applications* 80.11 (2020). High-Order Finite Element and Isogeometric Methods 2019, pp. 2586 –2603. ISSN: 0898-1221.

[52] G. Loli, G. Sangalli, and M. Tani. *Easy and Efficient preconditioning of the Isogeometric Mass Matrix*. Submitted to Computers & Mathematics with Applications. 2020. arXiv: 2006.02313.

[53] M. Łoś, M. Paszyński, A. Kłusek, and W. Dzwinel. "Application of fast isogeometric L2 projection solver for tumor growth simulations". In: *Comput. Methods Appl. Mech. Engrg.* 316 (2017), pp. 1257–1269.

[54] A. Mantzaflaris, B. Jüttler, B. N. Khoromskij, and U. Langer. "Low rank tensor methods in Galerkin-based isogeometric analysis". In: *Comput. Methods Appl. Mech. Engrg.* 316 (2017), pp. 1062–1085.

[55] A. Mantzaflaris, B. Jüttler, B. N. Khoromskij, and U. Langer. "Matrix generation in isogeometric analysis by low rank tensor approximation". In: *International Conference on Curves and Surfaces*. Springer, Cham. 2014, pp. 321–340.

[56] M. Montardini, M. Negri, G. Sangalli, and M. Tani. *Space-time least-squares isogeometric method and efficient solver for parabolic problems*. 2018. arXiv: 1809.10026 [math.NA].

[57] M. Montardini, G. Sangalli, and M. Tani. "Robust isogeometric preconditioners for the Stokes system based on the Fast Diagonalization method". In: *Computer Methods in Applied Mechanics and Engineering* 338 (2018), pp. 162 –185. ISSN: 0045-7825.

[58] J. Niiranen, J. Kiendl, A. H. Niemi, and A. Reali. "Isogeometric analysis for sixth-order boundary value problems of gradient-elastic Kirchhoff plates". In: *Computer Methods in Applied Mechanics and Engineering* 316 (2017). Special Issue on Isogeometric Analysis: Progress and Challenges, pp. 328 –348. ISSN: 0045-7825.

[59] A. Quarteroni, Saleri. F., and A. Veneziani. "Factorization methods for the numerical approximation of Navier-Stokes equations". In: *Computer Methods in Applied Mechanics and Engineering* 188.1 (2000), pp. 505 –526. ISSN: 0045-7825.

[60] A. Reali and H. Gómez. "An isogeometric collocation approach for Bernoulli-Euler beams and Kirchhoff plates". In: *Computer Methods in Applied Mechanics and Engineering* 284 (2015). Isogeometric Analysis Special Issue, pp. 623 –636. ISSN: 0045-7825.

[61] E. Sande, C. Manni, and H. Speleers. "Sharp error estimates for spline approximation: Explicit constants, n-widths, and eigenfunction convergence". In: *Math. Models Methods Appl. Sci.* (2019), pp. 1–31.

[62] G. Sangalli and M. Tani. "Isogeometric Preconditioners Based on Fast Solvers for the Sylvester Equation". In: *SIAM Journal on Scientific Computing* 38.6 (2016), A3644–A3671.

[63] G. Sangalli and M. Tani. "Matrix-free weighted quadrature for a computationally efficient isogeometric k-method". In: *Comput. Methods Appl. Mech. Engrg.* 338 (2018), pp. 117–133. ISSN: 0045-7825.

[64] D. Schillinger, I. Harari, M. Hsu, D. Kamensky, S. K. F. Stoter, Y. Yu, and Y. Zhao. "The non-symmetric Nitsche method for the parameter-free imposition of weak boundary and coupling conditions in immersed finite elements". In: *Computer Methods in Applied Mechanics and Engineering* 309 (2016), pp. 625 –652. ISSN: 0045-7825.

[65] L. Schumaker. *Spline Functions: Basic Theory*. Third. Cambridge Mathematical Library. Cambridge University Press, Cambridge, 2007.

[66] V. Simoncini. "Computational Methods for Linear Matrix Equations". In: *SIAM Review* 58.3 (2016), pp. 377–441.

[67] S. Takacs and T. Takacs. "Approximation error estimates and inverse inequalities for B-splines of maximum smoothness". In: *Math. Models Methods Appl. Sci.* 26.07 (2016), pp. 1411–1445.

[68] A. Tkachuk and M. Bischoff. "Direct and sparse construction of consistent inverse mass matrices: general variational formulation and application to selective mass scaling". In: *Internat. J. Numer. Methods Engrg.* 101.6 (2015), pp. 435–469.

[69] A. Toselli and O. Widlund. *Domain decomposition methods—algorithms and theory*. Vol. 34. Springer Series in Computational Mathematics. Springer-Verlag, Berlin, 2005, pp. xvi+450.

[70] R. Vázquez. "A new design for the implementation of isogeometric analysis in Octave and Matlab: GeoPDEs 3.0". In: *Computers and Mathematics with Applications* 72.3 (2016), pp. 523 –554. ISSN: 0898-1221.

[71] L. Beirão da Veiga, A. Buffa, J. Rivas, and G. Sangalli. "Some estimates for h–p–k-refinement in Isogeometric Analysis". In: *Numer. Math.* 118.2 (2011), pp. 271–305.

[72] L. Beirao da Veiga, A. Buffa, G. Sangalli, and R. Vázquez. "Mathematical analysis of variational isogeometric methods". In: *Acta Numerica* 23 (2014), pp. 157–287.

[73] L. Beirão da Veiga, D. Cho, L. F. Pavarino, and S. Scacchi. "Overlapping Schwarz Methods for Isogeometric Analysis". In: *SIAM J. Numer. Anal.* 50.3 (2012), pp. 1394–1416.

[74] B. I. Wohlmuth. "Discretization Techniques Based on Domain Decomposition". In: *Discretization Methods and Iterative Solvers Based on Domain Decomposition*. Berlin, Heidelberg: Springer Berlin Heidelberg, 2001, pp. 1–84.

[75] M. Woźniak, M. Łoś, M. Paszyński, L. Dalcin, and V. M. Calo. "Parallel fast isogeometric solvers for explicit dynamics". In: *Comput. Inform.* 36.2 (2017), pp. 423–448.

[76] L. Wunderlich, A. Seitz, M. D. Alaydın, B. Wohlmuth, and A. Popp. "Biorthogonal splines for optimal weak patch-coupling in isogeometric analysis with applications to finite deformation elasticity". In: *Comput. Methods Appl. Mech. Engrg.* 346 (2019), pp. 197–215.